UNCLASSIFIED

AD NUMBER

AD809541

NEW LIMITATION CHANGE

TO

Approved for public release, distribution unlimited

FROM

Distribution authorized to U.S. Gov't. agencies and their contractors; Critical Technology; NOV 1966. Other requests shall be referred to Air Force Flight Dynamics Lab., AFSC, Wright-Patterson AFB, OH 45433.

AUTHORITY

AFFDL ltr, 24 Jan 1973

THIS PAGE IS UNCLASSIFIED

AFFDL-TR-66-104

809541

DRAG AND DYNAMICS OF SINGLE AND CLUSTERED PARACHUTES IN FREESTREAM, AND WITH WAKE AND GROUND EFFECTS

H. G. HEINRICH
R. A. NOREEN

UNIVERSITY OF MINNESOTA

TECHNICAL REPORT AFFDL-TR-66-104

NOVEMBER 1966

MAR 2 4 1967

AIR FORCE FLIGHT DYNAMICS LABORATORY
RESEARCH AND TECHNOLOGY DIVISION
AIR FORCE SYSTEMS COMMAND
WRIGHT-PATTERSON AIR FORCE BASE, OHIO

DRAG AND DYNAMICS OF SINGLE AND CLUSTERED PARACHUTES IN FREESTREAM, AND WITH WAKE AND GROUND EFFECTS

H. G. HEINRICH
R. A. NOREEN

UNIVERSITY OF MINNESOTA

ABSTRACT

Results of wind tunnel studies concerned with transient and steady state performance of single and clustered parachutes in cargo extraction systems are presented.

In Part 1, circular flat and ringslot canopies singly suspended and in clusters of 2, 3, and 4, were deployed in freestream, in the wake of an aircraft, and near a simulated ground.

As a further means of analysis, wake pressure surveys were performed on the DHC-4 Caribou and the C-130 Hercules aircraft and are presented in Part 2.

TABLE OF CONTENTS

ILLUSTRATIONS

ILLUSTRATIONS (CONT.)

ILLUSTRATIONS (CONT.)

        Note: Figures 41-56 are included in Appendix II.

TABLES

SYMBOLS*

AW	deployment in the wake of the Caribou model aircraft
AW/GE	deployment in the wake of the aircraft near the ground
C	effective porosity
C_{D_O}	drag coefficient based on nominal diameter
D	steady state drag
D_O	nominal diameter
D_p	projected diameter of parachute
F_{max}	opening shock
FS	freestream deployment
GE	deployment near the simulated ground
h	distance between ground plane and parachute centerline
n	number of parachutes
q	dynamic pressure
t_f	filling time
S_O	nominal area
V	deployment velocity
X	opening shock factor
λ_t	total porosity

Subscripts

1	value for a single parachute
n	value for a parachute acting as a clustered unit
∞	freestream conditions

Superscripts

'	full scale values

Additional symbols, when used, are defined in the text.

---

* In view of definitions in Ref 1.

1. EXTRACTION PARACHUTE STUDIES

I. INTRODUCTION

This study is concerned with the opening and steady state performance of solid flat and ringslot extraction parachutes deployed singly and clustered in freestream and in the wake of an aircraft in free flight and near the ground.

In view of these objectives, the experiments were performed for the circular solid flat and circular flat ringslot parachutes in the following arrangements:

1) Deployment of single parachutes in freestream at velocities of 40, 50, 120, and 150 knots.

2) Deployment of single, and clusters of 2, 3, and 4 parachutes in freestream, and in the wake of a free-flying aircraft at the single velocity of 54 knots.

3) Deployment of single, and a cluster of two parachutes near the ground and in the wake of an aircraft near the ground at a velocity of 54 knots.

II. MODELS

In order to correlate model opening characteristics with those of full size parachutes, the models should be very flexible. To achieve this flexibility, the models must be as large as the wind tunnel blockage effects will permit. Considering the available wind tunnel with a 5' by 5' open jet area, the size of the individual parachute models was determined from the expected blockage caused by a cluster of four parachutes in the wake of the model aircraft. A nominal diameter of about 16 in. for the parachutes, and an aircraft model with a wing span of about 6 ft was selected. These dimensions correspond to a model scale factor of 1/16.

A. Parachute Models

1) Ringslot Parachutes

The ringslot parachute models were scaled from the standard 22-foot, 28 gore ringslot extraction parachutes.

They were made with a constructed diameter of 15 in., 28 gores, and a total calculated porosity of 12.7%. A typical gore pattern of the ringslot models is shown in Fig 1.

2) Solid Flat Parachutes

The circular solid flat models were scaled from a prototype parachute having the same drag area, $C_D S$, as the 22-ft diameter ringslot parachute, which yields a nominal diameter of 18.2 ft. Applying the 1/16 scale, the diameter of these models is 13.65 in. The solid flat parachute models having 28 gores were constructed of 1.1 oz standard parachute nylon cloth with a permeability of 90 - 120 ft^3/ft^2-min. A typical gore pattern is shown in Fig 1.

B.   Aircraft Model

The DeHavilland DHC-4 Caribou was chosen as a characteristic aircraft for extraction parachute deployment. Large three-views and other data were obtained from DeHavilland Aircraft of Canada, Ltd., on the basis of which the 1/16 scale model was constructed.

As shown in Fig 2, the model had a 6-ft wing span, and an overall length of 4.5 ft. The model was designed to withstand the opening forces of the parachutes, since the load extraction line must anchor to a force sensing element in the aircraft fuselage. Thus, the force balance was rigidly fastened to a steel framework, around which the fuselage of the model was built of mahogany. The wing, also constructed of mahogany, was equipped with engine nacelles and windmilling propellers. Wing and fuselage were separable for ease of handling.

Figure 3 shows the Caribou model mounted in the wind tunnel. The overhead struts fasten to the steel framework, leaving the outer structure free of all parachute forces. As shown in Fig 3, 6 in. of each wing tip were removed and tip plates attached for ease of installation. The tip plates, of course, suppress the formation of wing tip vortices, which was, in this case, considered to be immaterial.

III.   EXPERIMENTAL APPARATUS

A.   Wind Tunnel Facilities

The subsonic, horizontal return wind tunnel (Fig 4) of the University of Minnesota has both a closed,

2
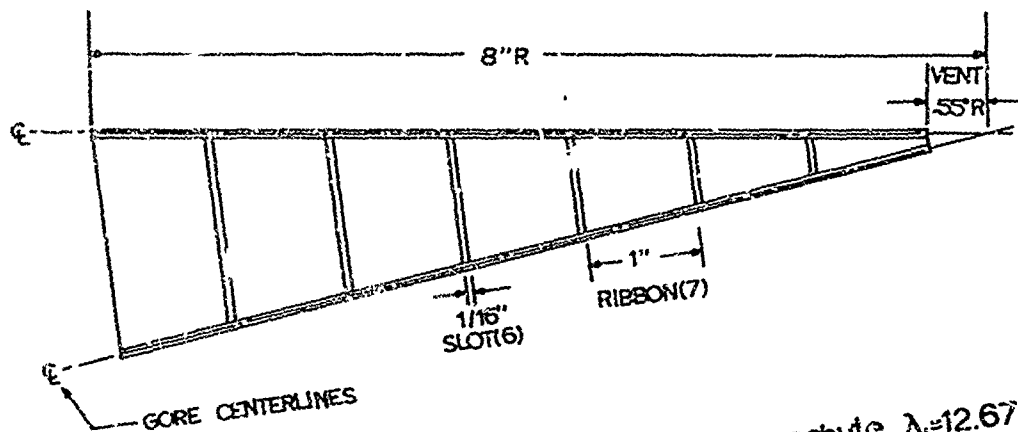
a. Gore Pattern for 28-Gore Ringslot Parachute, λ_t=12.67%

NOTE: 1.1 oz. NYLON CLOTH
90-120 ft³/ft²min PERMEABILITY
EVERY OTHER LINE CROSSES VENT
NUMBER OF GORES = 28
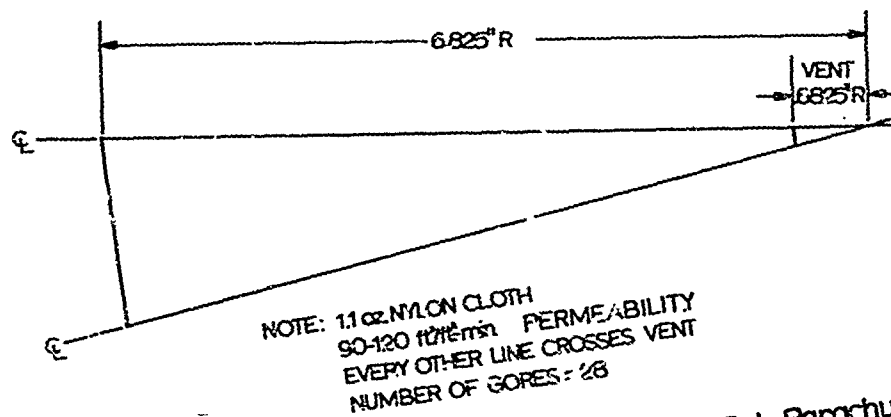
b. Gore Pattern for 28-Gore Circular Solid Flat Parachute

Fig 1.   Gore Patterns for Ringslot and Solid Flat Parachute Models
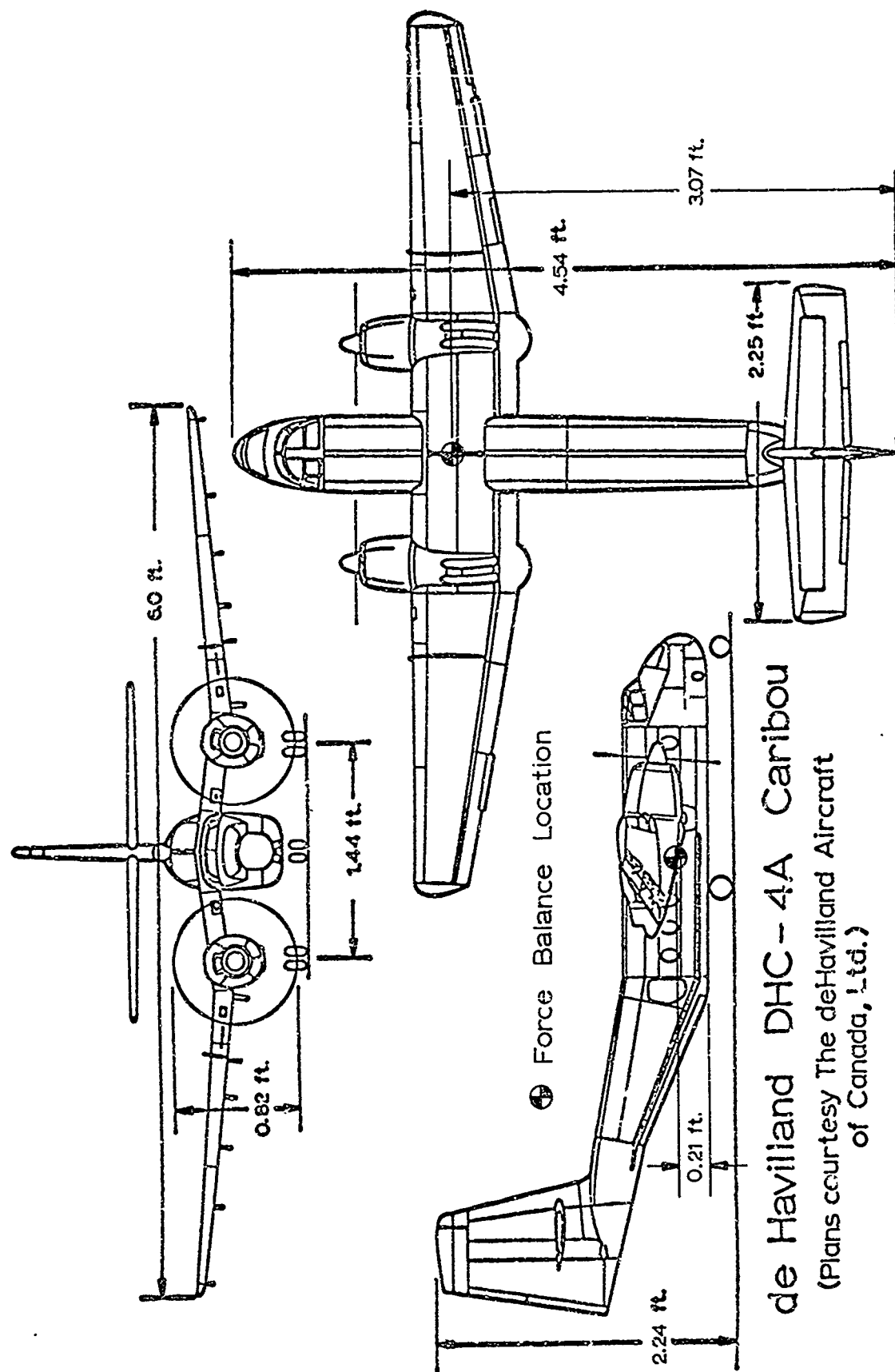
3

de Haviland DHC-4A Caribou

(Plans courtesy The deHavilland Aircraft of Canada, Ltd.)

● Force Balance Location

Fig 2.   Three-View of Model Aircraft Used for Extraction Parachute Studies

4

Fig 3.　Aircraft Model Installation

SECTION A-A   SECTION B-B   SECTION C-C   SECTION D-D   SECTION E-E

100 hp, 1200 rpm, 400 volt, 60 cycle 3 phase AC electric motor

STRAIGHTENER VANES

FAN (6' DIAM.)

SCREEN

HONEYCOMB

OPEN TEST SECTION 60'x60'

CLOSED TEST SECTION 38'x54"

BREATHER

CORNER VANE DETAIL

50'-2"

24'-0"

15'-4"

3.5°

2°

TEST SECTION VELOCITY RANGE 0 - 200 mph
CONTRACTION RATIO = 6.16 : 1

Fig 4.   University of Minnesota Horizontal Return Wind Tunnel

6

high velocity test section, and an open, lower velocity jet. Velocities of up to 150 knots may be obtained when the open jet nozzle has been removed and replaced by a simple connecting diffuser section. Single parachutes were deployed at velocities from 40 to 150 knots in this closed test section. All other tests with the Caribou model, ground plane, and clustered parachutes were performed in the much larger open-jet test area of the wind tunnel.

B.   Force Balances and Recording Apparatus

Three force balances of similar construction were used. All consisted of a standard strain gage bridge affixed to a cantilever beam. The balance mounted within the Caribou fuselage was capable of measuring loads of up to 50 lbs. The other two were designed to be mounted on a strut far upstream of the parachute model. One had a load capacity up to 300 lbs, while the other could measure loads to 50 lbs. The 300 lb balance was needed for the high velocity tests on a single circular flat parachute where the opening shock approached 120 lbs.

For all of the force balances, the output of the strain gage bridge was amplified, then fed to an oscillograph recorder. The recorder paper speed was 25 in/sec with timing marks every .01 sec.

C.   Parachute Deployment Cylinders

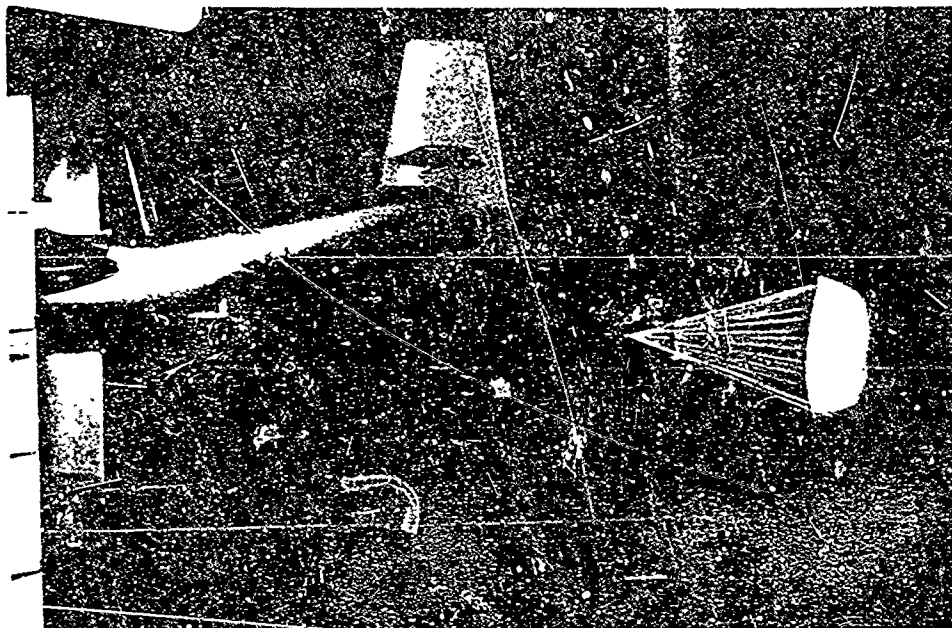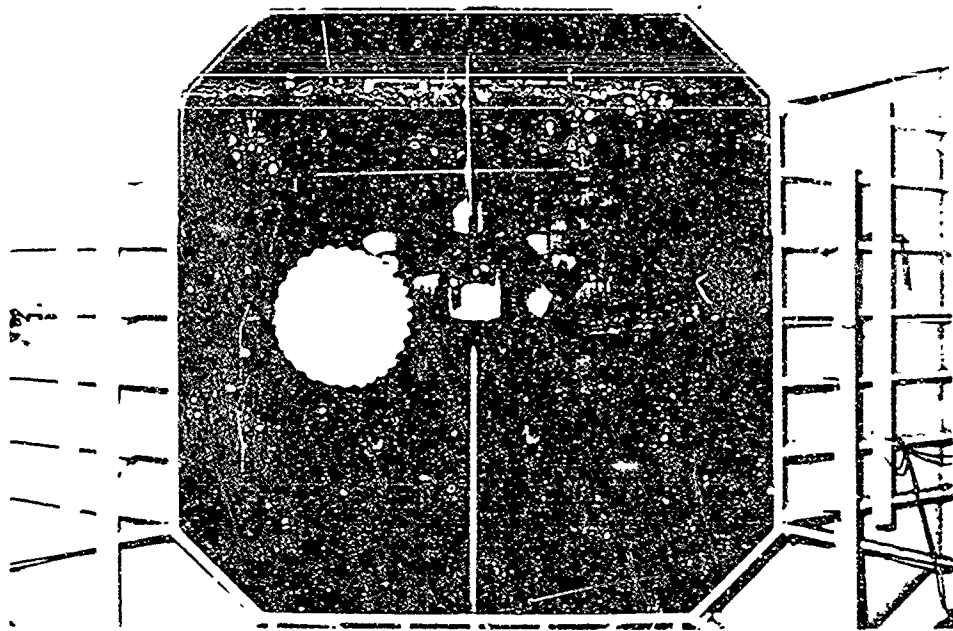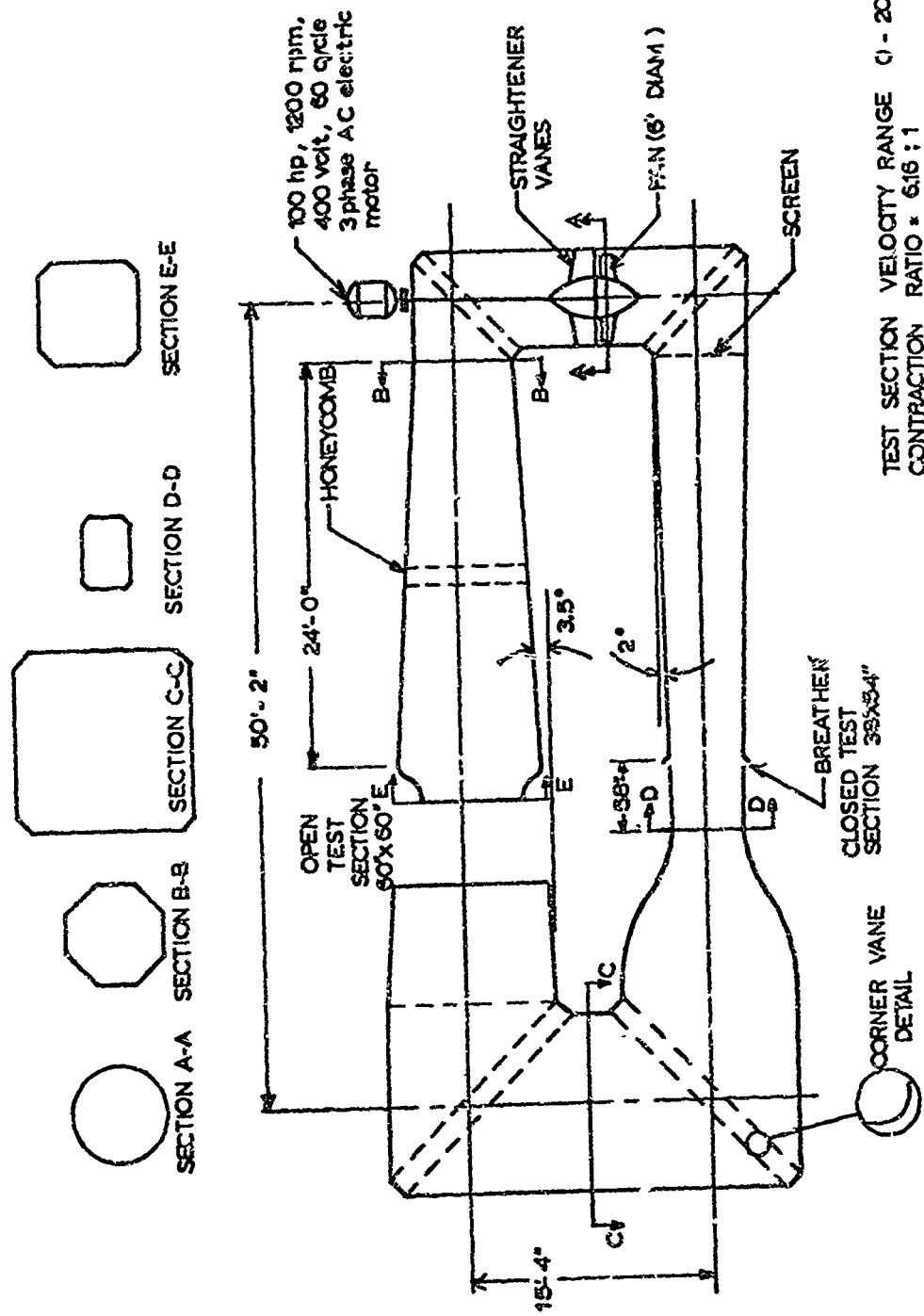The model parachutes were deployed into the airstream in a manner similar to that used for full-size extraction parachutes (Section IV, A). In the model deployments, the parachutes were packed into one of three deployment cylinders (Fig 5). These cylinders, attached to either a support in the wind tunnel or inside the model aircraft, held the parachutes out of the flow until the deployment sequence began. Three cylinders of different sizes were needed to hold the various numbers of parachutes tested.

The first two cylinders (Fig 5 a,b) were of similar construction and consisted of a brass tube that was split and hinged. A helical spring, wrapped around the cylinders, provided a moment which tended to open them. A loop of stainless steel wire held the cylinders closed. Burning the wire with an electrical current initiated the rapid opening of the cylinder.

The third cylinder, designed to hold clusters of 3 and 4 parachutes (Fig 5 c) consisted of a flat piece of spring steel, which was wrapped around the clustered parachutes, held closed by a loop of wire, and opened as described above.
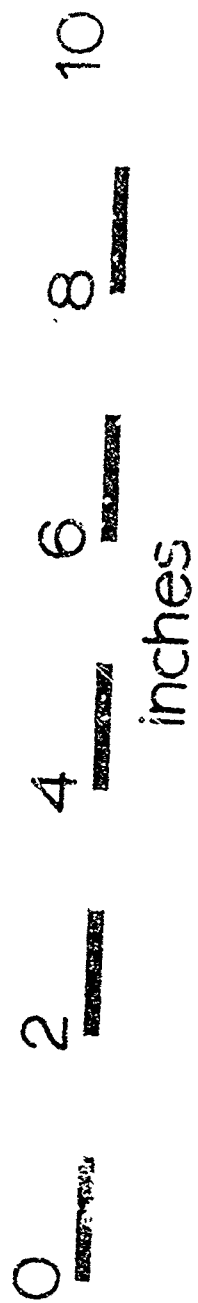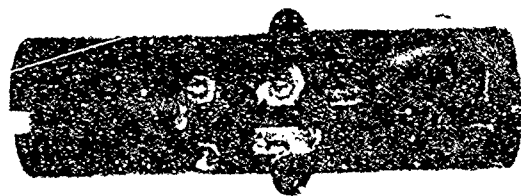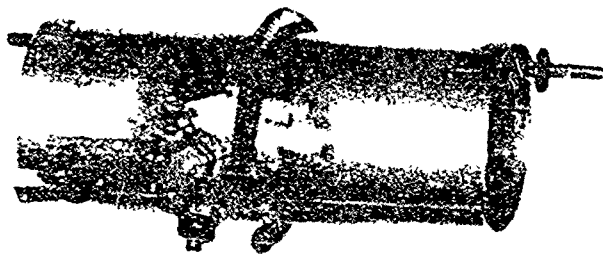
7

Fig 5. Parachute Deployment Cylinders

8

IV. EXPERIMENTAL PROCEDURE

A. Parachute Deployment and Packing

The accuracy of the opening characteristics of model parachutes depends very strongly upon the deployment and packing methods used in the tests. The model deployment method should allow the parachutes to open under conditions identical to those of full scale parachutes, and model packing procedure must insure uniformity and repeatability of the opening process.

After investigating several parachute deployment and packing methods, the deployment method chosen for the tests was very similar to that of the "pendulum deployment" used in full-scale cargo extraction procedures (Ref 1). However, the packing procedures used on full-scale parachutes are much too complex to duplicate on small parachute models so a simple, repeatable model packing procedure was chosen. The parachute deployment and packing procedures used in all tests are given below.

In the wind tunnel, the parachute deployment cylinder mounts above and downstream of the force balance, and a nylon extraction line connects the parachute confluence point to the force balance. All cluster configurations had a 3.75 in. riser (full scale 5 ft) between parachute confluence points and extraction line. The model parachute(s) was packed tightly and placed in the deployment cylinder as outlined in Fig 6. First, the skirt of the parachute was gathered by "accordion pleating" one gore upon the next (Fig 6 a,b). Next, the suspension lines were folded doubled over the lines, holding everything in position (Fig 6d). The bundle was then placed in the deployment cylinder (Fig 6e), the cylinder closed, and fastened with a wire loop (Fig 6f). When the cylinder was opened, the parachute fell into the flow and moved downstream. Although the model parachutes were used without deployment bags, as full size parachutes usually are, the models did not inflate until the suspension lines were deployed and snatch force had occurred. Hence, gravity and aerodynamic drag deployed the model parachutes just as in full-size extraction procedures.

Figures 7 and 8 show the deployment of a single parachute and a cluster of 4 parachutes, respectively.

B. Test Procedure

The parachutes were packed as described above and the freestream dynamic pressure of the wind tunnel was

9
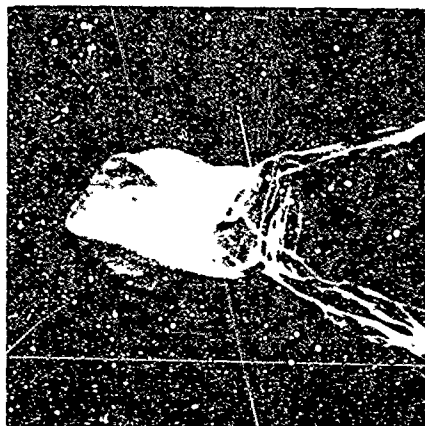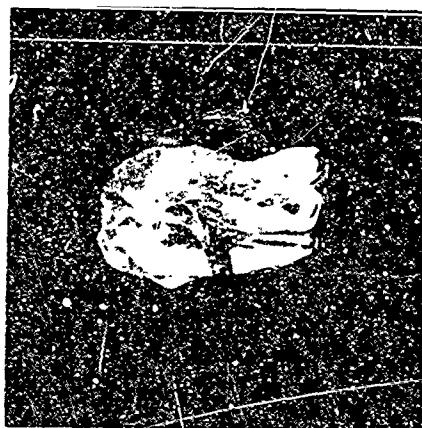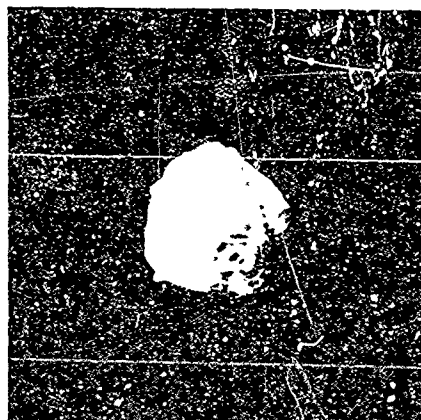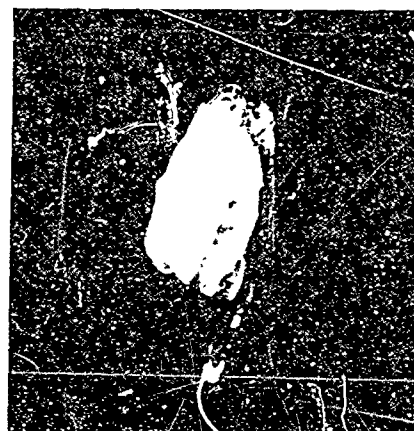
Fig 6. Parachute Model Packing Sequence
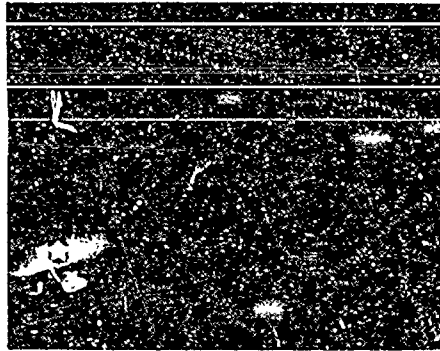
a. Packed Parachute
   Leaving Airplane
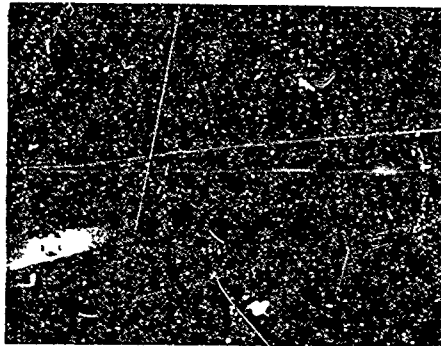
b. Parachute Falling
   Downstream
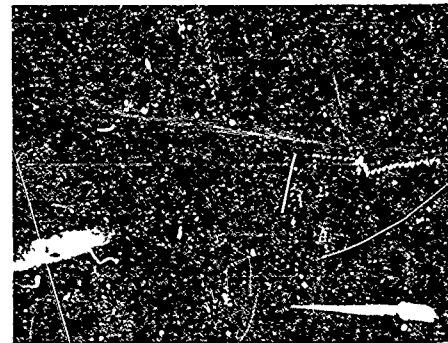
c. Snatch Force
   Occurrence

d. Parachute Inflating
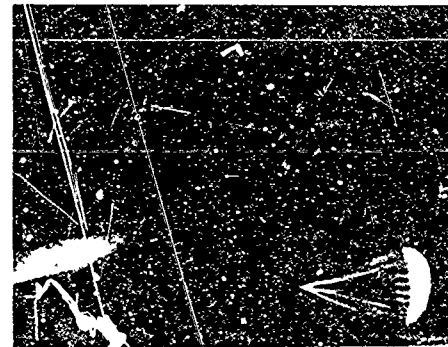
e. Parachute Fully
   Inflated

Fig 7. Film Sequence of the Deployment of a Single
       Solid Flat Parachute
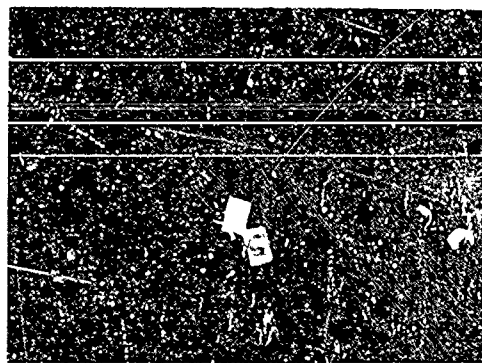
a) Packed Parachutes Leaving
Deployment Cylinder

b) Parachutes Moving
Downstream
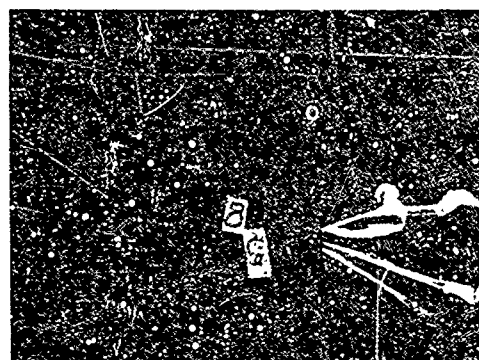
c) Snatch Force
Occurrence
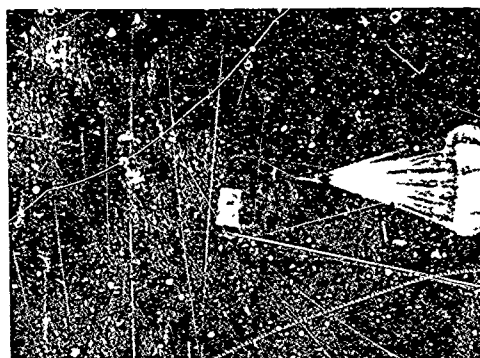
d) Parachutes Inflating
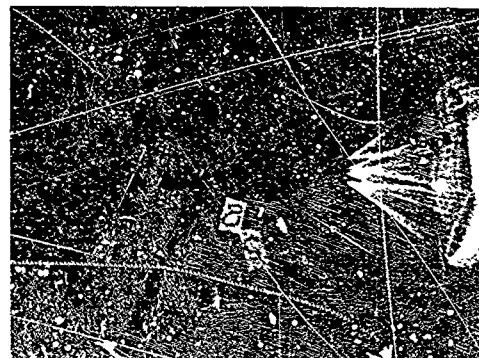
e) Fully Inflated
Clusters

Fig 8. Film Sequence of the Deployment of a Cluster of
4 Ringslot Parachutes

12

adjusted. Subsequently, the recorder paper was started and the deployment cylinder opened.

Fifteen to twenty tests were performed for each deployment configuration and velocity condition to provide data points for a statistical analysis.

Movies with 700 frames/sec were taken of selected runs of each configuration to provide a means of checking the parachute deployment.

The measurement of parachute opening dynamics presents difficulties because the wind tunnel velocity decreases due to the increasing blockage of the inflating parachute. A few tests using an electrical differential pressure gage showed that the significant decrease in flow velocity did not occur until after the parachute was fully inflated. Thus, the opening for ? occurred in freestream dynamic pressure, but the steady ate drag following inflation occurred at a reduced (nic pressure. Steady state drag forces used for determining opening shock factors were obtained from separate wind tunnel measurements where the freestream dynamic pressure was adjusted with the parachute fully inflated, restrained merely by the confluence points.

In the following, the various configurations and arrangements will be described. Table I may serve as a general orientation. Details of the different phases are presented below.

1) Single and Clustered Parachute in Freestream

Singly suspended parachutes were deployed in the 38 in. x 54 in. closed test section of the wind tunnel to establish the opening characteristics over a velocity range of 40 to 150 knots. The deployment cylinder was mounted on the roof of the test section, and force sensing element on a strut far upstream. A steel cable extended from the force balance to the front of the test section where it was supported by a small washer which was centered in the test section (Fig 9). A nylon extraction line connected the parachute to the end of this cable.

Single and clustered parachutes were tested in the open test section with essentially the same test arrangement as described above (Fig 10). The deployment cylinder mounted on the strut used for supporting the aircraft model. Single parachutes were tested at velocities of 43 and 54 knots to obtain correlation of opening characteristics between open and closed test sections.

2) Single and Clustered Parachutes in the Aircraft Wake

13

TABLE I

TEST PROGRAM FOR ONE PARACHUTE TYPE

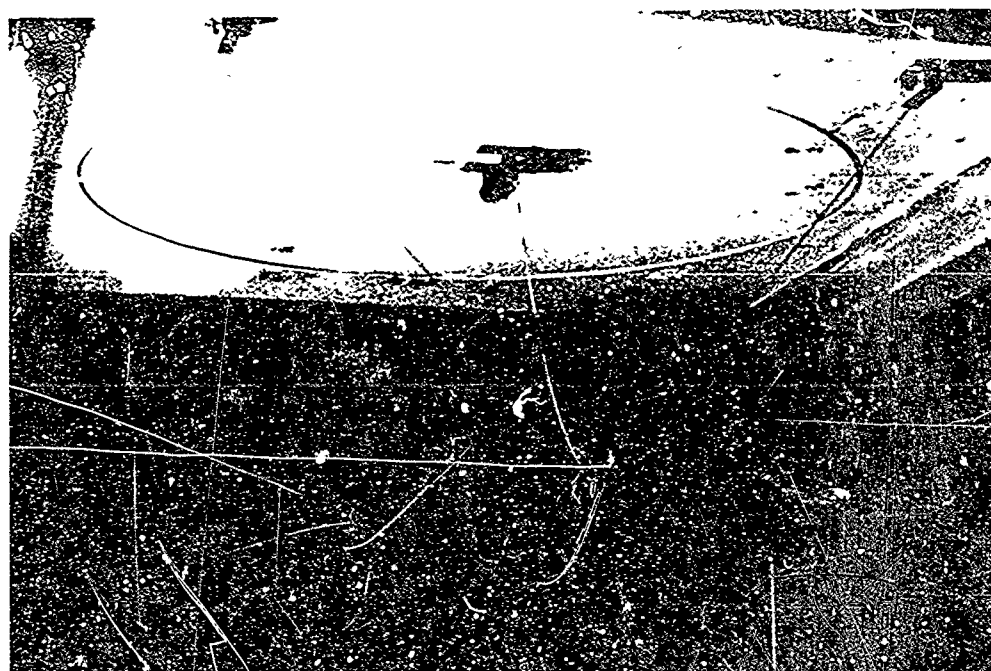| Flow Condition	Parachutes	Deployment Velocities (knots)
Freestream (FS)	1	40, 50, 80, 120, 150
Freestream (FS)	1, 2, 3, and 4	54
Aircraft Wake (AW)	1, 2, 3, and 4	54
Ground Effect (GE)	1, 2	54
Aircraft Wake With Ground Effect (AW/GE)	1, 2	54

14

Fig 9. Closed Test Section Installation for Freestream
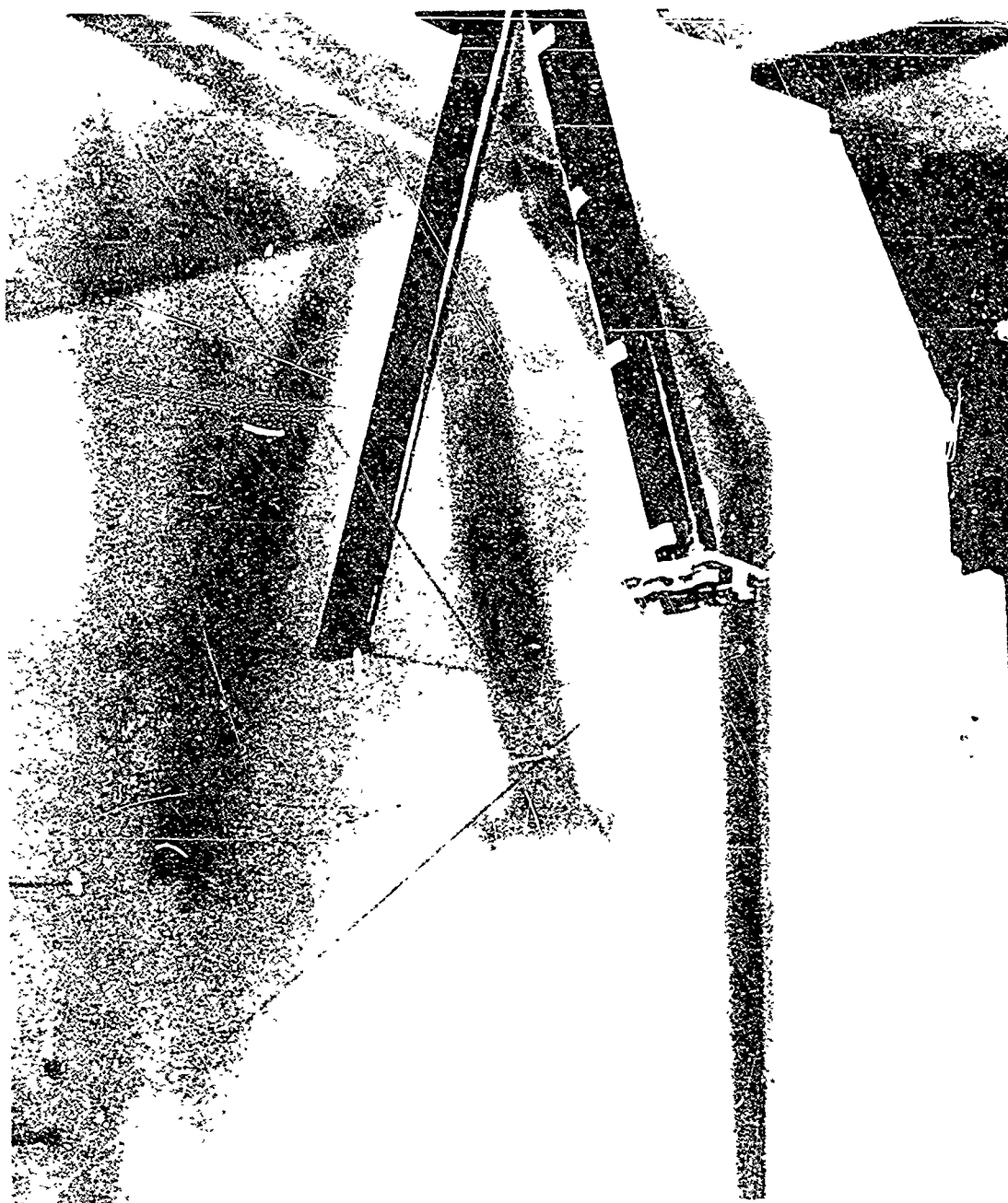   Deployment

15

Fig 10. Open Test Section Installation for Freestream
Deployment

16

The installation of the Caribou model was shown in Fig 3. The model was positioned so the wing's leading edge was slightly upstream of the nozzle exit. The deployment cylinder was mounted above and behind the loading ramp of the Caribou (Fig 11), with the extraction line extending up to the force balance. The force balance was positioned to simulate a load placed at the mean center of gravity of the aircraft, with the extraction line fastened at a height of 27.5 in. above the cargo compartment floor (Fig 2). The extraction line length was scaled from the standard 60-ft line used in the pendulum deployment system.

3) Single and Clustered Parachutes With Ground Effect

A large plane of plywood was installed in the open section for simulation of the ground (Fig 12). The plane was equipped with adjustable supports for varying the height of the simulated ground. A door in the ground plane allowed easy access to the deployment cylinder.

The dimensions of the ground plane were such that when used with the Caribou model, it extended one mean aerodynamic chord ahead of the leading edge of the wing. Downstream, the ground plane extended 1.5 parachute nominal diameters past the vent position of the fully inflated parachute.

The height of the ground plane was set at $h/D_O=0.5$, where h is the distance between the ground plane and the parachute centerline and D_O is the nominal diameter of the parachute.

The position of the deployment cylinder and force balance was identical to that of freestream testing in the open section.

4) Aircraft Wake with Ground Effect Experiments

Since the ground plane could be installed and adjusted without removal of the aircraft model, the deployment cylinder and force balance of the Caribou model were used (Fig 13).

With the ground plane positioned at $h/D_O = 0.50$, an attempt was made to simulate a Caribou aircraft flying 5 ft above the ground.

V. RESULTS

The data obtained from the tests consists of the opening shock factor, filling time, the respective standard
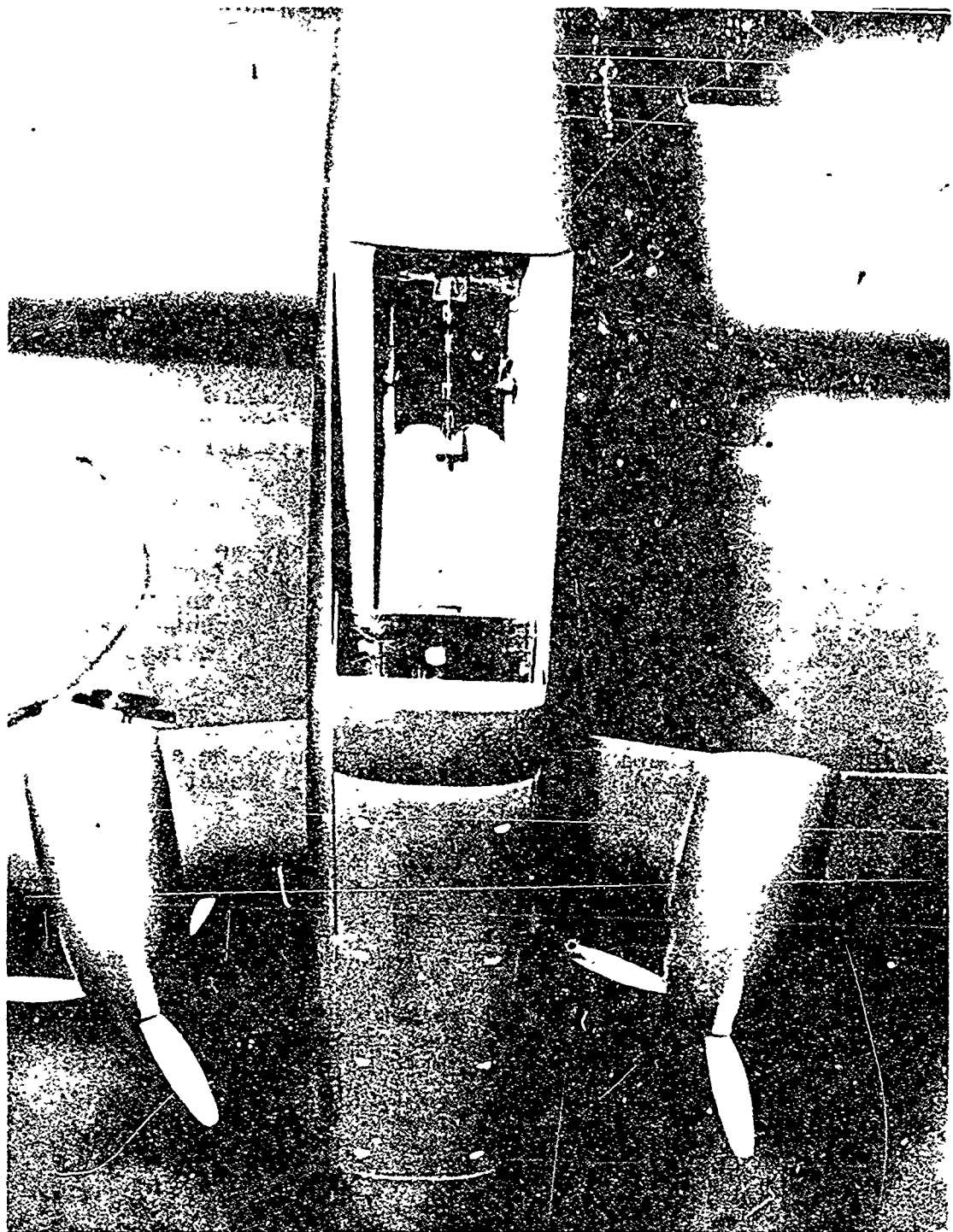
17

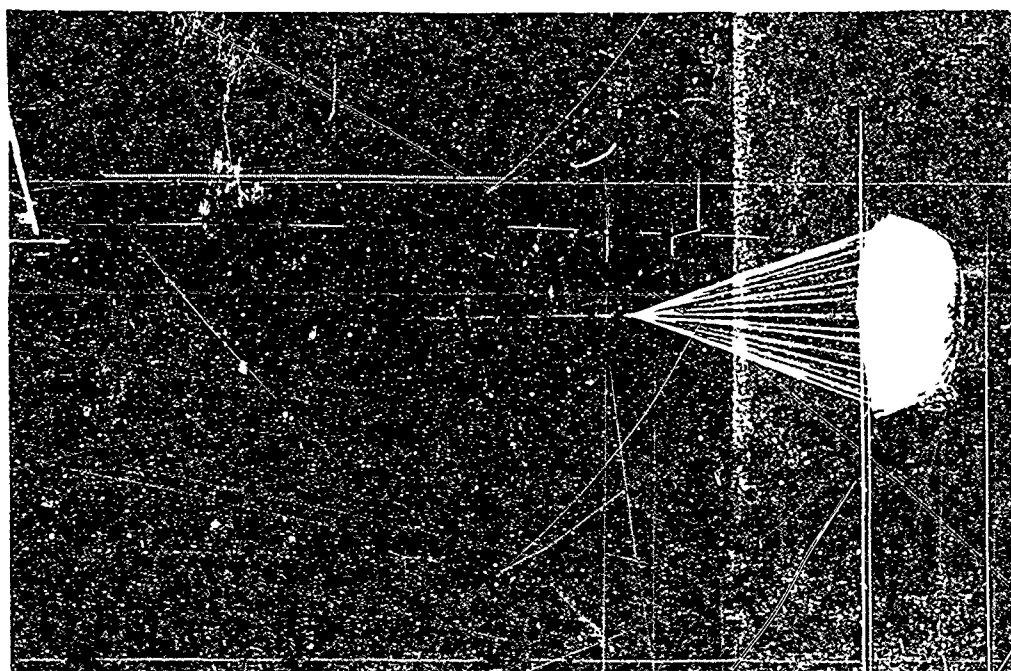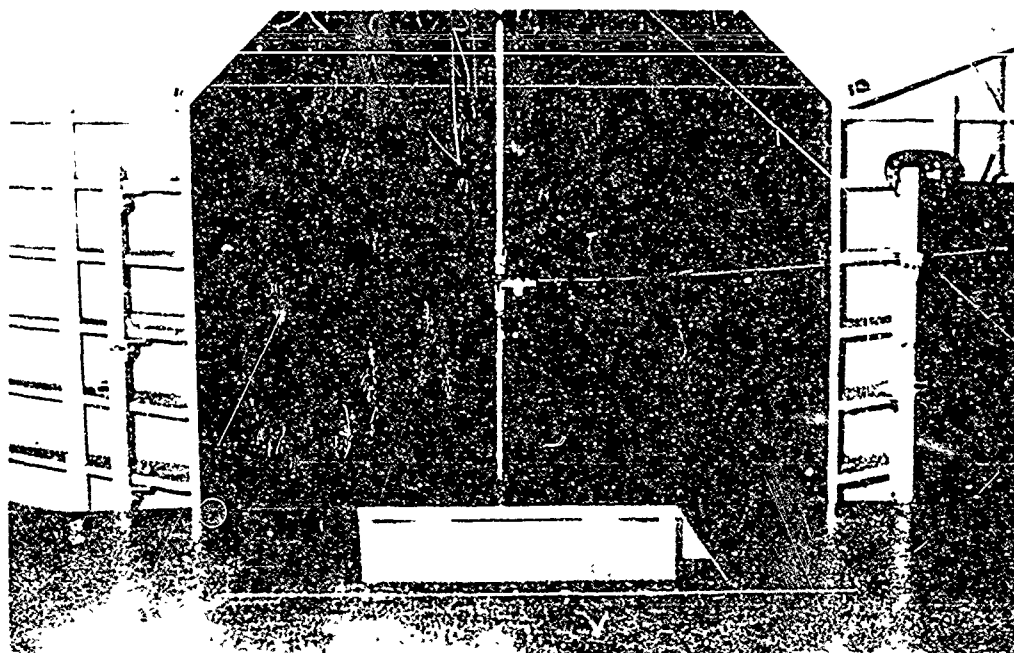Fig 11.   Deployment Cylinder Installation in Aircraft
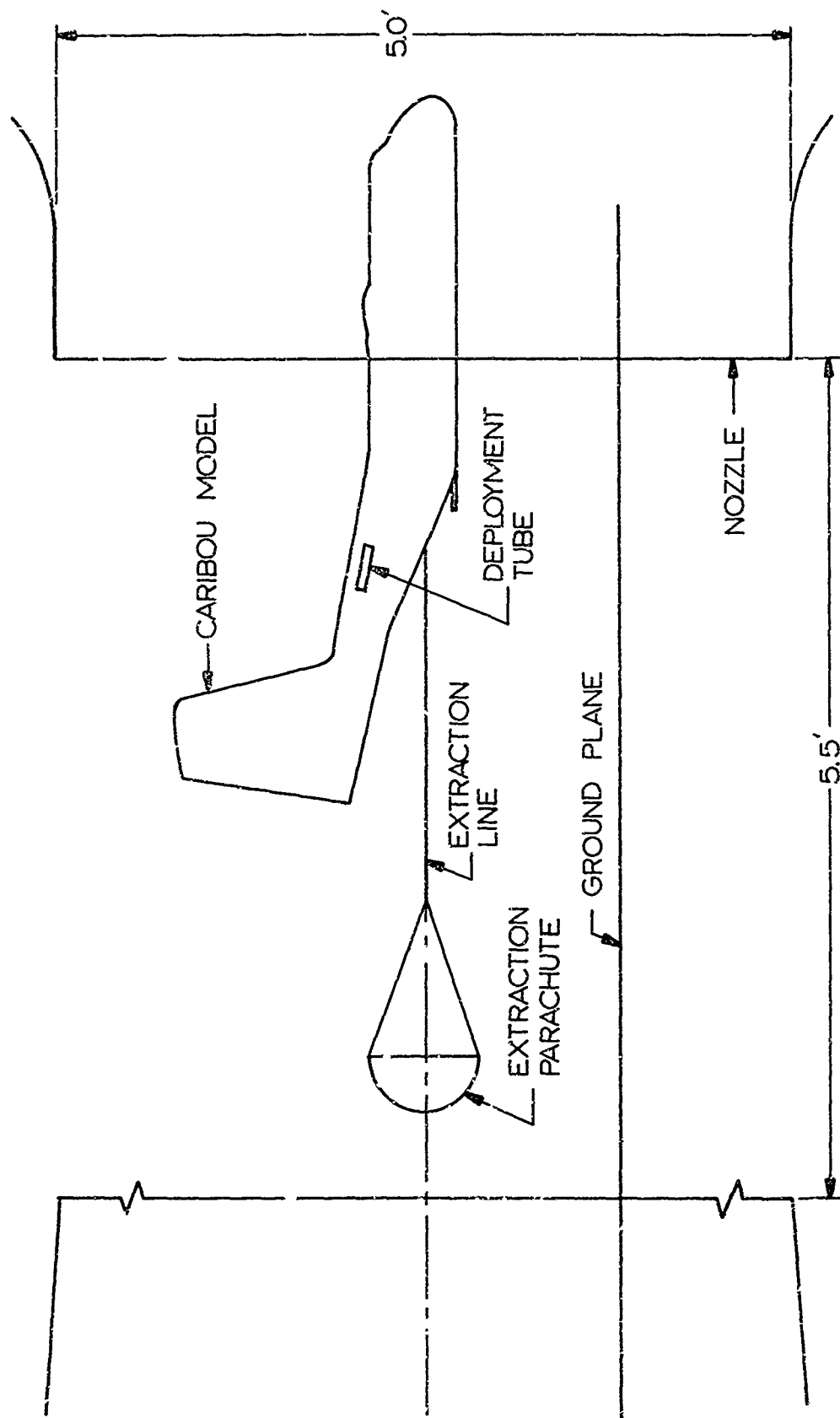Model

18

Fig 12. Ground Plane Installation

19

Fig 13. Aircraft-Ground Plane Installation

deviations of each group (Appendix I), and the steady state drag coefficient. Figures 14 to 17 are typical force traces illustrating the definition of filling time and the opening shock factor.

Filling time is defined as the time from snatch force occurrence to the first time the opening force reaches steady state drag after the opening shock.

The opening shock factor is the ratio of the maximum opening force to the steady state drag (Ref 1).

The steady state drag coefficient is

$$C_{D_O} = \frac{D}{nqS_O} \tag{1}$$

where

D = steady state drag of the particular deployment

n = the number of parachutes

q = dynamic pressure

S_O = the nominal area of one parachute

Histograms of the individual values of filling time and opening shock factor are given in Appendix II.

A.   Single Parachutes in Freestream

     1)   Solid Flat Parachutes

The steady state drag coefficients are shown in Table II and Fig 18. The drag coefficients determined in the closed test section were corrected for solid blockage using experimental values established for this wind tunnel. No blockage corrections were used for the data obtained in the open test section. The drag coefficients obtained in the open test section were somewhat higher than those of the closed test section. The drag coefficient of the solid flat parachute was essentially constant (C_{D_O} = 0.65) over the velocity range studied.

The filling time (Table II and Fig 19) decreases with velocity as expected, and amounts to 0.062 sec and 0.026 sec at velocities of 40 and 149 knots, respectively. An empirical curve ($t_f V$ = 2.65 knot-sec) determined by the method of least squares is indicated (Appendix I).

Opening shock factors (Table II and Fig 20) were determined as the ratio of opening shock force to steady

21
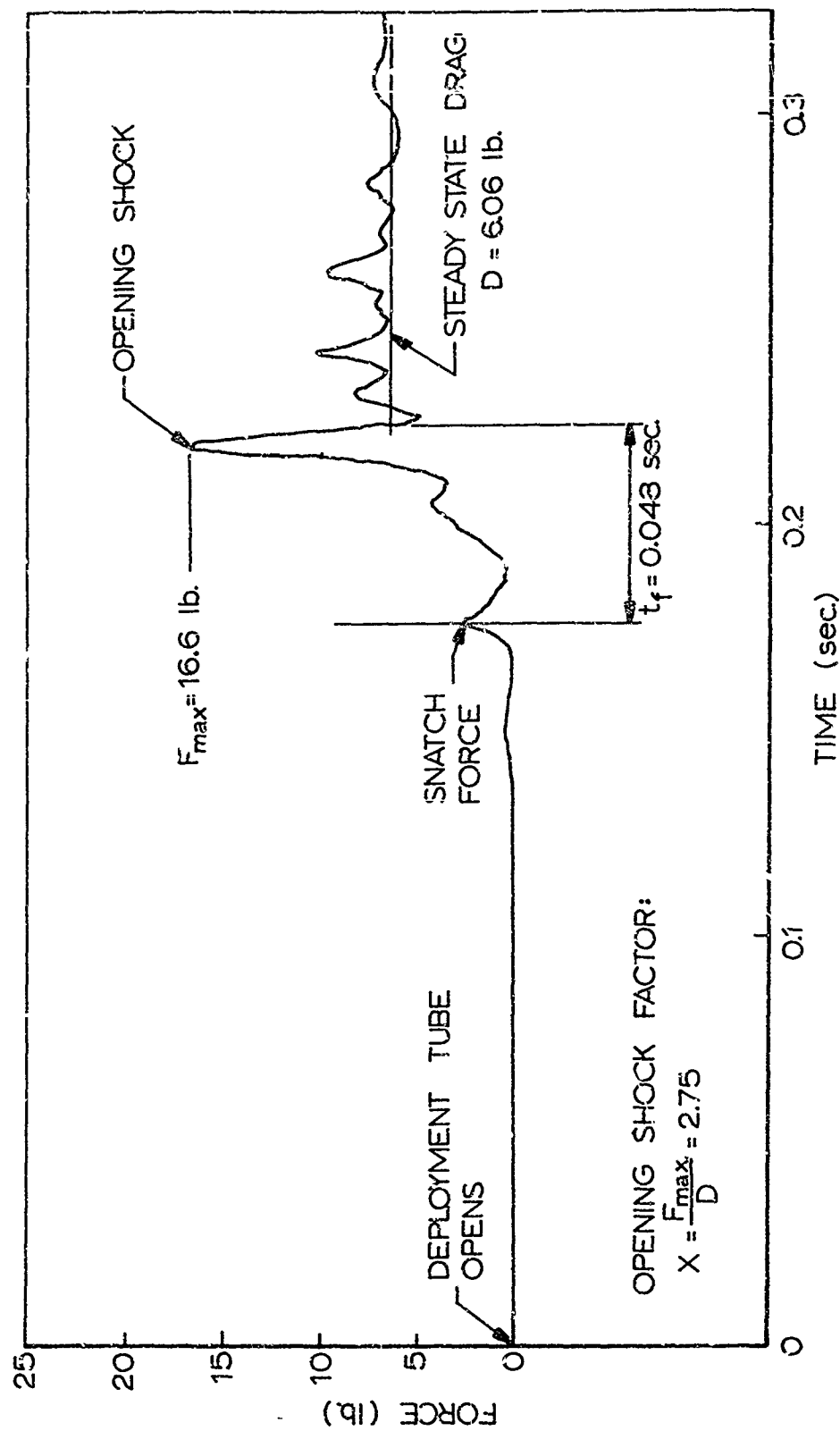
Fig 14. Typical Opening Force-Time History for a Single Solid Flat Parachute

22
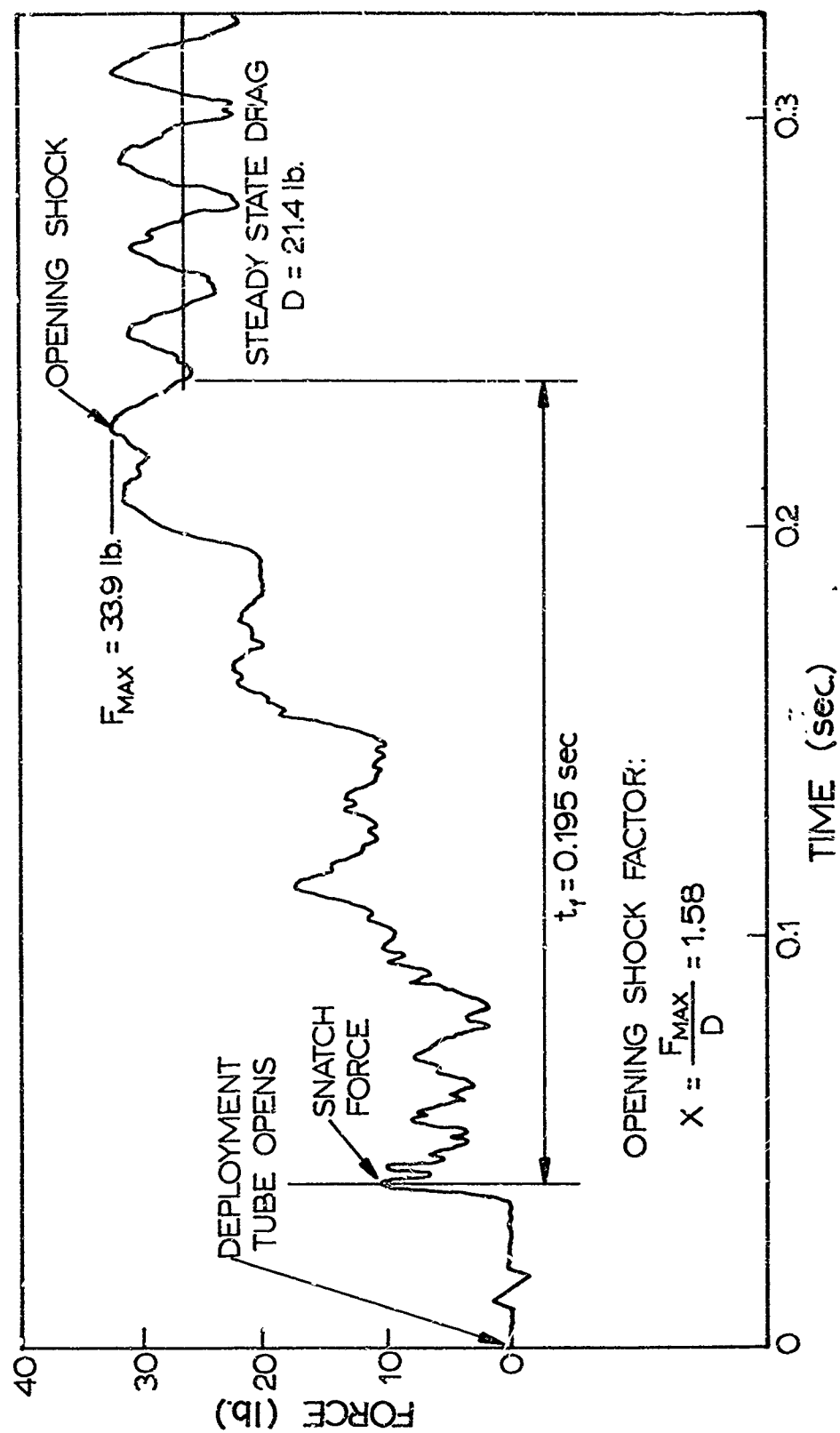
Fig 15. Typical Opening Force-Time History for a Cluster of 4 Solid Flat Parachutes
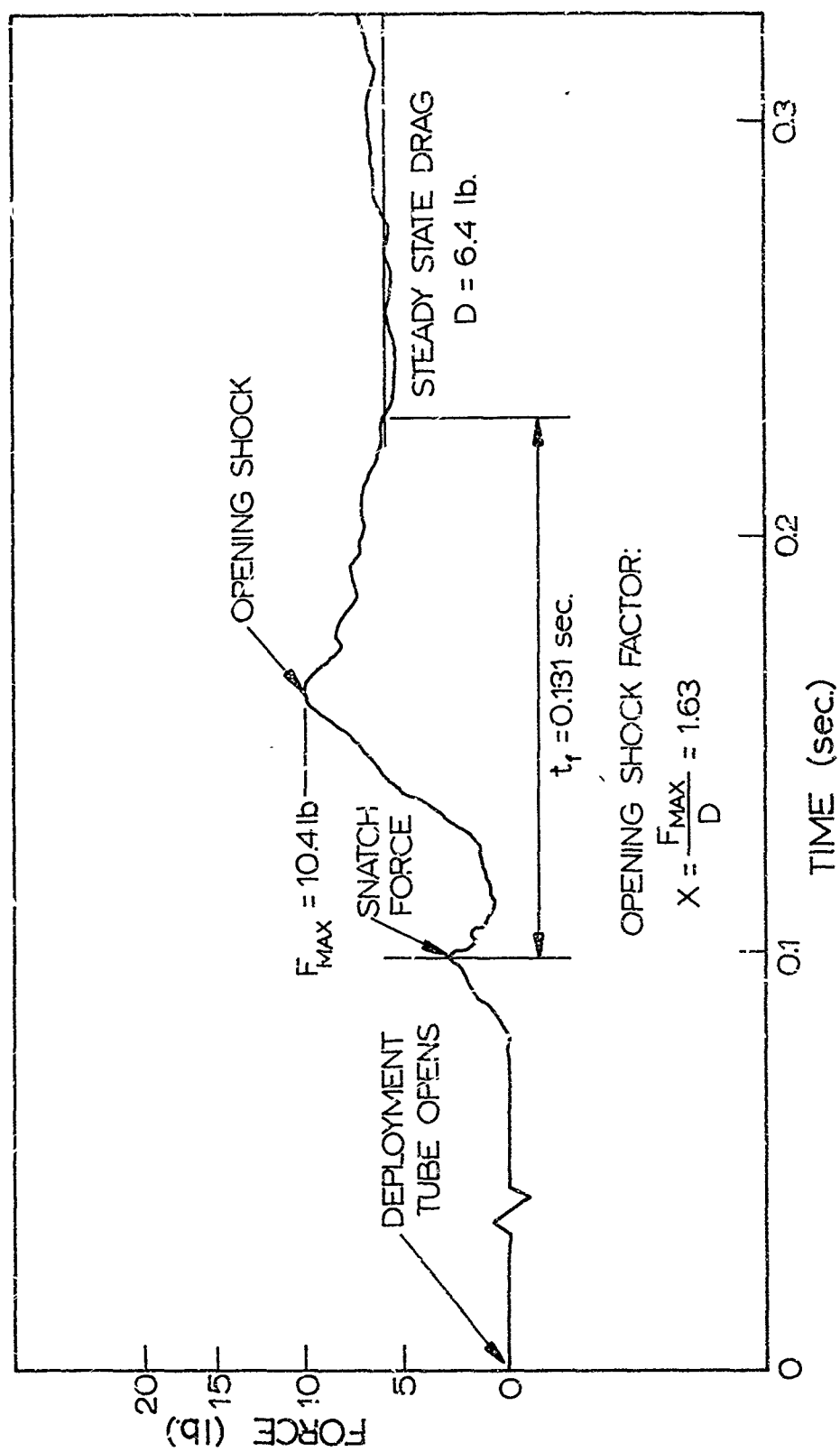
Fig 16. Typical Opening Force–Time History for a Single Ringslot Parachute

FORCE (lb)

TIME (sec.)

DEPLOYMENT TUBE OPENS

SNATCH FORCE

$F_{MAX} = 10.4$ lb

OPENING SHOCK

STEADY STATE DRAG
D = 6.4 lb.

$t_f = 0.131$ sec.

OPENING SHOCK FACTOR:
$X = \dfrac{F_{MAX}}{D} = 1.63$
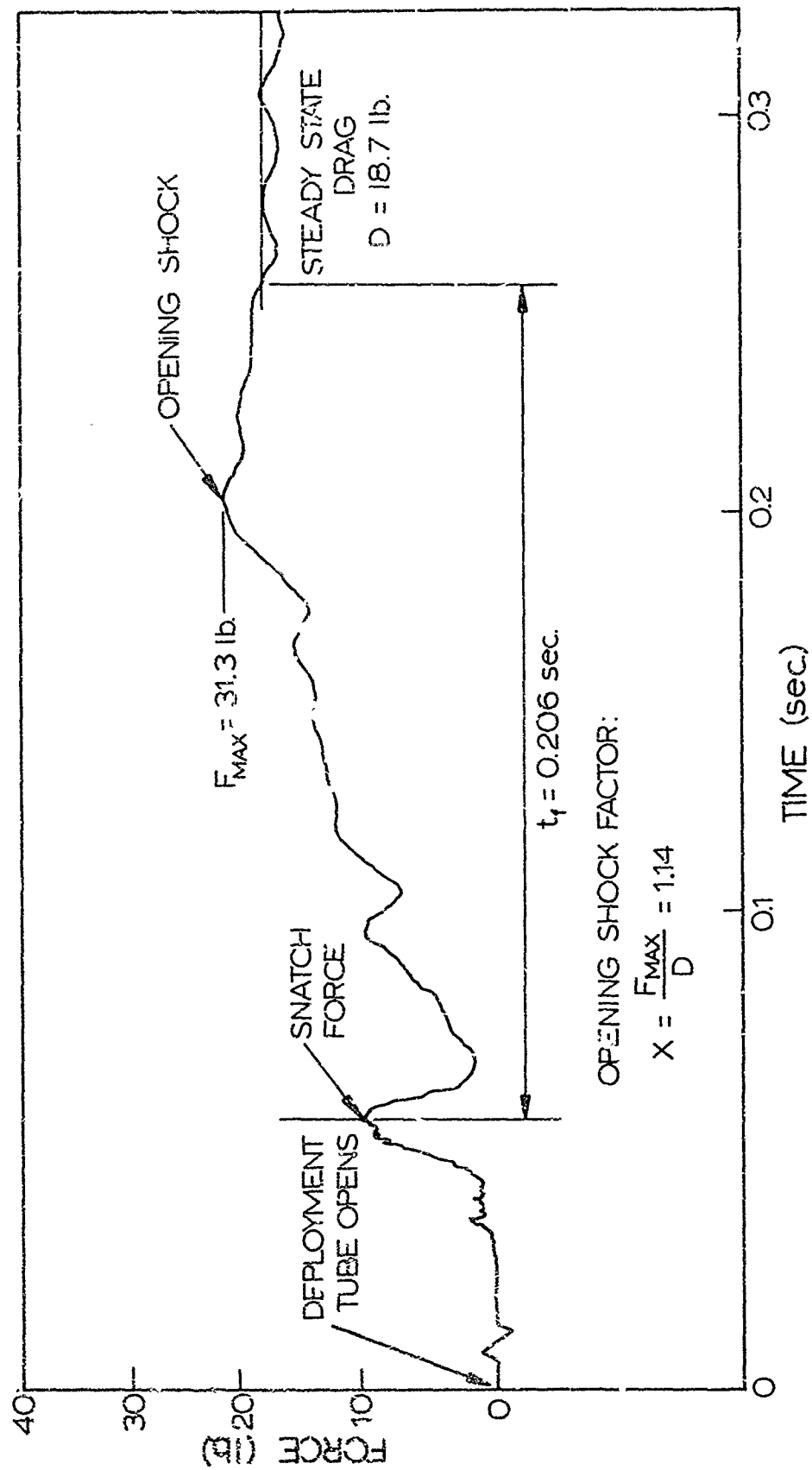
Fig 17. Typical Opening Force–Time History for a Cluster of 3 Ringslot Parachutes

25

TABLE II

OPENING SHOCK FACTORS, FILLING TIMES, AND DRAG COEFFICIENTS AT VELOCITIES FROM 40-150 KNOTS FOR A SINGLE SOLID FLAT PARACHUTE

V_∞ (knots)	$X \pm \sigma_X$	$t_f \pm \sigma_{t_f}$ (sec)	c_{D_O}
40	$2.70 \pm .44$	$.062 \pm .008$	.638
50	$2.69 \pm .48$	$.048 \pm .006$	.6..
82	$2.75 \pm .68$	$.038 \pm .008$	.579
121	$2.26 \pm .13$	$.027 \pm .005$	.622
149	$1.63 \pm .09$	$.024 \pm .004$	.665
43*	$2.79 \pm .19$	$.062 \pm .009$	.682
54*	$2.37 \pm .14$	$.047 \pm .006$	.711

* Open Test Section

Fig 18. Freestream Drag Coefficient versus Velocity for a Single Solid Flat Parachute

Fig 19. Freestream Filling Time versus Velocity for a Single Solid Flat Parachute
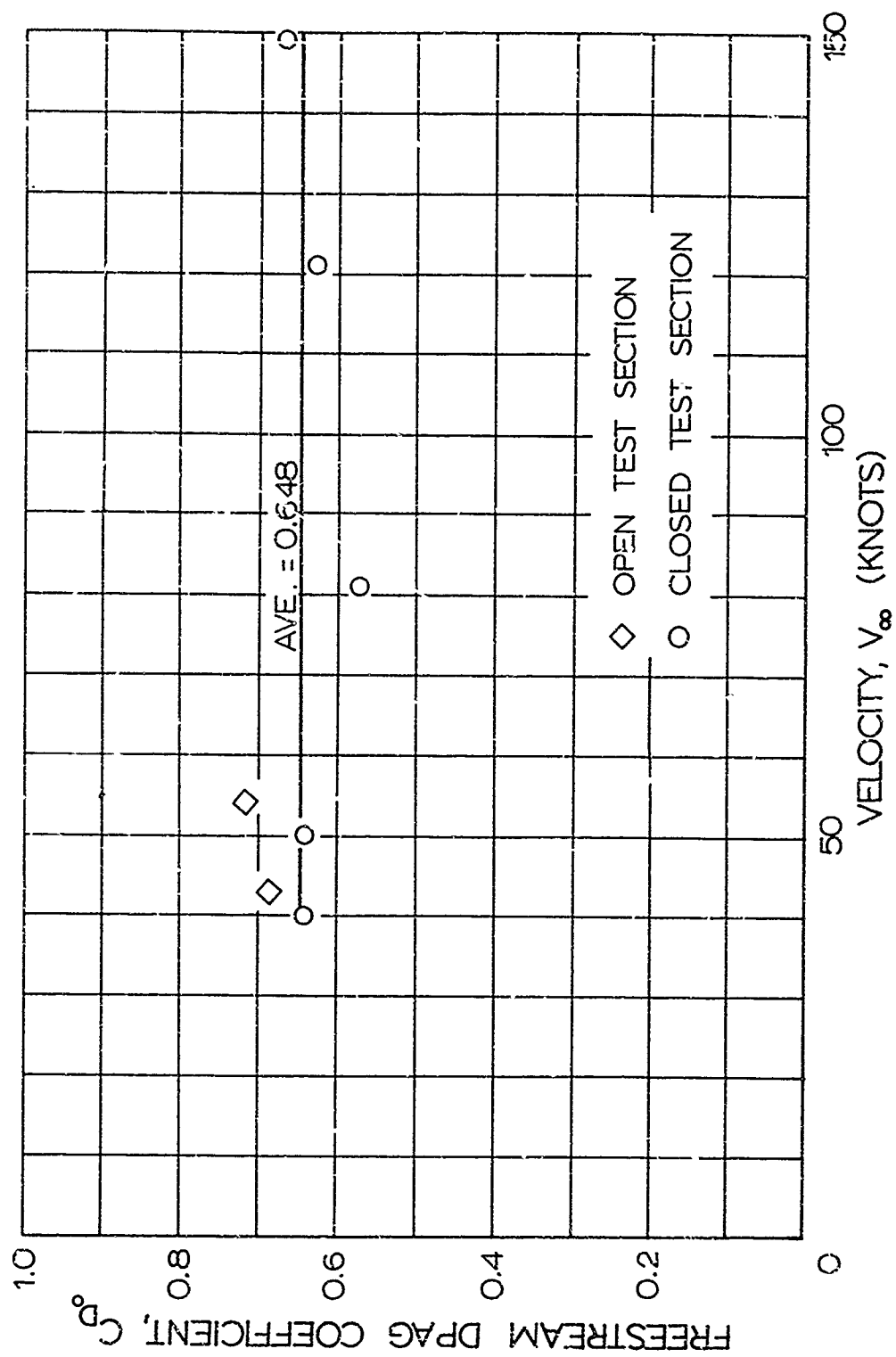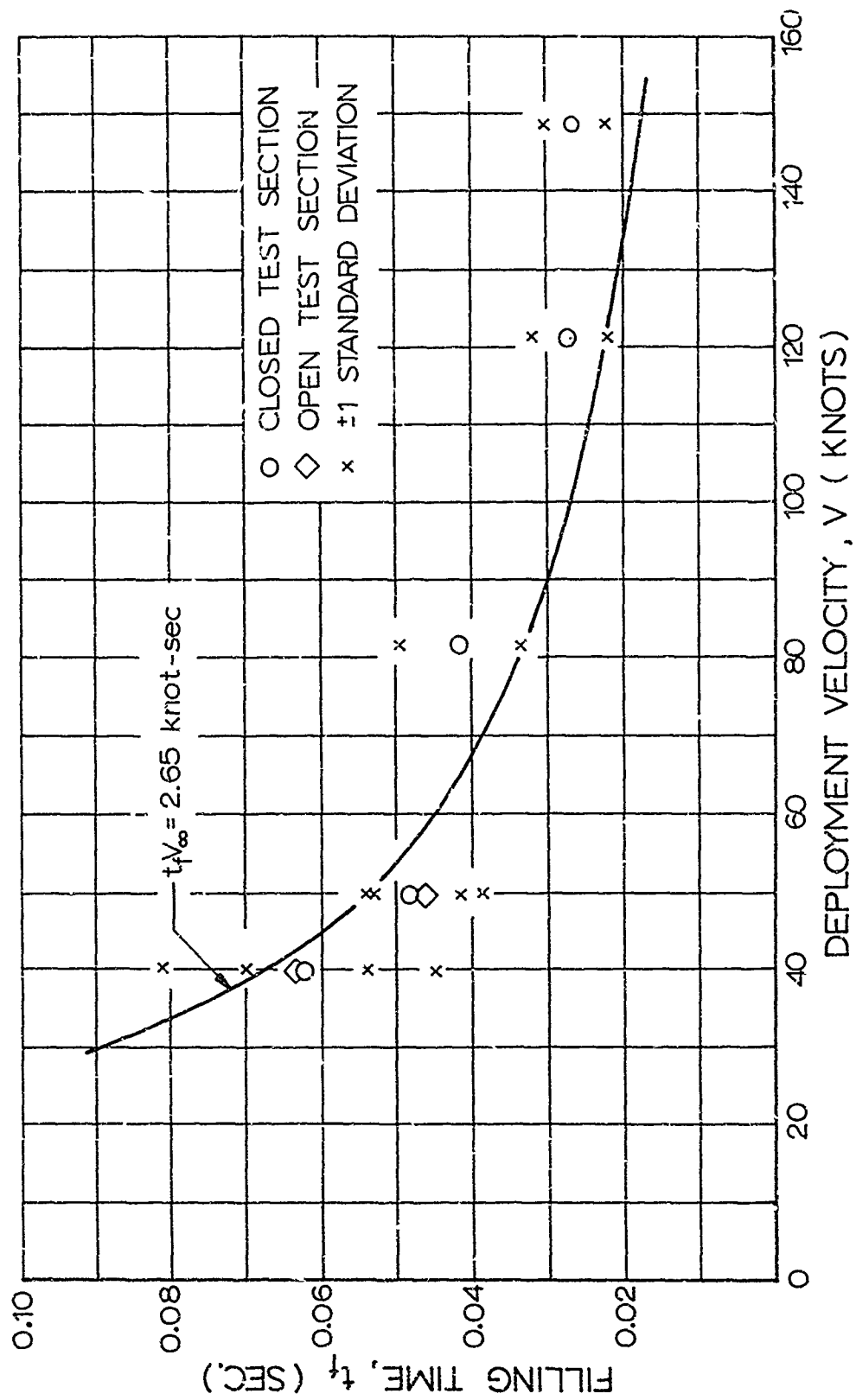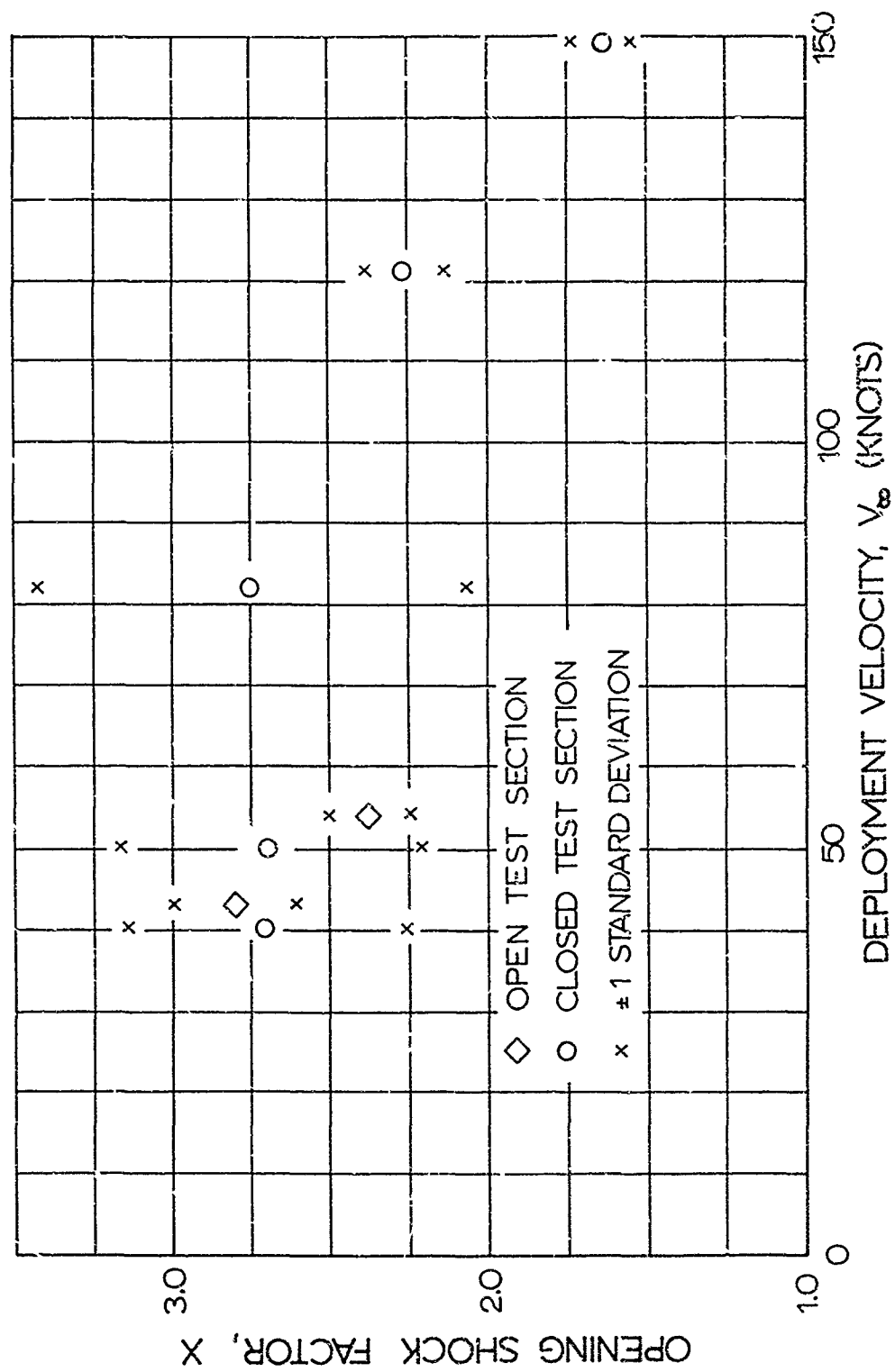
Fig 20. Freestream Opening Shock Factor versus Velocity
for a Single Solid Flat Parachute

state drag force. A decrease in opening shock factor at the higher velocities was noted. Reference 1 gives an average shock factor of $X \geq 2.5$ for small solid flat parachutes.

The following observations may be significant in considering the opening shock variations. The large variation in opening shock factor and the lower values at higher velocities may be caused by a velocity dependent oscillation of the solid flat parachute models. High-speed movies show that the projected diameter of the parachute varies by $\div 10\%$ of a mean projected diameter at 120 knots, and by nearly $\pm 20\%$ at 150 knots. The initial stages of opening appeared similar in both speed ranges because the most violent oscillations at the higher speed developed in a later phase of inflation. The ringslot models did not show this characteristic and as Fig 23 shows, their opening shock factor varies only slightly with speed. Therefore, the opening shock factor dependency observed in the solid flat parachute experiments may be a consequence of the structural instability of the solid flat parachute models.

2) Ringslot Parachute

The steady state drag coefficients are shown in Table III and Fig 21. Again, the closed section values are corrected for wind tunnel blockage effects. Good agreement was obtained between the drag coefficients determined in the two test sections; being essentially constant $(C_{D_O} = 0.52)$ over the velocity range studied.

The filling times (Table III and Fig 22) again decrease with velocity as expected, changing from 0.147 at $V_\infty = 40$ knots to 0.049 at $V_\infty = 150$ knots. An empirical curve of $t_f V_\infty = 6.14$ is drawn through the data.

Table III and Fig 23 show the opening shock factors of the single ringslot parachute. There is little dependence of opening shock factor on velocity, the average value is 1.67. This value is also somewhat higher than the value of $X \geq 1.50$ given in Ref 1 for small ringslot parachutes.

The X-factors of the single and the clustered parachutes, which will be given below, indicate that the measured values of the model opening characteristics differ somewhat from values for full scale parachutes (Ref 1). This does not necessarily imply that the measured values are incorrect, but rather that the canopy inertia and flexibility of the 16-in parachute models are not and could not be scaled from the full-size 22 ft parachute. Reference 1 also shows that differences in opening characteristics between small and large parachutes do exist by giving opening shock factors of small pilot parachutes that are considerably greater than

30

TABLE III

OPENING SHOCK FACTORS, FILLING TIMES, AND DRAG COEFFICIENTS AT VELOCITIES FROM 40-150 KNOTS FOR A SINGLE RINGSLOT PARACHUTE

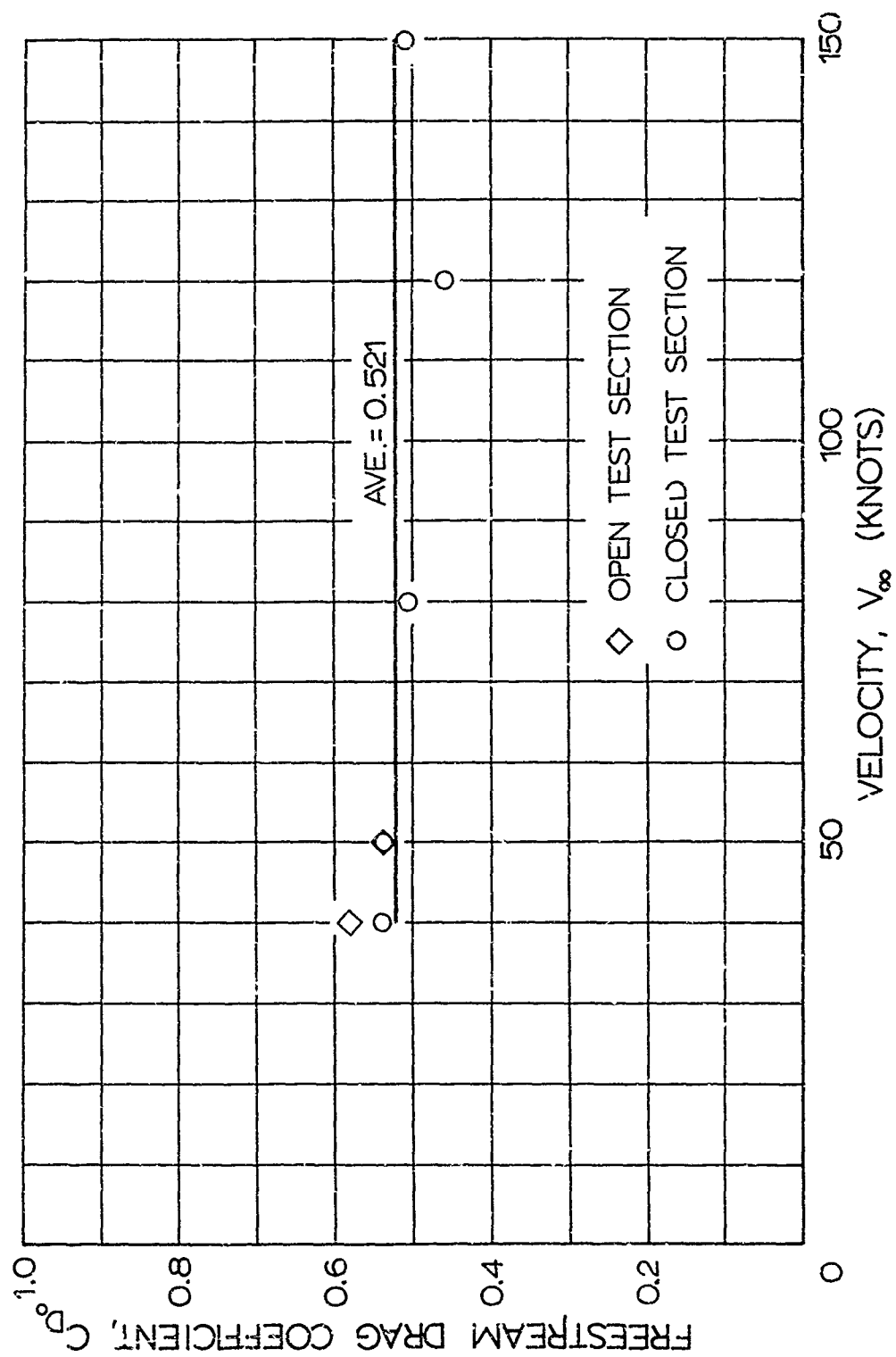| V_∞ (knots)	$\bar{x} \pm \sigma_x$	$t_f \pm \sigma_{t_f}$ (sec)	c_{D_O}
40	$1.85 \pm .18$	$.147 \pm .020$	.538
50	$1.89 \pm .15$	$.122 \pm .005$	.533
80	$1.65 \pm .10$	$.091 \pm .022$	.502
120	$1.72 \pm .09$	$.046 \pm .004$	.457
150	$1.41 \pm .10$	$.049 \pm .021$	.506
43*	$1.55 \pm .07$	$.151 \pm .058$	.580
54*	$1.62 \pm .11$	$.124 \pm .032$	.534

* Open Test Section

31

Fig 21. Freestream Drag Coefficient versus Velocity for a Single Ringslot Parachute
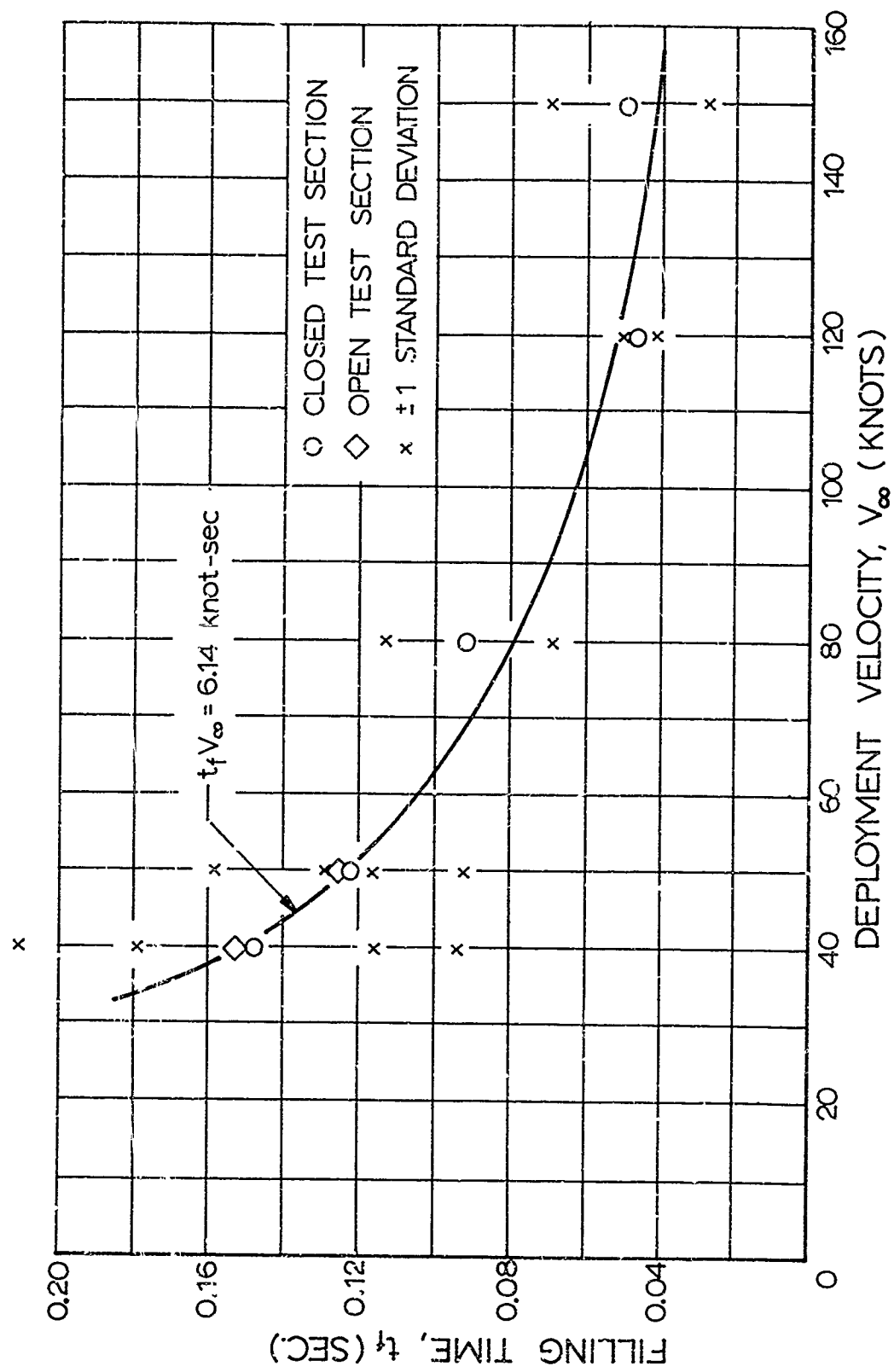
Fig 22. Freestream Filling Time versus Velocity for a Single Ringslot Parachute
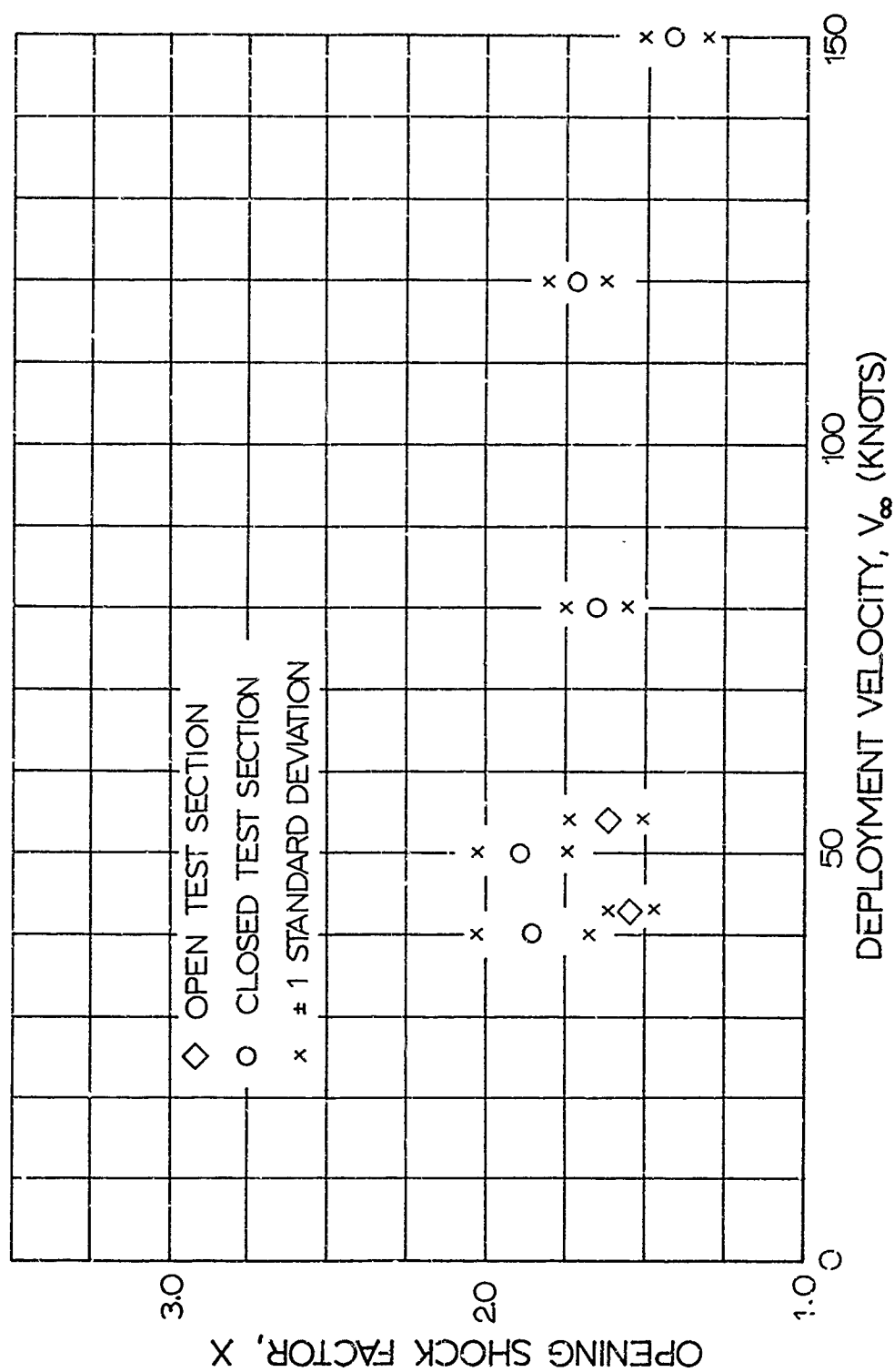
33

Fig 23. Freestream Opening Shock Factor versus Velocity
for a Single Ringslot Parachute

34

those of larger parachutes of the same type. By using
dimensionless ratios which are characteristic of a par-
ticular case, effects due to the size of the parachute will
be eliminated and laboratory experiments can be related to
full-scale conditions. In this manner, changes in the
opening characteristics of full-scale parachutes due to
changes in deployment configuration can be predicted from
model tests.

B.   Single and Clustered Parachutes with Wake and
           Ground Effects

The measured opening shock factors, filling times,
and drag coefficients for the various parachute and flow
configurations are given in Tables IV and V for the solid
flat and ringslot parachutes, respectively. In these tables
each configuration is identified with the following initials:

FS - Freestream Deployment

AW - Deployment in the Wake of the Caribou Model
     Aircraft

GE - Deployment near the Simulated Ground

AW/GE - Deployment in the Wake of the Aircraft
        Near the Ground

Because of the inertia and scaling differences,
the absolute values of these data should not be accepted
as typical for full-size parachutes. Rather, the effects of
clustering and flow conditions should be obtained from ratios
of the opening characteristics of a parachute deployed in a
particular configuration, to the corresponding characteristics
of a single parachute deployed in the freestream of the wind
tunnel. Finally, the freestream wind tunnel values should be
compared with the freestream full-size data.

In the following sections these ratios and the
limits of the standard deviations are presented. Furthermore,
the procedure to be followed in order to determine full scale
characteristics from the experimental ratios is illustrated.

1) Performance Ratios of Solid Flat Parachutes

The drag coefficient ratios for circular flat
parachutes deployed in the various configurations are shown
in Fig 24 a and b.

The subscript "∞" identifies freestream conditions
and the subscript "1" refers to values for a single para-
chute. Thus, Fig 24a shows the drag coefficient of a
cluster in freestream compared to the drag coefficient of
a single parachute in freestream. All values are taken
from wind tunnel measurements. Figure 24b compares the

35

TABLE IV

OPENING SHOCK FACTORS, FILLING TIMES, AND DRAG
COEFFICIENTS FOR SOLID FLAT PARACHUTES
V_∞ = 54 KNOTS

Configuration	n	$X \pm \sigma_x$	$t_f \pm \sigma_{t_f}$	c_{D_o}
FS	1	2.37 ± .14	.047 ± .006	.711
	2	1.53 ± .15	.099 ± .021	.634
	3	1.37 ± .10	.152 ± .008	.6147
	4	1.42 ± .17	.160 ± .039	.530
AW	1	1.93 ± .16	.057 ± .009	.669
	2	1.42 ± .10	.123 ± .028	.6147
	3	1.43 ± .10	.160 ± .023	.604
	4	1.60 ± .12	.215 ± .044	.522
GE	1	2.22 ± .14	.050 ± .006	.607
	2	1.59 ± .12	.110 ± .015	.629
AW/GE	1	2.16 ± .13	.057 ± .005	.606
	2	1.45 ± .12	.130 ± .030	.620

TABLE V

OPENING SHOCK FACTORS, FILLING TIMES, AND DRAG
COEFFICIENTS FOR RINGSLOT PARACHUTES
$V_\infty = 54$ KNOTS

Configuration	n	$X \pm \sigma_x$	$t_f \pm \sigma_{t_f}$	c_{D_o}
IS	1	$1.62 \pm .11$	$.124 \pm .032$	.534
	2	$1.26 \pm .08$	$.227 \pm .047$	.460
	3	$1.28 \pm .05$	$.249 \pm .034$	.423
	4	$1.21 \pm .06$	$.283 \pm .045$	.408
AW	1	$1.45 \pm .07$	$.124 \pm .035$	.513
	2	$1.35 \pm .09$	$.240 \pm .034$	.448
	3	$1.20 \pm .08$	$.227 \pm .035$	.416
	4	$1.16 \pm .06$	$.299 \pm .051$	.404
GE	1	$1.61 \pm .08$	$.149 \pm .034$	.514
	2	$1.35 \pm .14$	$.273 \pm .049$	.448
AW/GE	1	$1.63 \pm .06$	$.131 \pm .024$	.463
	2	$1.36 \pm .10$	$.196 \pm .030$	.426

37
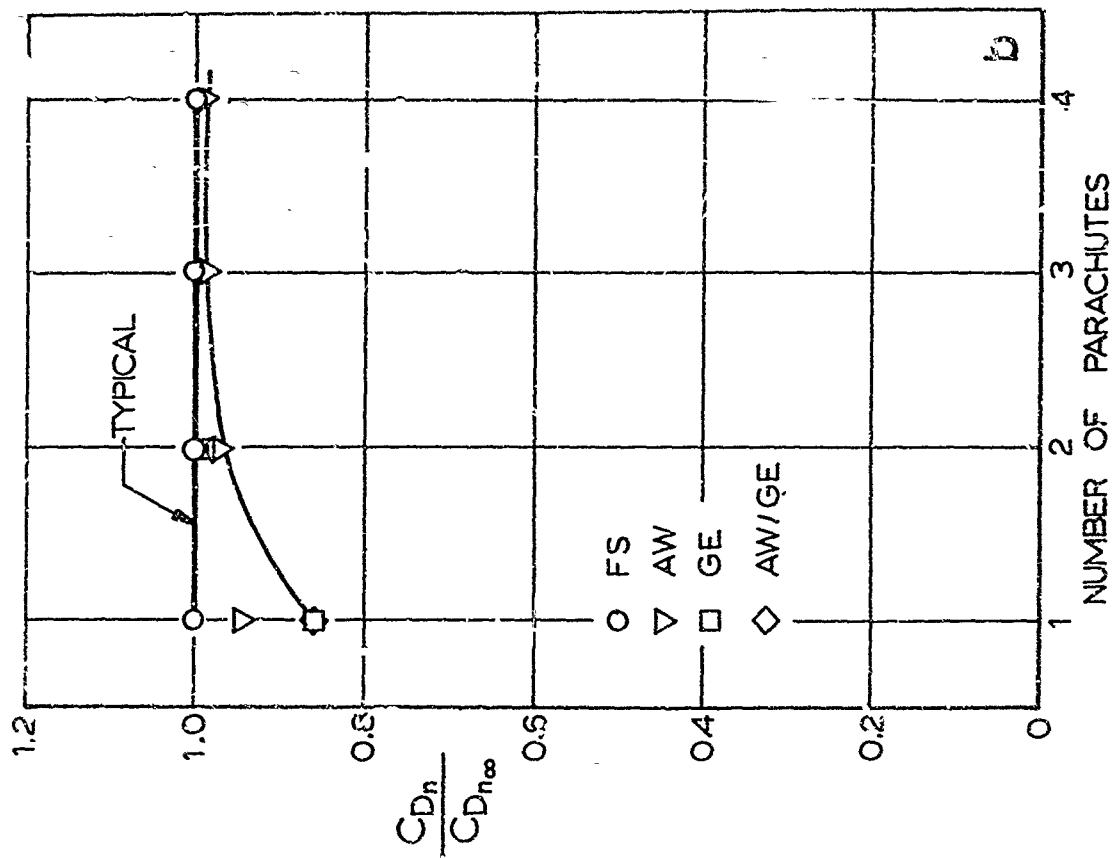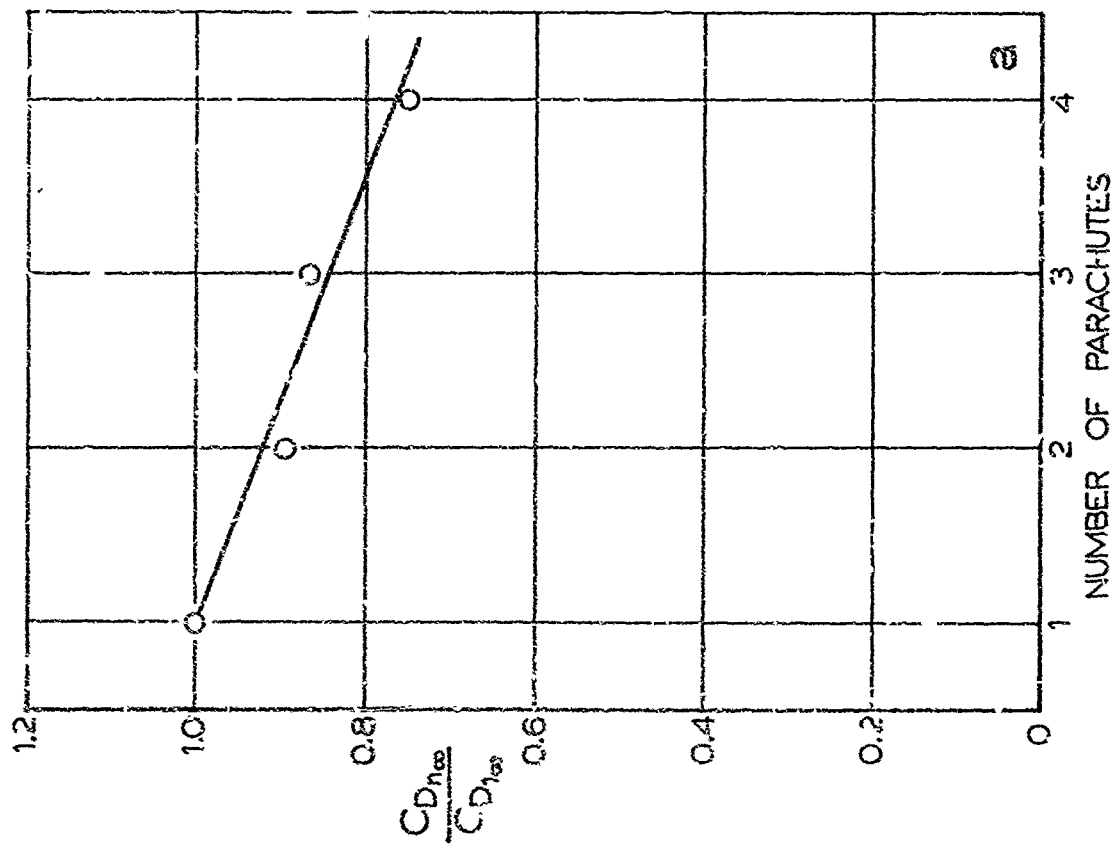
Fig 24. Drag Coefficient Ratios for Solid Flat Parachute Clusters

drag coefficient of a particular number of parachutes in the aircraft wake or with ground effect, to the drag coefficient of the same number of parachutes in freestream. Hence, the first plot gives the effect of clustering while the second gives the effect of changing flow condition. Average lines are drawn through the data in Fig 24 and in the following figures.

It can be seen that clustering the solid flat parachutes reduces the drag coefficient gradually to a ratio of about 0.75 for a cluster of 4 parachutes. The aircraft wake also reduces the drag coefficients of a single parachute from 5% with the aircraft wake alone to 15% with the combined effect of wake and ground. The drag of the clustered solid flat parachutes does not seem to be affected by the simulated ground.

Under similar deployment conditions, the opening shock and filling time ratios are shown in Figs 25 and 26, respectively.

The clusters of 2, 3, and 4 parachutes in freestream have nearly equal opening shock ratios, with an average ratio of 0.62. The aircraft wake and ground effect decrease the opening shock ratio of a single and cluster of 2 parachutes, but the influence of the aircraft wake decreases for clusters of 3 and 4 solid flat parachutes.

The filling time ratio of the solid flat parachutes increases linearly with the addition of parachutes up to a cluster of 3 parachutes; the filling time for a cluster of 4 solid flats is only slightly greater than that of a cluster of 3 parachutes.

The influence of the aircraft wake on the solid flat filling times is stronger than that of the ground. In the aircraft wake the filling time ratios are increased about 25%, while the ratios for the ground effect alone are nearly one.

2) Performance Ratios of Ringslot Parachutes

The drag coefficient ratios for single and clustered ringslots are shown in Fig 27 a and b. The drag efficiency of the ringslot cluster decreases to about 0.8 for clusters of 3 and 4 parachutes. Neither the aircraft wake nor the ground effect alter the ringslot drag coefficient appreciably. There is a decrease of about 10% caused by the combination of aircraft wake and ground effect.

Figures 28 and 29 present the opening shock and filling time ratios for the ringslot parachutes. In freestream, the opening shock ratio decreases to a nearly constant
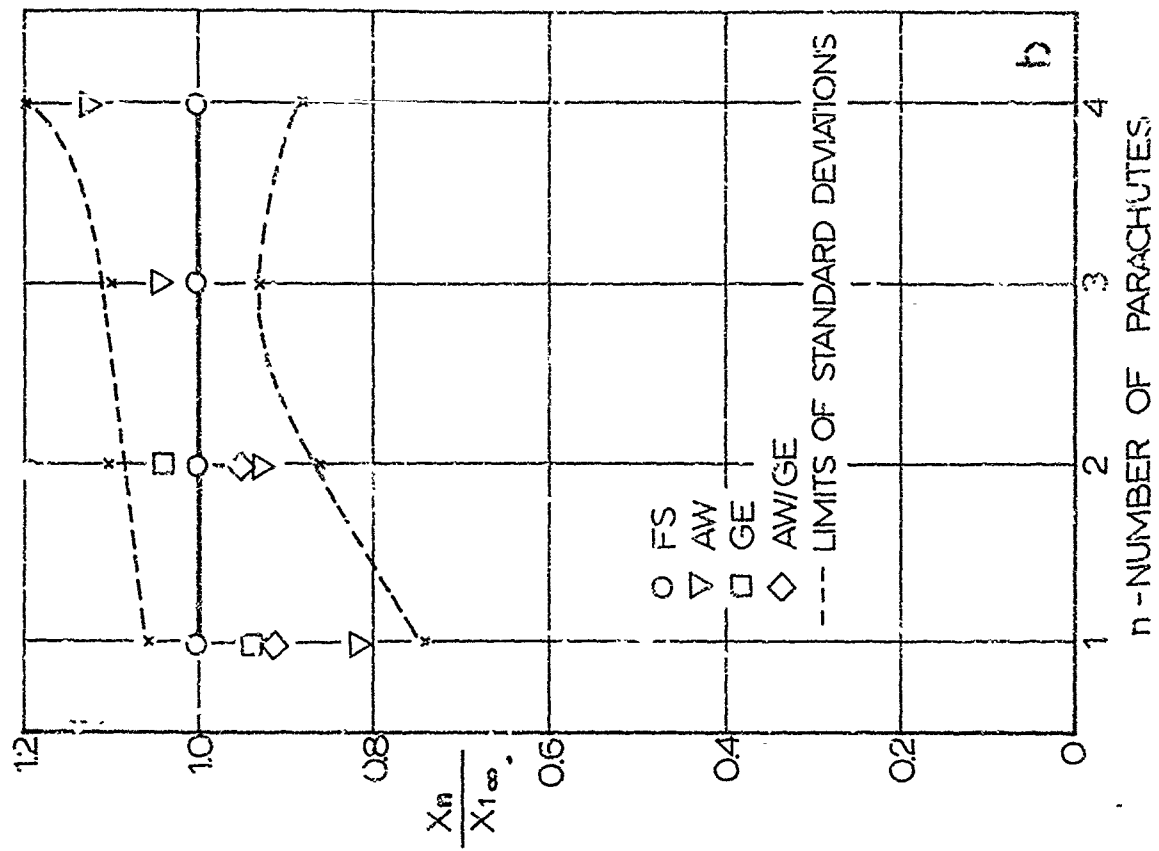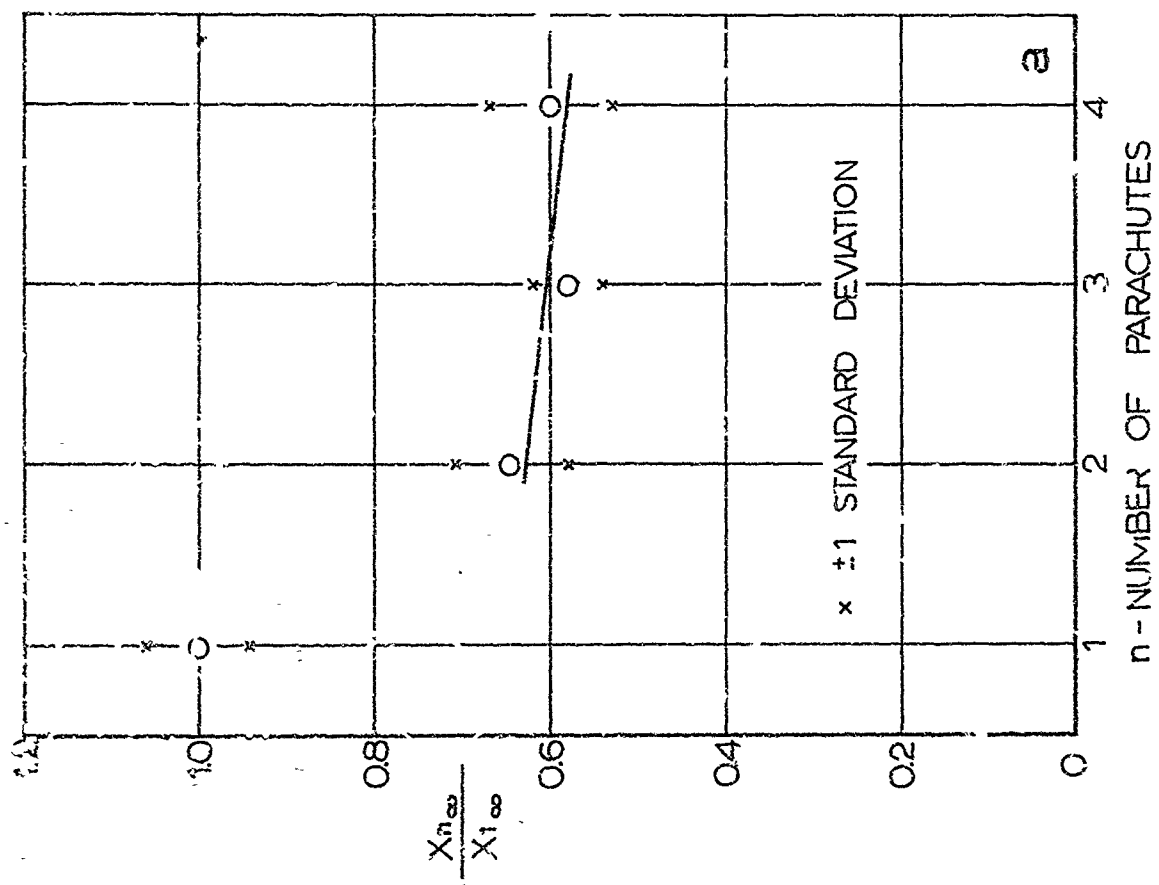
39

Fig 25. Opening Shock Ratios for Solid Flat Parachute
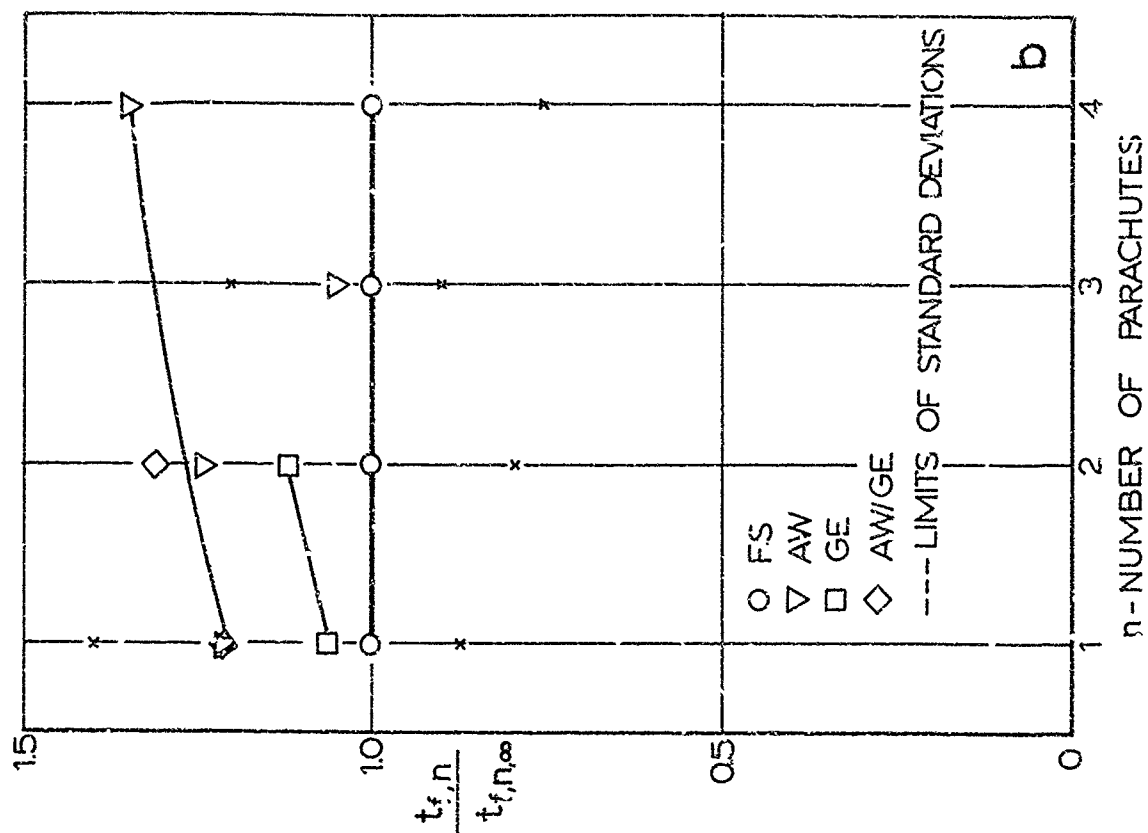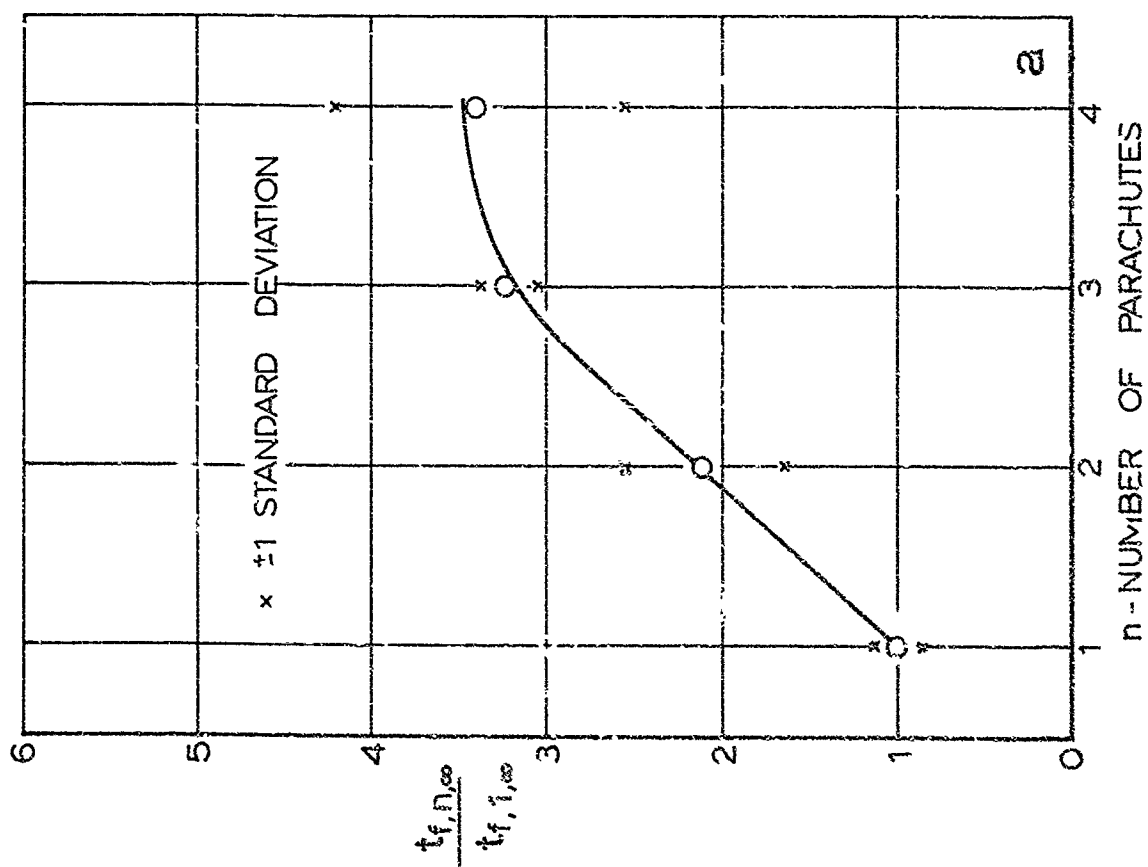Clusters

40

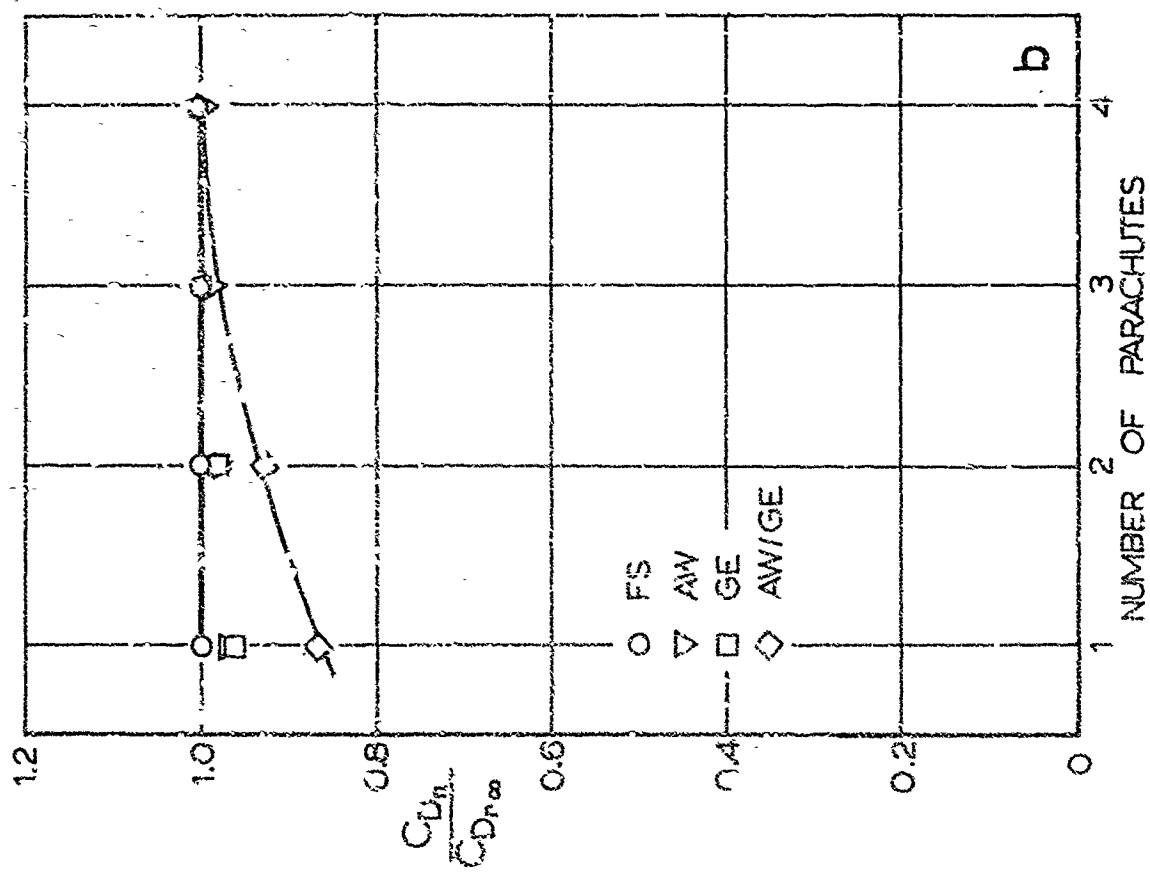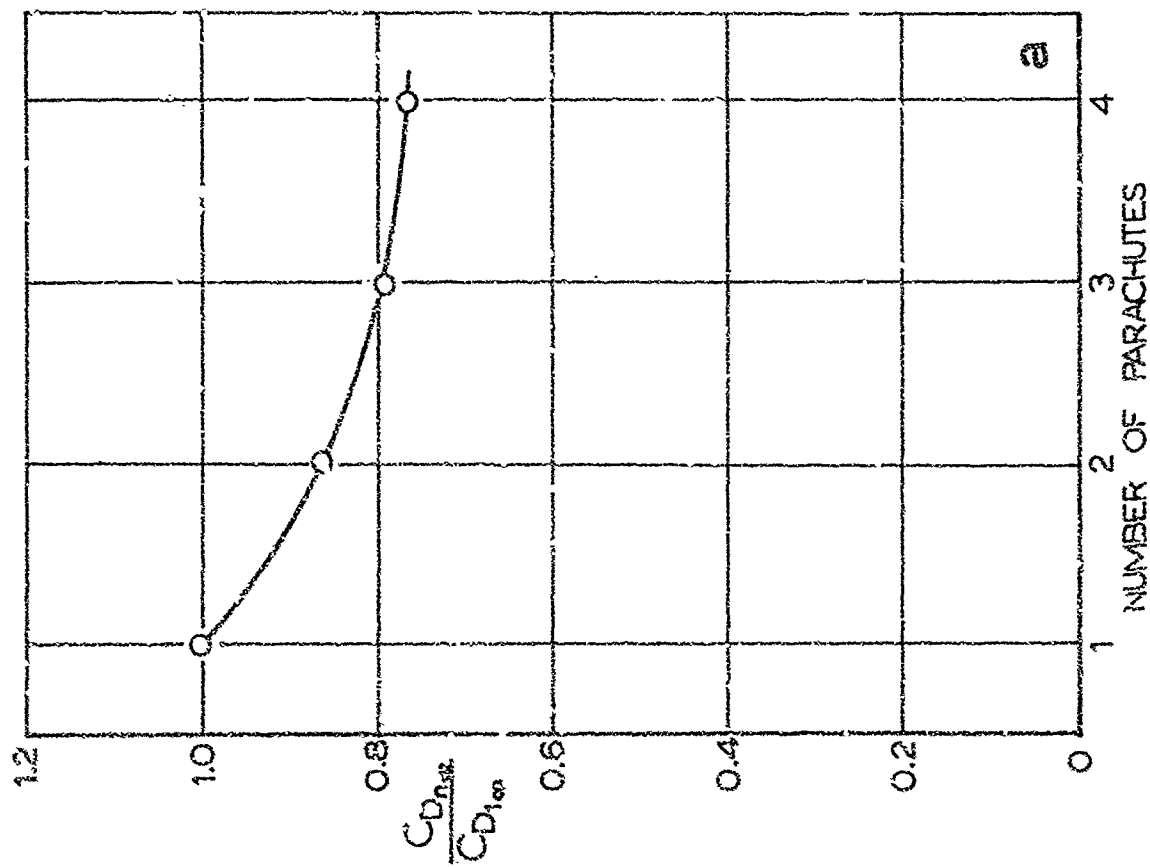Fig 26. Filling Time Ratios for Solid Flat Parachute Clusters

41

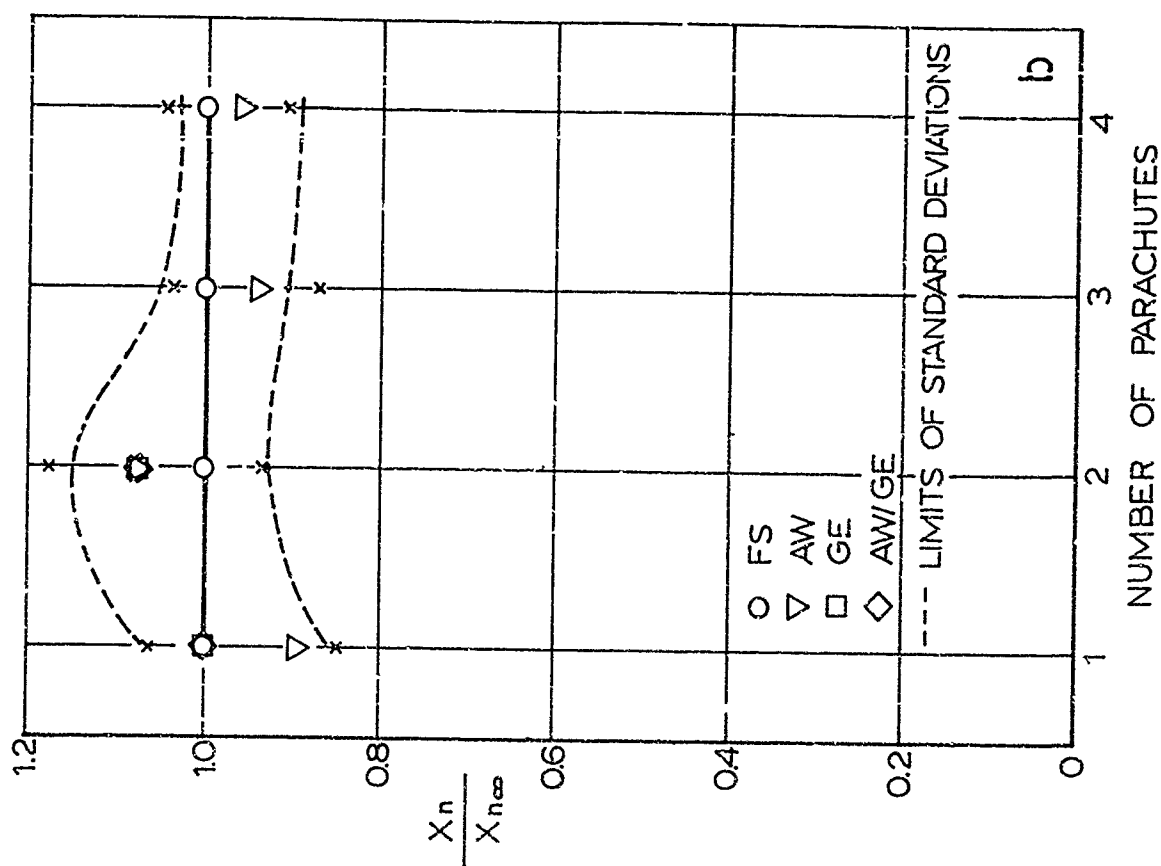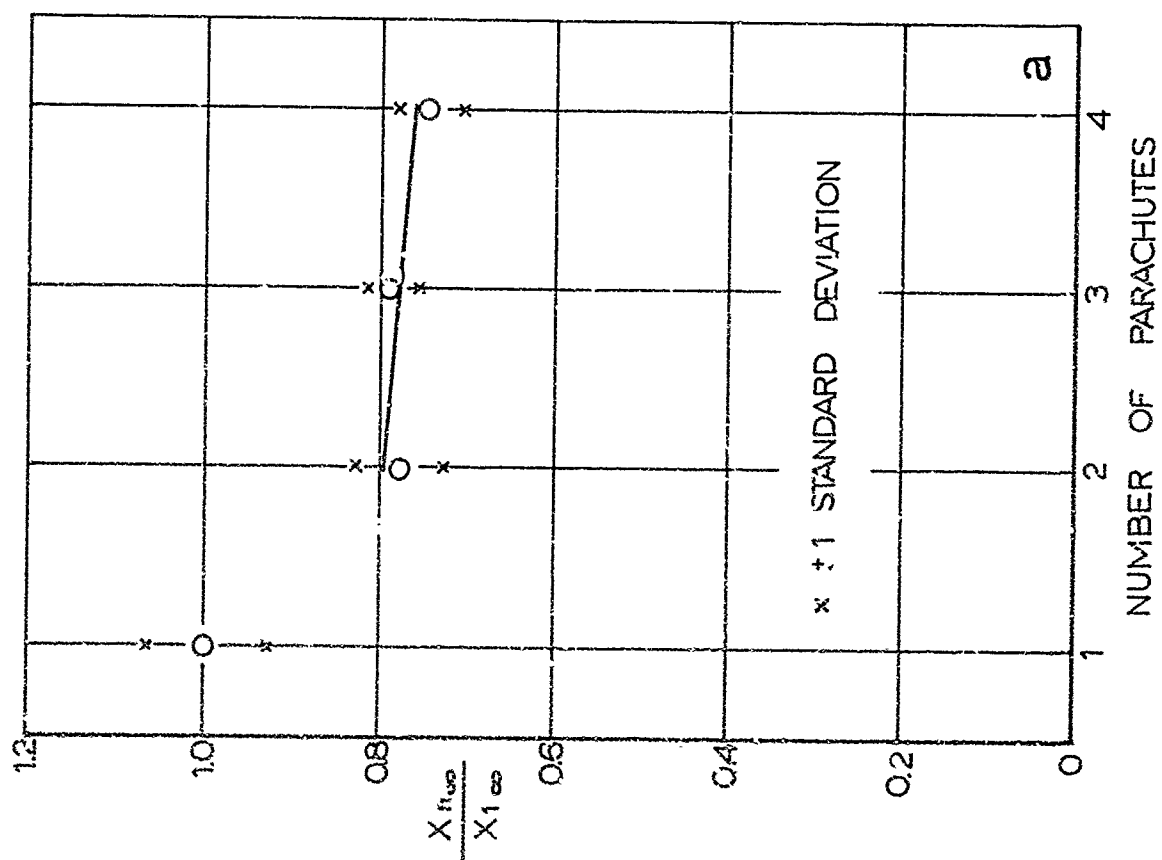Fig 27. Drag Coefficient Ratios for Ringslot Parachute Clusters

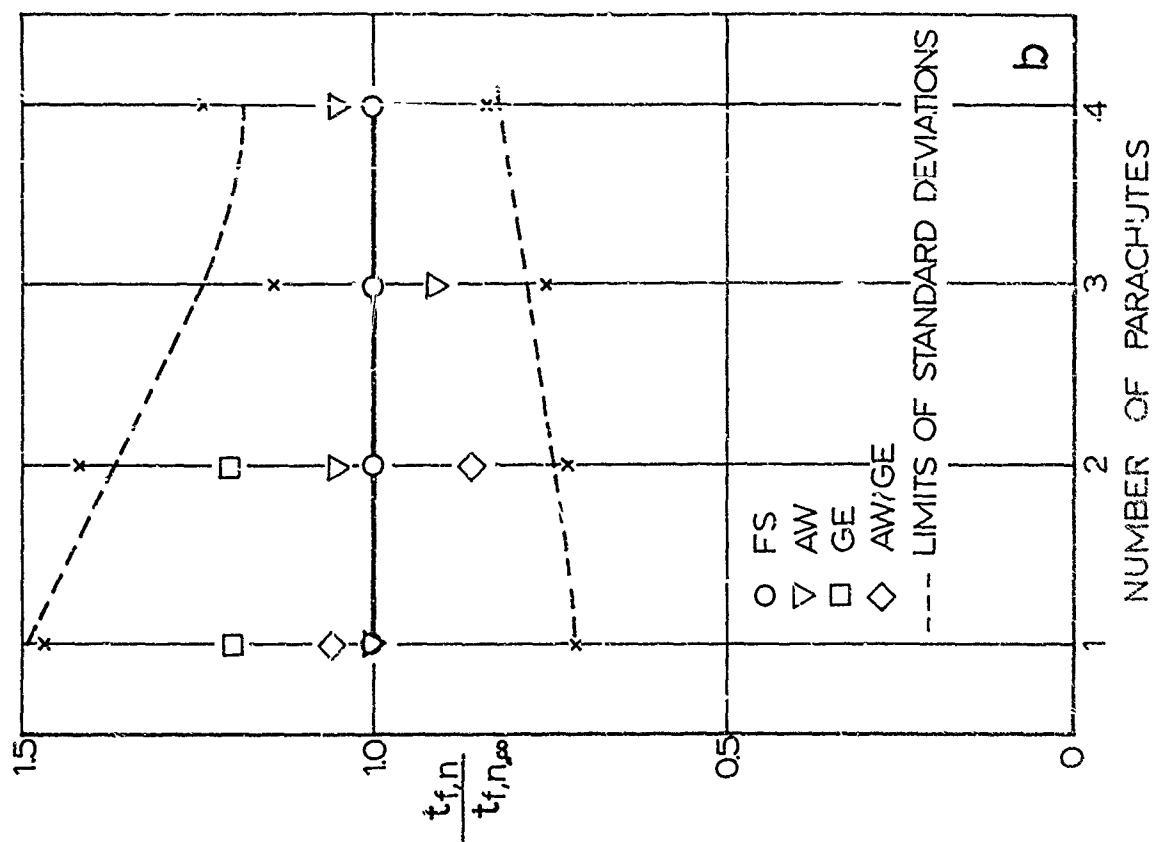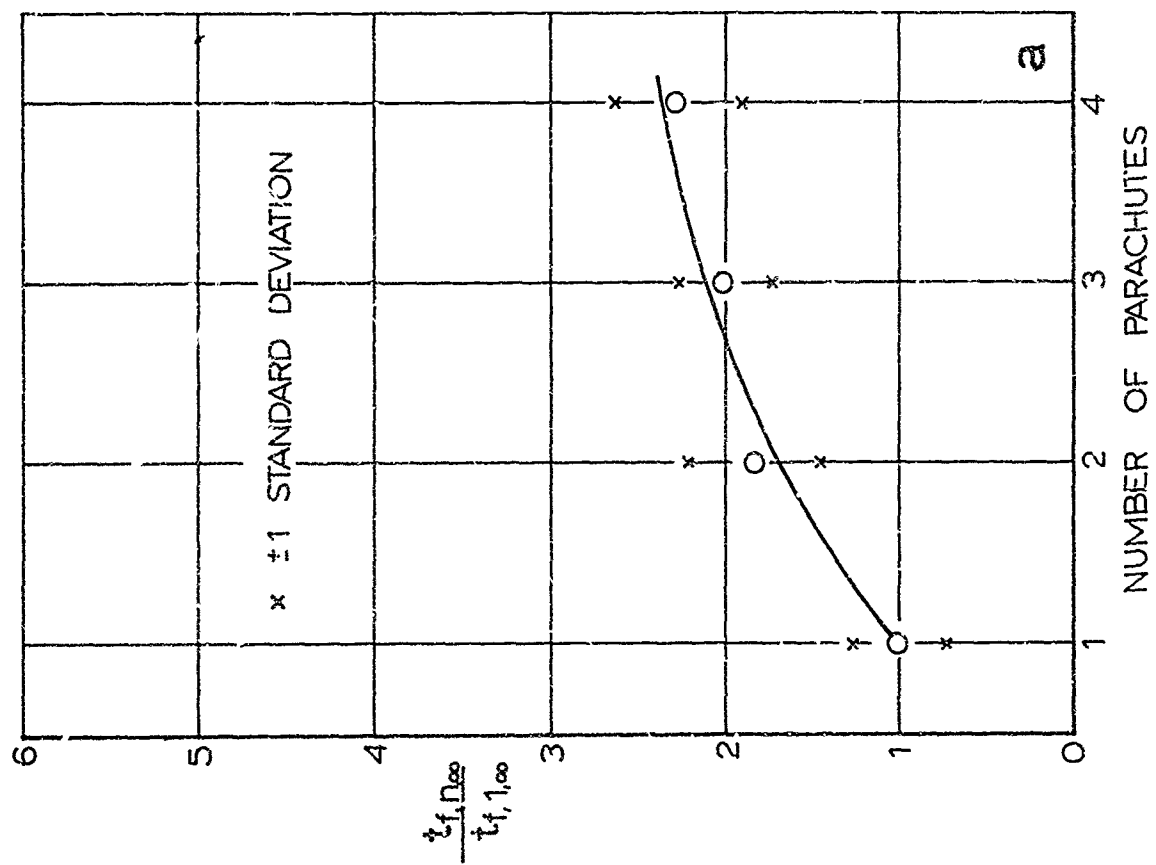Fig 28. Opening Shock Ratios for Ringslot Parachute
Clusters

43

Fig 29. Filling Time Ratios for Ringslot Parachute Clusters

value of 0.78 for any cluster and the filling time ratio increases to 2.3 for a cluster of 4.

The changes in opening shock and filling time caused by the aircraft wake or the ground effect are small. The following behavior, which was observed during the tests may have contributed to this result. Because the ringslot models were considerably heavier than the solid flats, they dropped a greater distance before opening. When they did open, they had fallen below the aircraft into a region of essentially freestream velocity. Hence, the average lines are shown at a ratio of 1.0 for both the opening shock and filling time ratios. This behavior may also exist to a certain extent in full-size experiments.

The presence of the ground effect does not appreciably alter the filling time ratios of the ringslot parachutes but gives very large standard deviations for these values. This may be caused by the ringslot models actually falling on the ground plane and sliding along it before they open. The average line is placed at a ratio of 1.0, but near the ground, the filling times will be random and the filling time ratio may vary between 0.8 and 1.2 or larger.

3) Illustrative Example

By means of the established values for any of the measured combinations,

$$\frac{X_n}{X_{n_\infty}} \, , \quad \frac{X_n}{X_{1_\infty}} \, , \quad X_{1_\infty} \, , \quad \text{and} \quad c_{D_n} \, ,$$

one can determine the maximum opening force of a model configuration as follows:

$$F_n \; = \; X_n \cdot c_{D_n} \cdot \frac{\rho}{2} \, V^2 \cdot S_n$$

or expanded,

$$F_n \; = \; \frac{X_n}{X_{n_\infty}} \; \cdot \; \frac{X_n}{X_{1_\infty}} \; \cdot X_{1_\infty} \cdot c_{D_n} \; \cdot qS_n$$

For full size configurations one may proceed similarly,

$$F_n' \; = \; \frac{X_n'}{X_{n_\infty}'} \; \cdot \; \frac{X_{n_\infty}'}{X_{1_\infty}'} \; \cdot \; X_{1_\infty}' \cdot c_{D_n}' \cdot \; qS_n'$$

45

For a first approximation one may assume that the effects of clustering and flow conditions on the small and large size parachutes are the same, also, that the drag coefficients of the model and full size configurations are identical. That is

$$\frac{X_n}{X_{n_\infty}} = \frac{X_n'}{X_{n_\infty}'} \quad , \qquad \frac{X_{n_\infty}}{X_{1_\infty}} = \frac{X_{n_\infty}'}{X_{1_\infty}'} \quad , \qquad C_{D_n} = C_{D_n}'$$

Through substitution, one obtains

$$F_n' = \frac{X_n}{X_{n_\infty}} \cdot \frac{X_{n_\infty}}{X_{1_\infty}} \cdot X_{1_\infty}' \cdot C_{D_n} \cdot q S_n'$$

This equation can be further expanded into

$$F_n' = \frac{X_n}{X_{n_\infty}} \cdot \frac{X_{n_\infty}}{X_{1_\infty}} \cdot \frac{X_{1_\infty}'}{X_{1_\infty}} \cdot X_{1_\infty} \cdot C_{D_n} \cdot q S_n'$$

All terms on the right-hand side of this equation have been determined experimentally in this study, with the exception of

$$\frac{X_{1_\infty}'}{X_{1_\infty}} \quad .$$

As a first approximation, this term can be obtained from combinations of values X_{1_∞}, given in this study, and values of

$$X_{1_\infty}'$$

from Ref 1. However, in order to make this study really applicable to full-size drop procedures, it is suggested that experiments be made, which would establish the relationship of

$$\frac{X_{1_\infty}'}{X_{1_\infty}}$$

over the speed range of interest.

The determination of the full scale drag coefficient and filling times would proceed in a similar manner.

Assuming the experimental ratios,

$$\frac{C_{D_n}}{C_{D_{n\infty}}}, \quad \frac{C_{D_{n\infty}}}{C_{D_{1\infty}}}, \quad \frac{t_{f_n}}{t_{f_n}}, \quad \frac{t_{f_{n\infty}}}{t_{f_{1\infty}}}$$

equal to the corresponding full scale ratios and obtaining

$$C'_{D_n} = \frac{C_{D_n}}{C_{D_{n\infty}}} \cdot \frac{C_{D_{n\infty}}}{C_{D_{1\infty}}} \cdot \frac{C'_{D_{1\infty}}}{C_{D_{1\infty}}} \cdot C_{D_{1\infty}}$$

$$t'_{f_n} = \frac{t_{f_n}}{t_{f_{n\infty}}} \cdot \frac{t_{f_{n\infty}}}{t_{f_{1\infty}}} \cdot \frac{t'_{f_{1\infty}}}{t_{f_{1\infty}}} \cdot t_{f_{1\infty}}$$

C.   Review

In general, the results of this study show certain
tendencies which agree with physical reasoning. However,
the large standard deviations and certain data points show
phenomena that cannot be explained at present. It is possible
that the opening of clustered parachutes in different con-
figurations is far more sensitive to environmental conditions
than originally expected. Therefore, the experiments may
not have encompassed and considered all parameters involved
and the presented values should be considered as boundaries
of performance characteristics.

Furthermore, a few experiments should be made to
prove or disprove the assumptions that the performance
ratios are identical as shown below:

$$\frac{X'_n}{X'_{n\infty}} = \frac{X_n}{X_{n\infty}} \qquad\qquad \frac{X'_{n\infty}}{X'_{1\infty}} = \frac{X_{n\infty}}{X_{1\infty}} \, .$$

With these proofs established, the presented laboratory study
would be applicable to a wide range of configurations.

47

2. WAKE SURVEYS

I. INTRODUCTION

The differences between the opening character-
istics of a parachute deployed in freestream and behind an
aircraft are caused by the velocity defects and directional
changes in the wake of the aircraft. Since the parachute
opening characteristics had been established in the wake of
the DHC-4 aircraft, the parachute characteristics in the wake
of another aircraft, specifically the C-130, can be roughly
predicted if wake pressure surveys are available for both
aircraft.

Scale models of both aircraft were made and the
distribution of total and static pressures was established
at several positions behind the aircraft.

II. MODELS

The DeHavilland Caribou and C-130 aircraft models
used in the wake studies had windmilling propellers and
open cargo doors. The sixe of the models was adjusted to
the dimensions of the available wind tunnel. This reduced
the Caribou and the C-130 to scales of 1/48 and 1/140,
respectively. The Caribou model was made at the University
of Minnesota (Fig 30) whereas a commercially available
model ofthe C-130 was modified for use in the tests (Fig 31).
The surface of the C-130 model was sanded smooth, the pro-
pellers replaced, and the propeller hubs modified to allow
windmilling.

III. EXPERIMENTS

The tests were conducted in the closed section
of the University of Minnesota subsonic wind tunnel.

The test velocity was 140 fps with a Reynolds
number of $Re = 1.65 \times 10^6$, for the Caribou and 100 fps for
the C-130 with $Re = 5.9 \times 10^6$. At these velocities the
turbulence factor of the wind tunnel is 1.40.

48
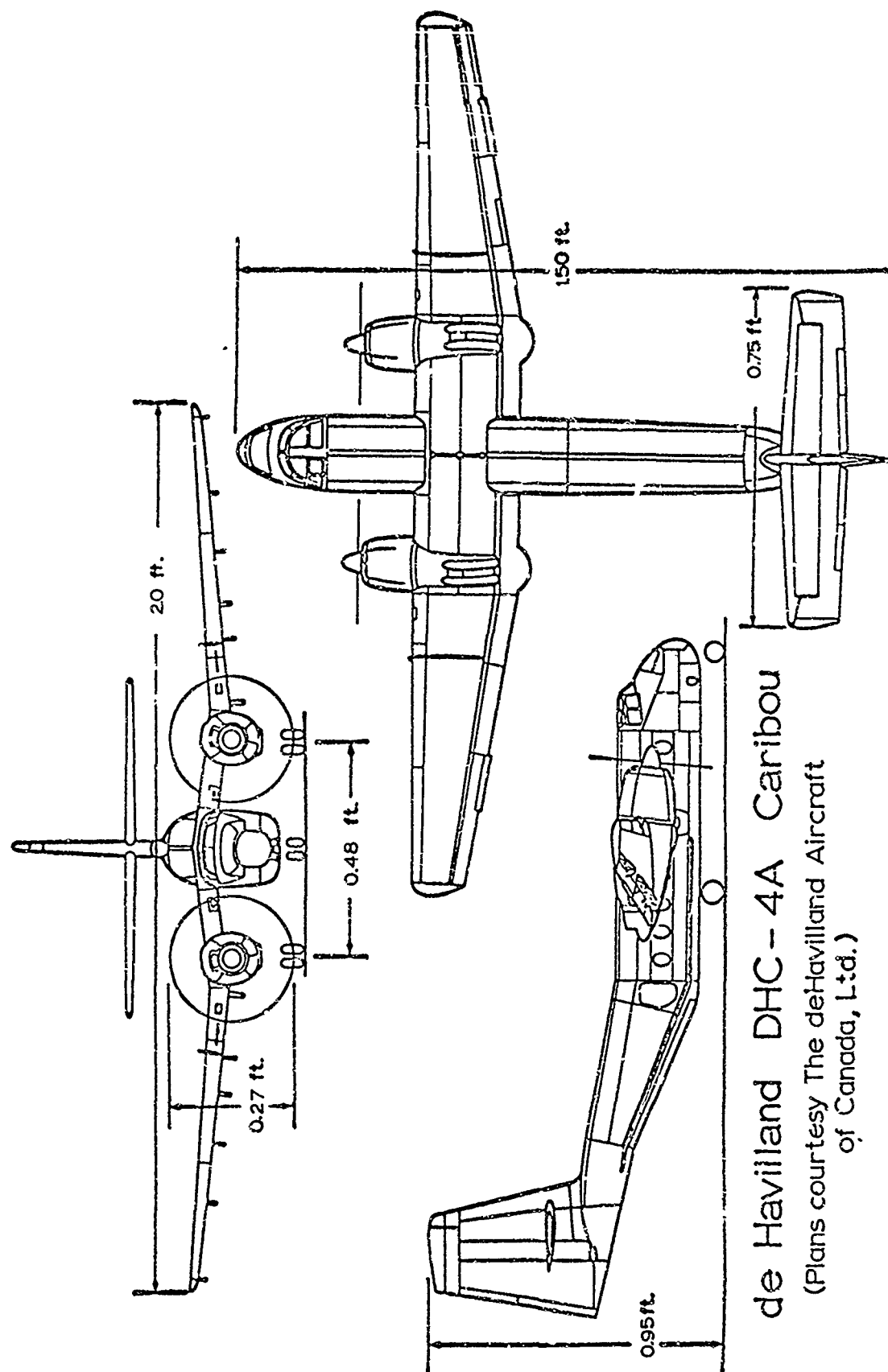
de Havilland DHC-4A Caribou
(Plans courtesy The deHavilland Aircraft
of Canada, Ltd.)

Fig 30.   Three View of Caribou Model Aircraft Used for
Wake Surveys

49
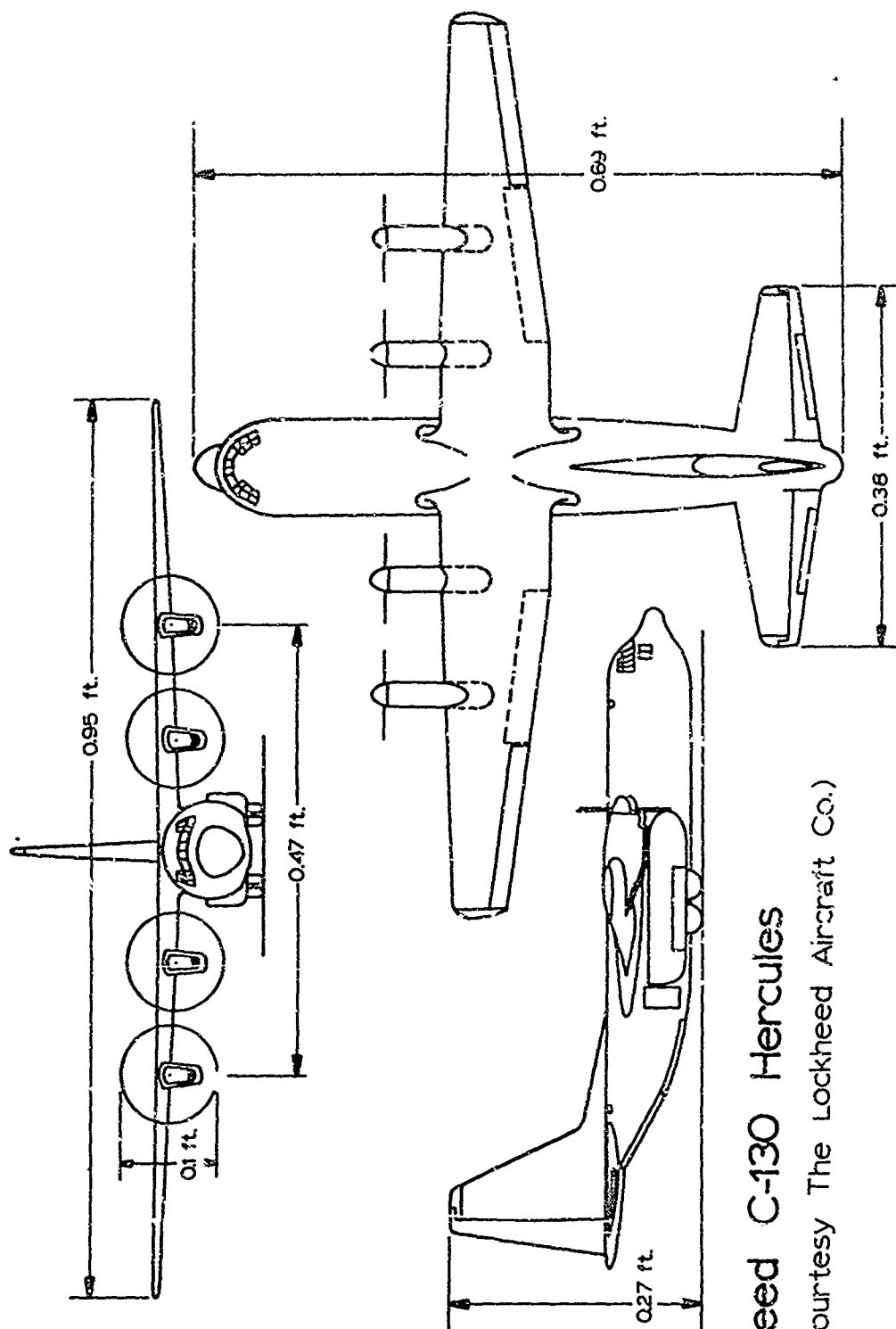
Lockheed C-130 Hercules

(Plans courtesy The Lockheed Aircraft Co.)

Fig 31. Three View of C-130 Model Aircraft Used for Wake Surveys

Figure 32 shows the models supported in the wind tunnel by a thin vertical sting. The model wing tips were wired to the floor and ceiling to provide limited adjustment and rigidity.

The total-static pressure rake is shown installed and schematically in Figs 32 and 33.

Pressure data was obtained at several stations behind each aircraft model (Fig 34). These stations represent the plane of the tailcone, and intermediate station, and the plane of the canopy skirt when fully inflated with a 60 ft extraction line attached at the aircraft center of gravity. At each of these stations, the pressure was measured in three vertical rake positions, which represent the plane of the cargo door top, and one projected diameter of a 22 foot extraction parachute above and below this first position.

IV. RESULTS

The measured total and static pressures were converted to local velocities, and ratioed to the free-stream velocity. Lines of constant velocity ratios were then superimposed on the aircraft profiles as shown in Figs 35 — 40.

The general observations indicate that the area directly downstream of the fuselage and propeller disk have the most notable velocity defect. Furthermore, there is a significant recovery at the position of the parachute skirt. The approximate projected diameter of a fully inflated 22 ft extraction parachute is shown to illustrate the wake region where the canopy operates.

Figures 35 to 40 show that the wake of the larger 4 engine C-130 has a stronger velocity defect and influences a greater region behind the aircraft than the Caribou. In the Caribou wake the parachute is in a region where the velocity ratio is 0.95 to 0.90, while in the wake of a C-130 the parachute stands in a field with a velocity defect of 10 to 15 per cent. It is safe to assume that the characteristic drag reductions behind the C-130 are larger than behind the Caribou, perhaps in the order of the pressure ratio defects.

As pointed out earlier, these surveys were performed with windmilling propellers, and the velocity defect

51
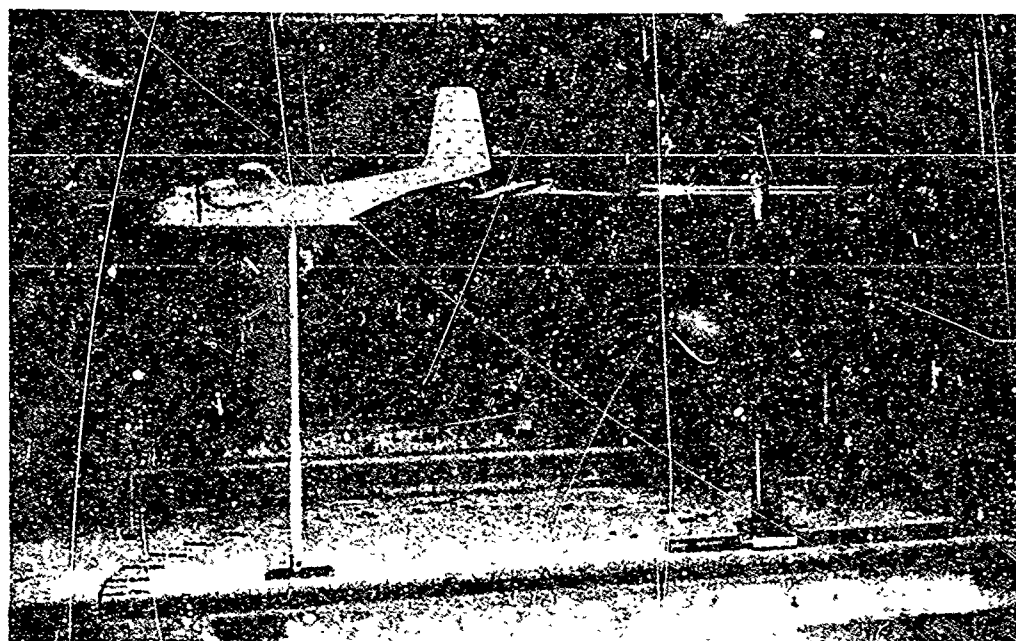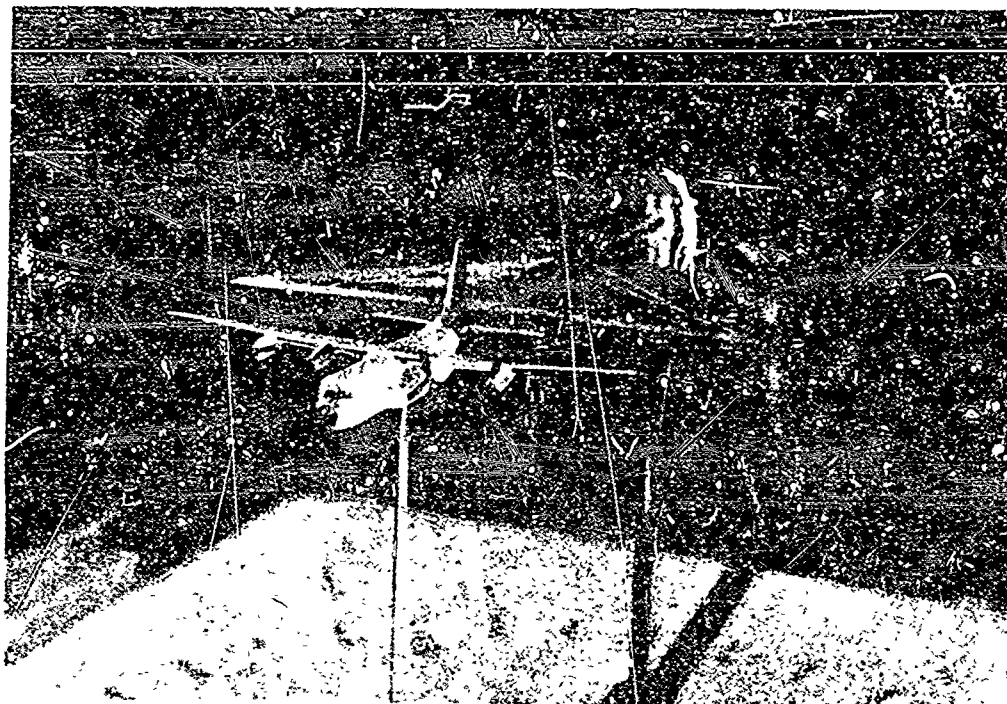
Fig 32. Aircraft Models and Survey Rake Mounted in
Wind Tunnel

1.315" long

1.0" long

1.0" (0.10 ea.)

2.5" (0.25 ea.)

3.0" (0.75 ea.)

15.0"

NOTE: RAKE HAS
ALTERNATING TOTAL
AND STATIC
PRESSURE PROBES,
DIAM. = 0.035"
TAP DIAM = 0.0135"
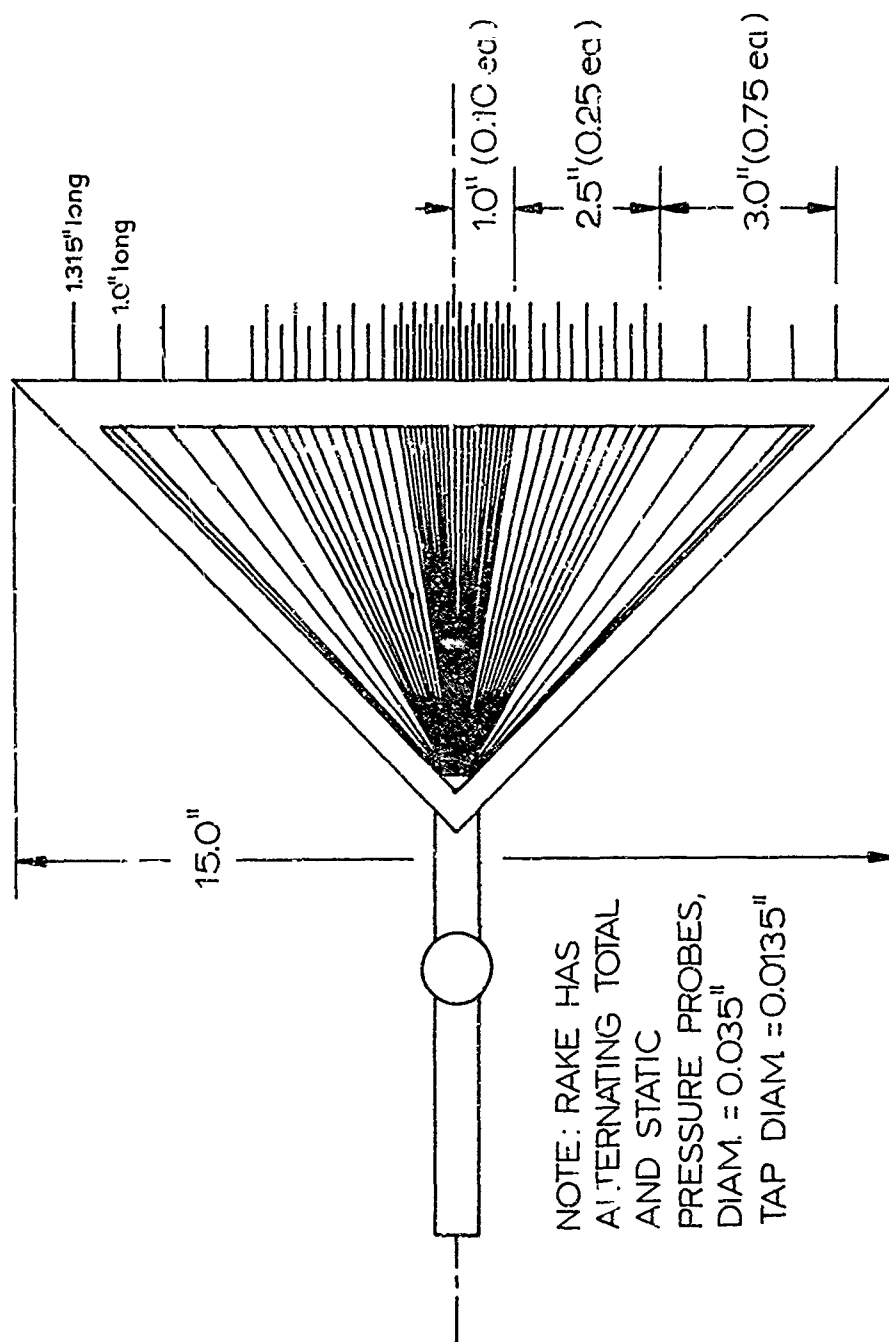
Fig 33. Pressure Survey Rake

53
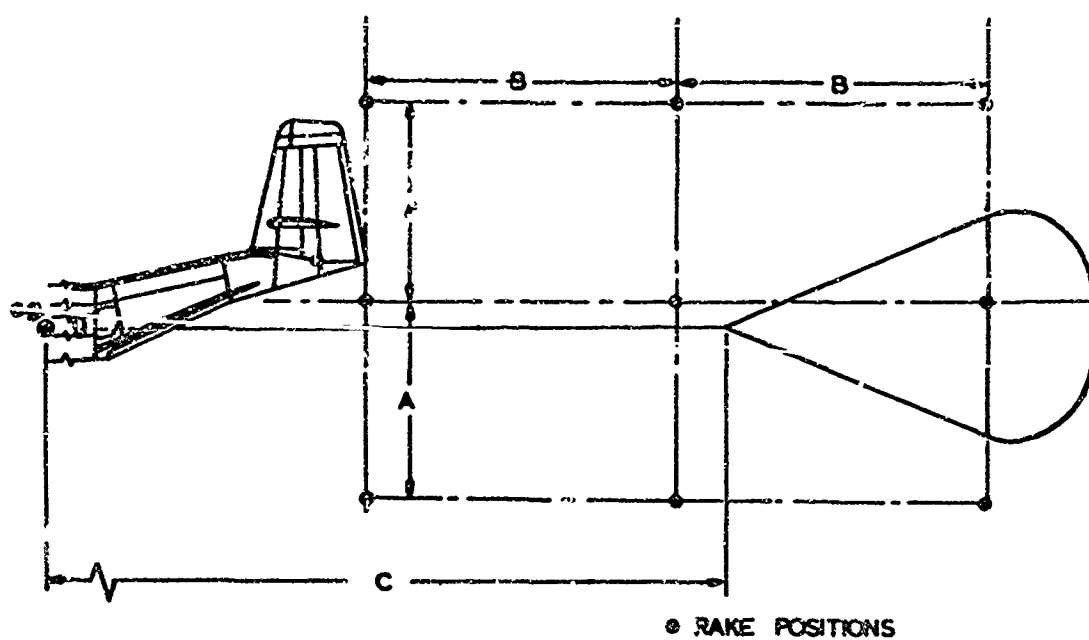
⊚ RAKE POSITIONS

	CARIBOU			C-130	
	MODEL	FULL-SCALE		MODEL	FULL-SCALE
A	3.68"	14.7'	A	1.26"	14.7'
B	4.1"	16.4'	B	1.11"	13.0'
C	15.0"	60.0'	C	5.15"	60.0'

FIG 34   Pressure Survey Rake Positions

54
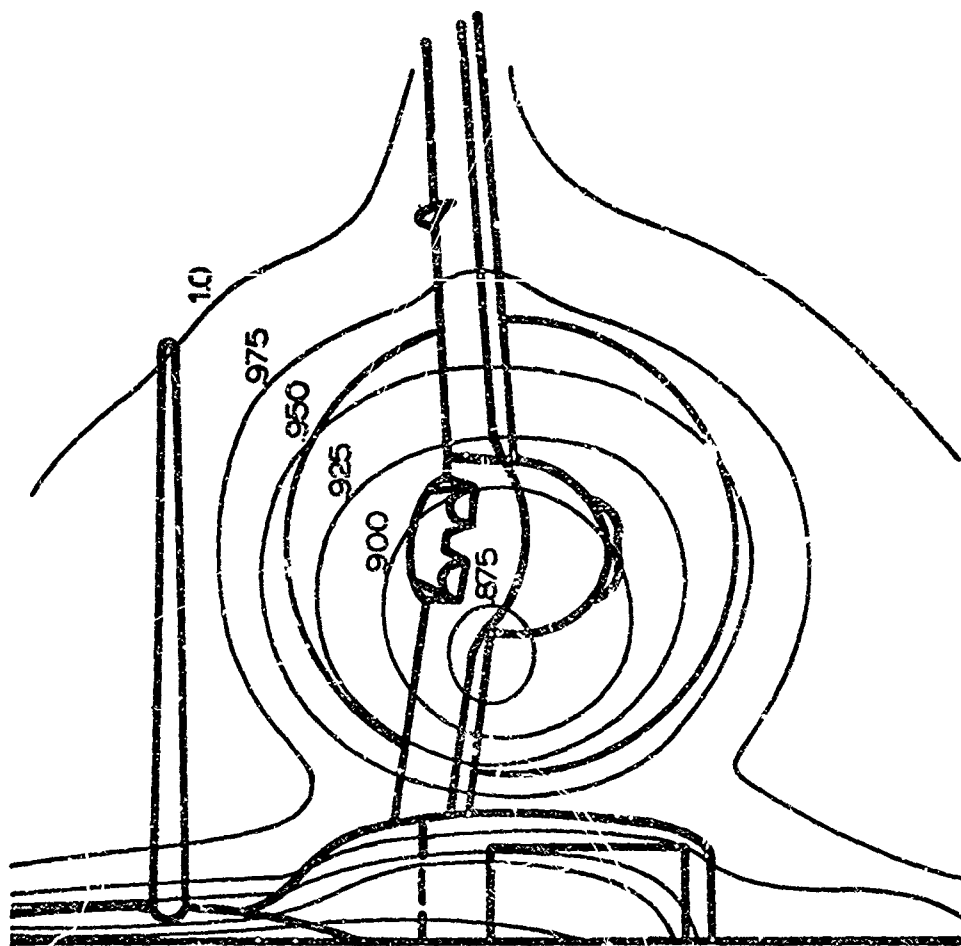
Fig 35. Velocity Distribution in the Wake of the Caribou Aircraft with Windmilling Propellers; Rake Station 1

55
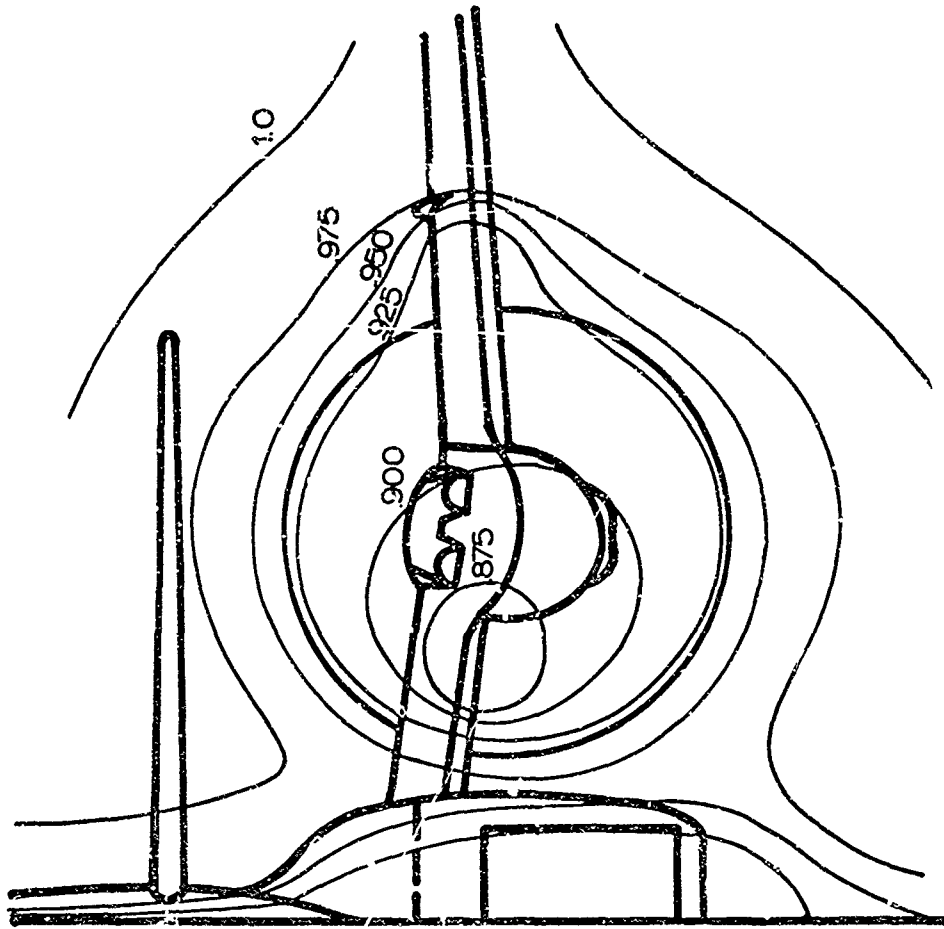
Fig 36. Velocity Distribution in the Wake of the Caribou Aircraft with Windmilling Propellers; Rake Section 2
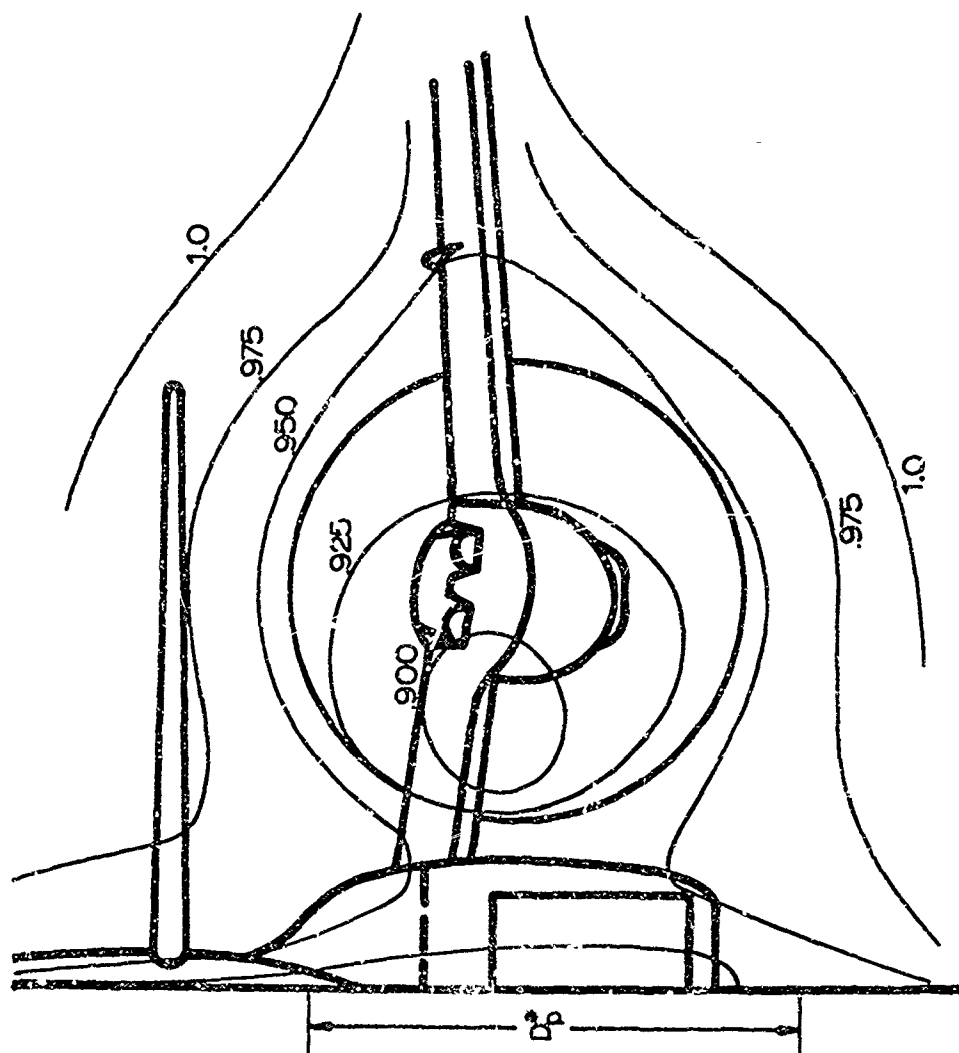
Fig 37. Velocity Distribution in the Wake of the Caribou Aircraft with Windmilling Propellers; Rake Section 3. *D_p = Projected Diameter of 22' Extraction Parachute
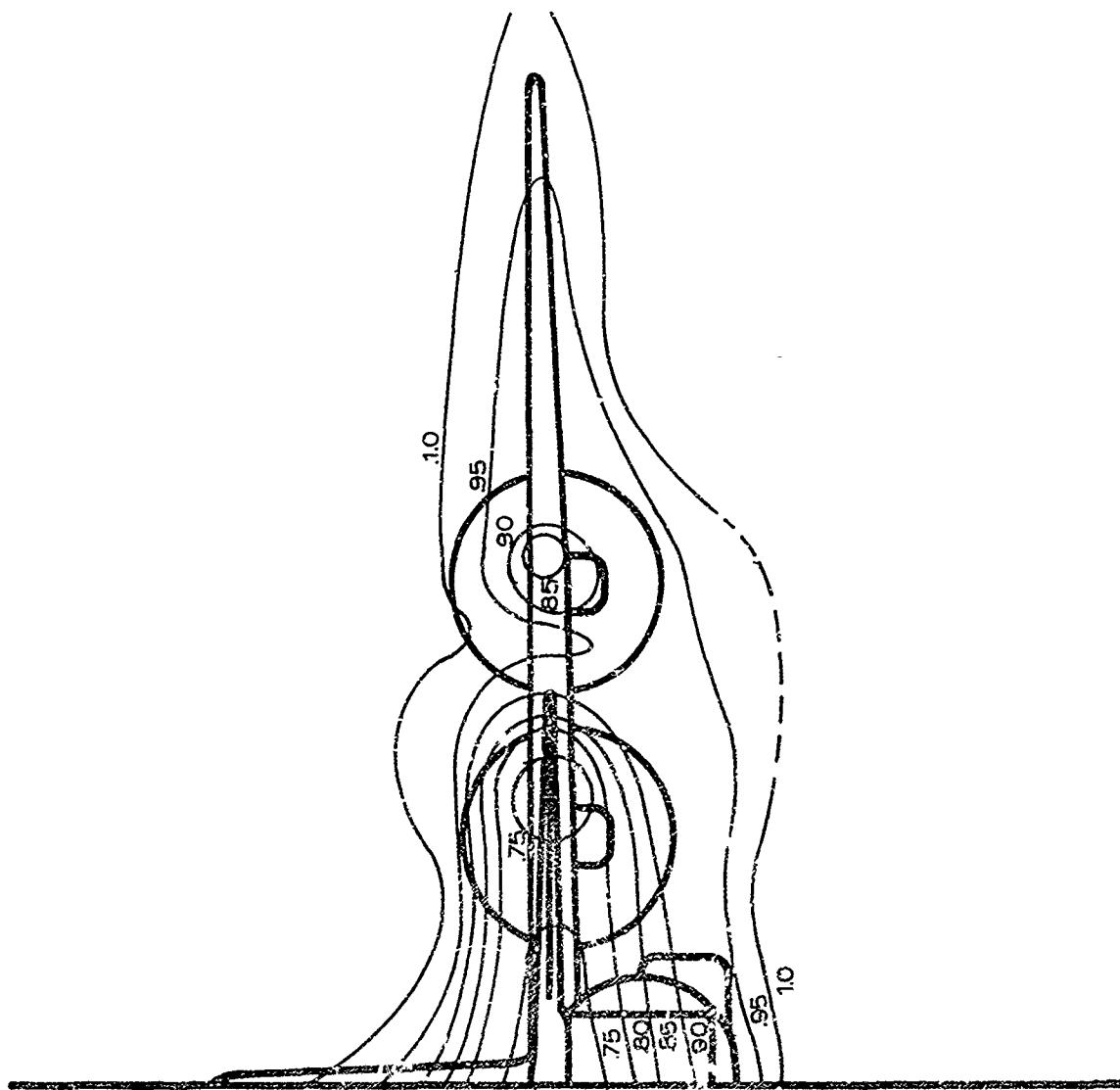
Fig 38. Velocity Distributions in the Wake of the C-130 Aircraft with Windmilling Propellers; Rake Section 1

58
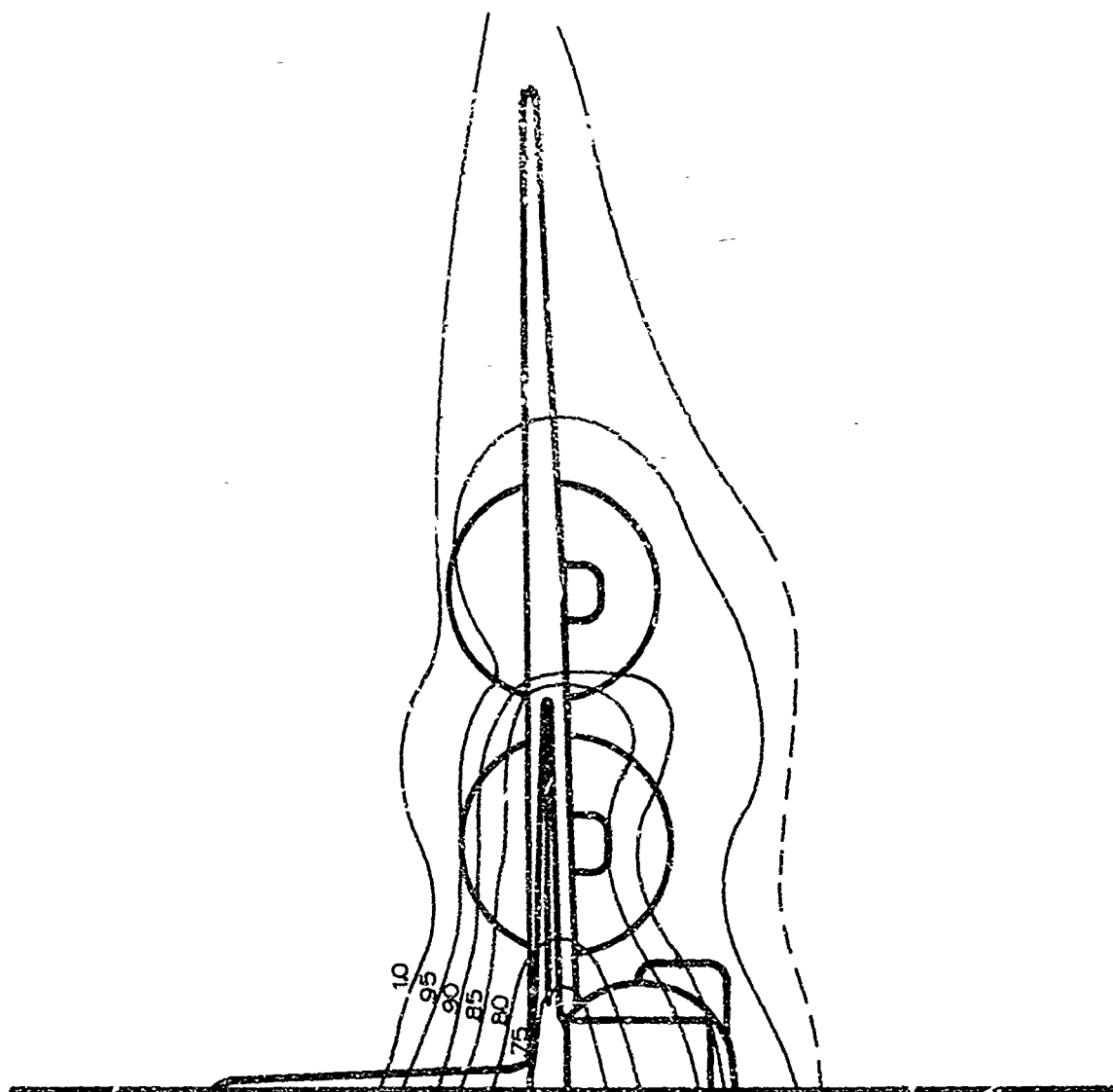
Fig 39. Velocity Distributions in the Wake of the C-130 Aircraft with Windmilling Propellers; Rake Section 2
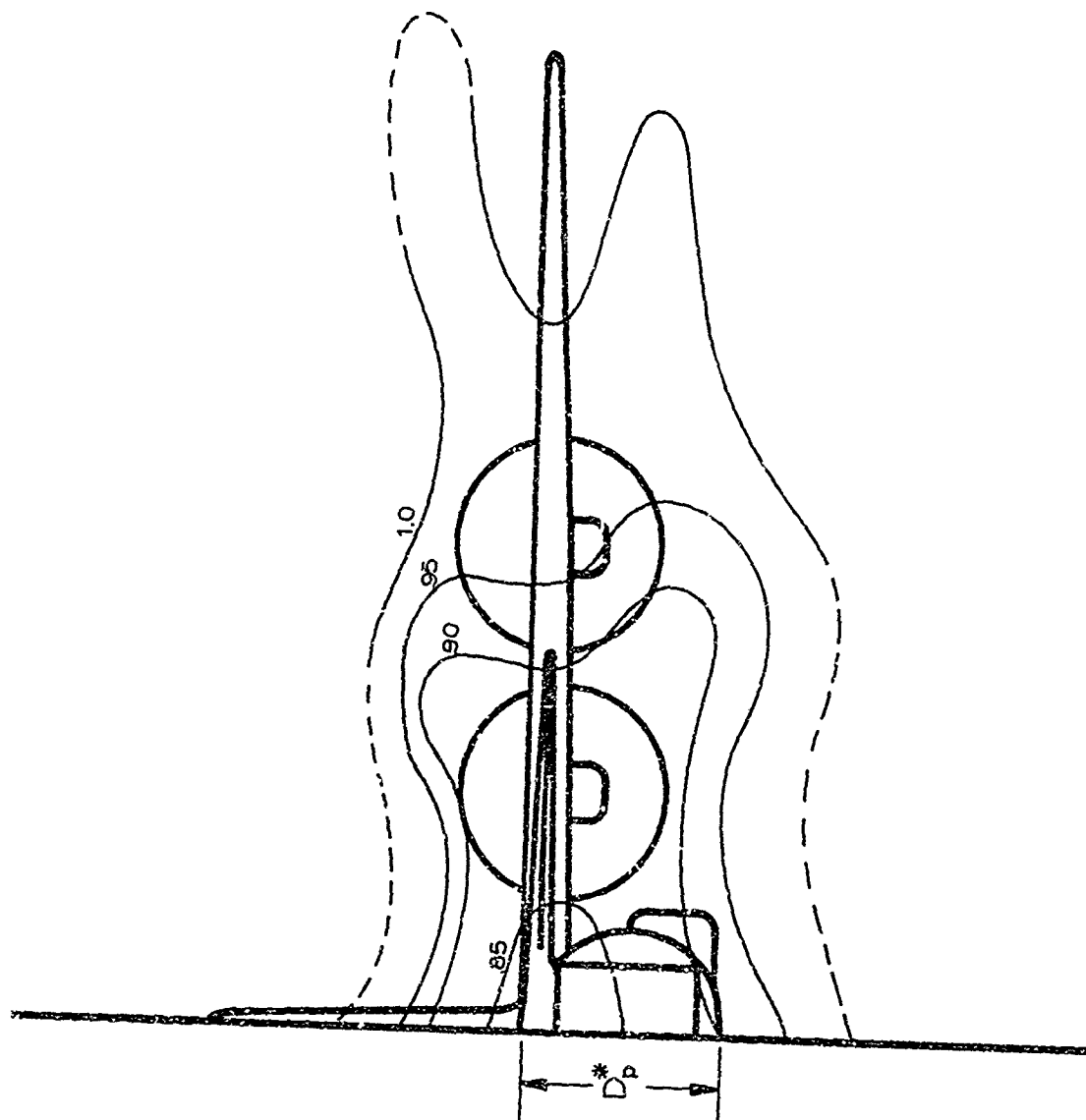
Fig 40. Velocity Distributions in the Wake of the C-130 Aircraft with Windmilling Propellers; Rake Section 3. * Dp = Projected Diameter of 22' Extraction Parachute

60

in the propeller wake is significant. For cargo release, this poses one boundary condition. When the engines produce thrust, the velocity in the propeller wake will increase above unity in certain areas. For this condition, the results are not directly applicable, and the general wake pattern will be altered. This condition would establish the other boundary and measurements of the parachute performance under both conditions will provide more specific information of the interaction between wake and parachute performance.

61

V. REFERENCES

1.   Performance of and Design Criteria for Deployable
      Aerodynamic Decelerators, ASD-TR-61-579.

2.   H. D. Young.   Statistical Treatment of Experimental
      Data,   McGraw-Hill Book Company Inc., New York, 1962.

62

APPENDIX I

STATISTICAL CONSIDERATIONS

Assuming the dispersion of values of individual measurements is normally distributed (the Gauss distribution), the most probable value of the quantity is simply the arithmetic mean of the measurements (Ref 2). The most probable values of filling time and opening shock factor are then,

$$t_f = \frac{1}{N} \sum_{i=1}^{N} t_{f_i} \tag{2}$$

and

$$X = \frac{1}{ND} \sum_{i=1}^{N} F_{max_i} \tag{3}$$

Equations 2 and 3 were used to determine the values of filling time and opening shock factor. The standard deviations of the values were determined in the conventional manner:

$$\sigma_{t_f} = \left[\frac{1}{N} \sum_{i=1}^{N} (t_f - t_{f_i})^2 \right]^{\frac{1}{2}} \tag{4}$$

and

$$\sigma_x = \left[\frac{1}{N} \sum_{i=1}^{N} (X - X_i)^2 \right]^{\frac{1}{2}} \tag{5}$$

The method of least squares was used to determine the best hyperbolic fit through the data for filling time versus velocity (Figs 19 and 22). The problem was to determine the constant A in

$$t_f V_\infty = A . \tag{6}$$

If there were no deviations in the individual data from the assumed relation, we would have $t_{f_i} - A/V_{\infty_i} = 0$, but

63

in reality the error in t_{f_1} is represented by $d_i = t_{r_1} - A/V_{\infty_1}$. Defining $Z_1 = 1/V_{\infty_1}$, and minimizing the least-squares sum, we obtain

$$\frac{d}{dA} \sum d_i^2 = \sum 2(t_{f_1} - AZ_1) Z_1 = 0 \qquad (7)$$

or

$$A = \frac{\sum t_{f_1} Z_1}{\sum Z_1^2} \quad . \qquad (8)$$

The constant A was then easily determined.

APPENDIX II.

HISTOGRAMS OF OPENING SHOCK FACTOR AND FILLING TIME

The following diagrams represent the statistical evaluations of the various measurements. They are merely added to this report for completeness and as a matter of record.
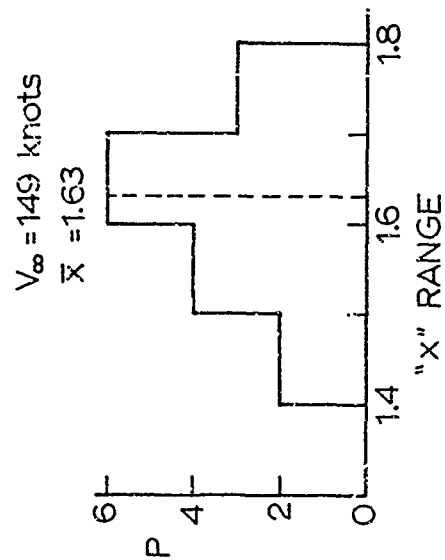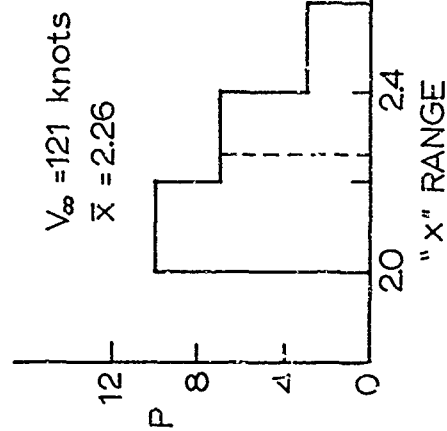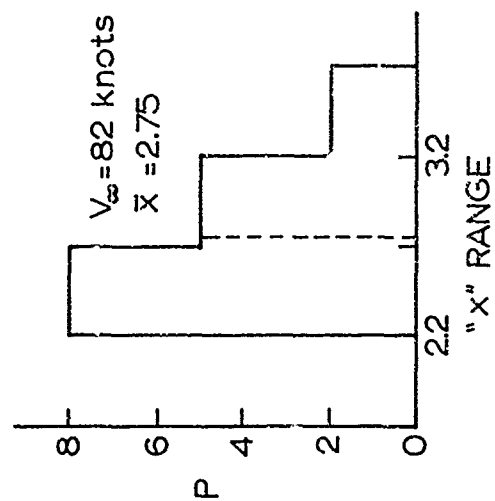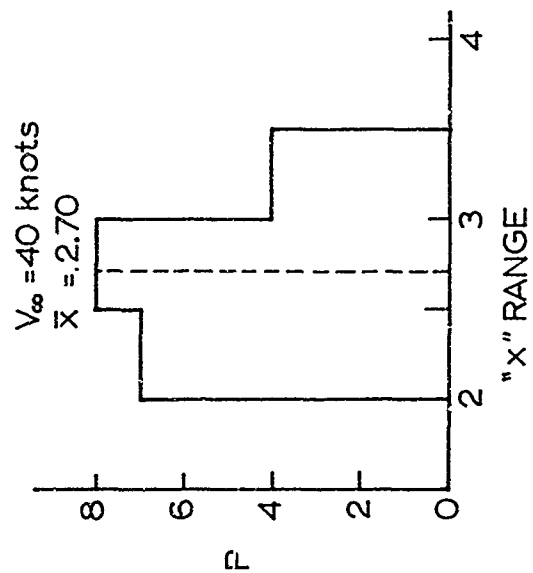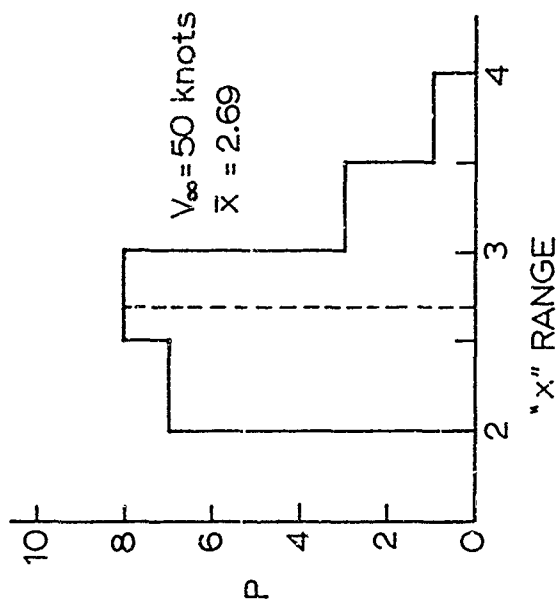
Fig 41. X Distributions for a Single Solid Flat Parachute in Freestream at Velocities from 40 to 150 knots.

66
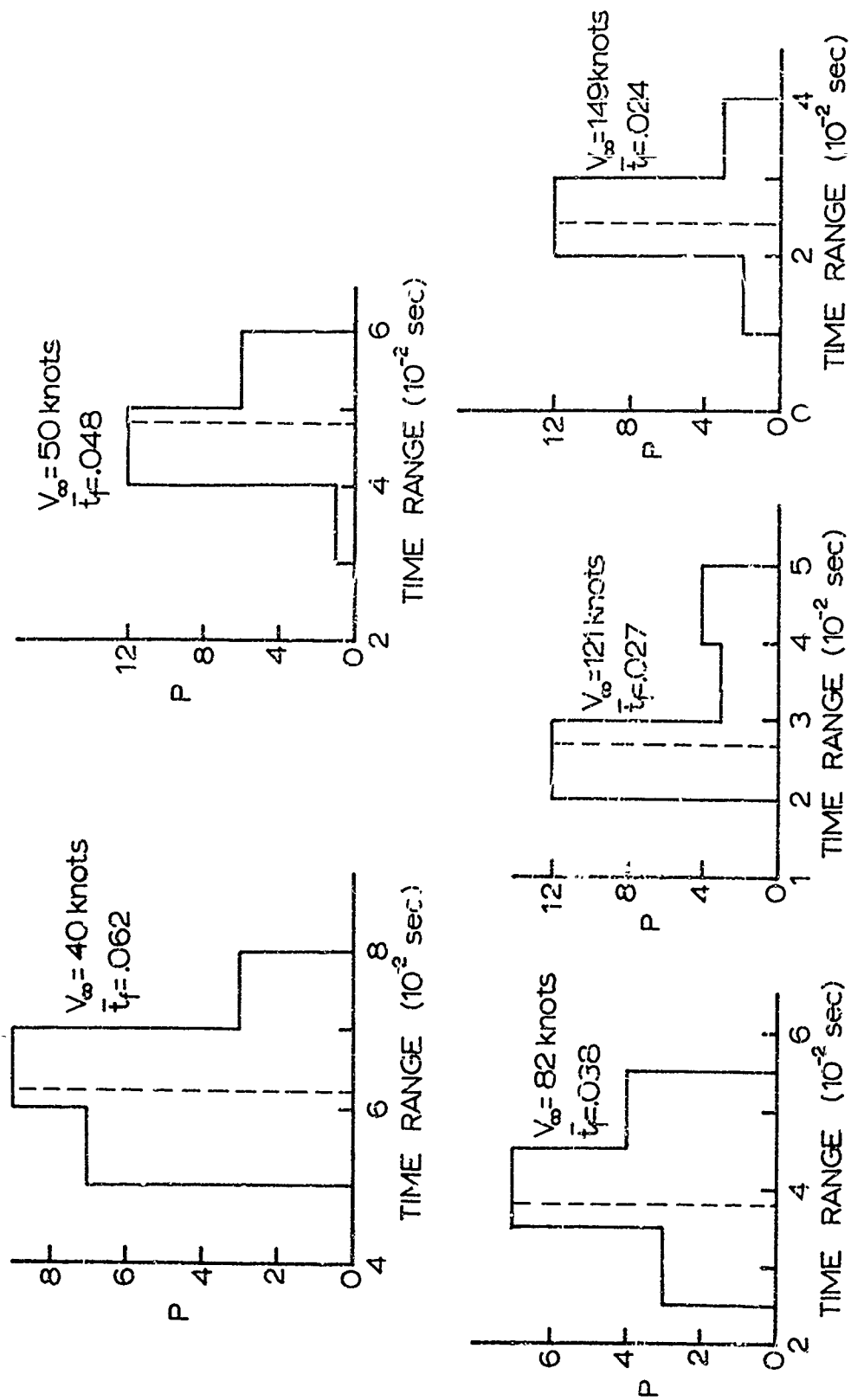
Fig 42. t_f Distributions for a Single Solid Flat Parachute in Freestream at Velocities from 40 to 150 knots.

67
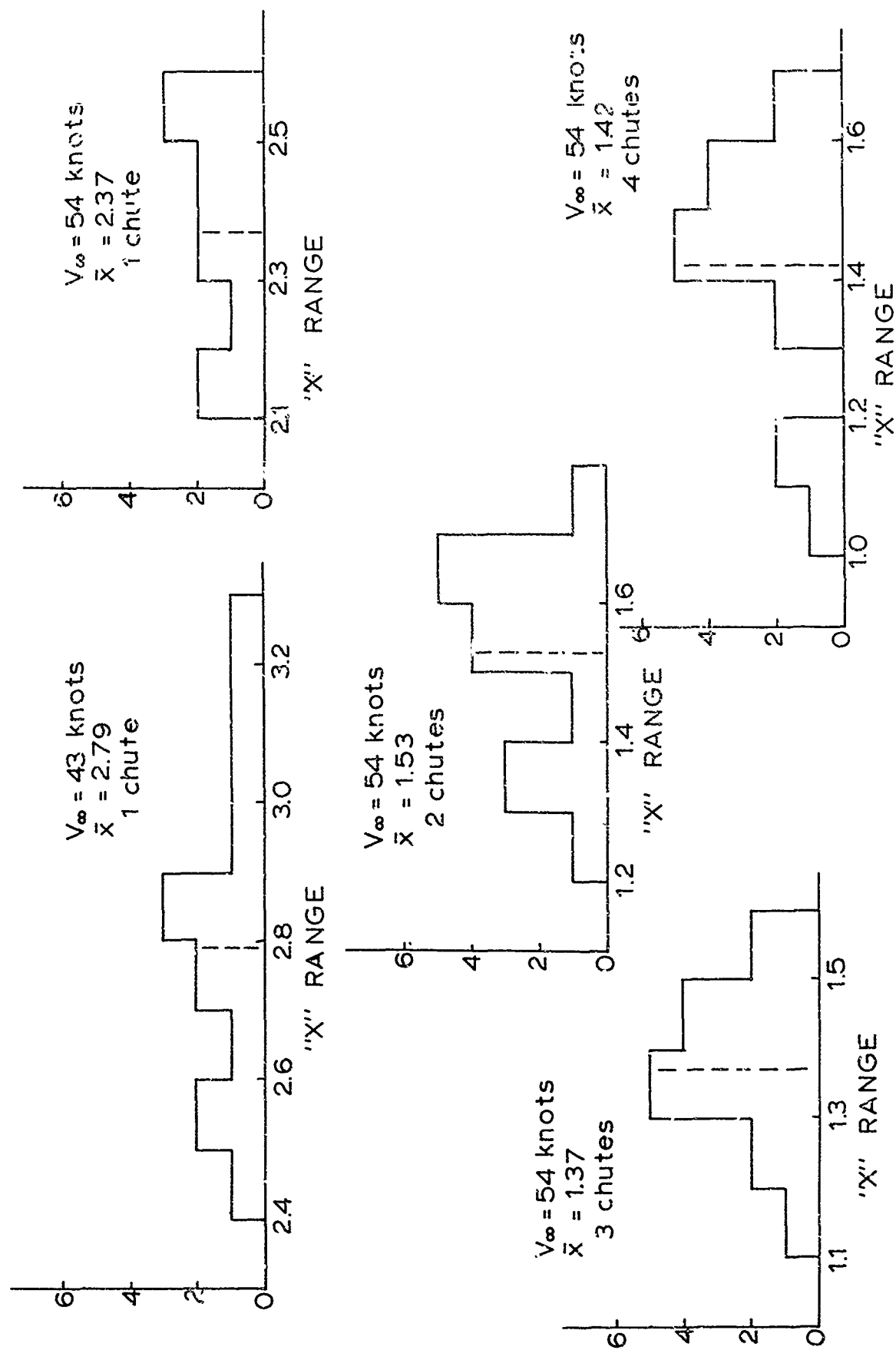
Fig 43. X Distributions for 1, 2, 3 and 4 Solid Flat Parachutes in Freestream
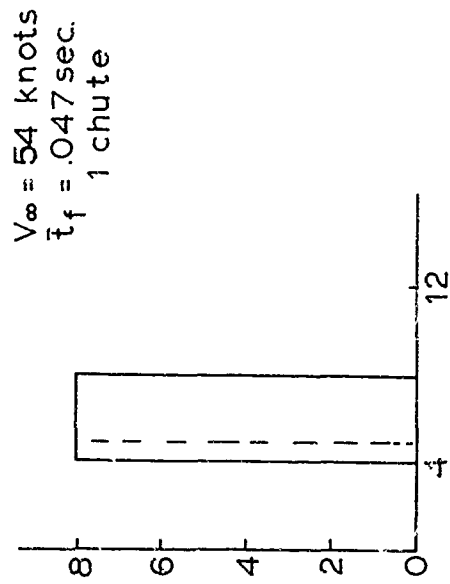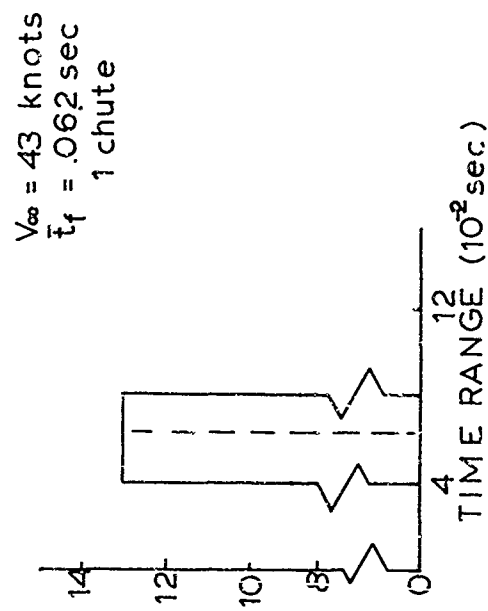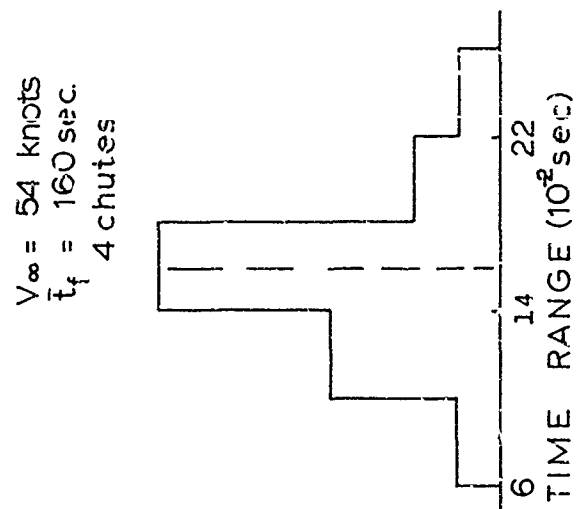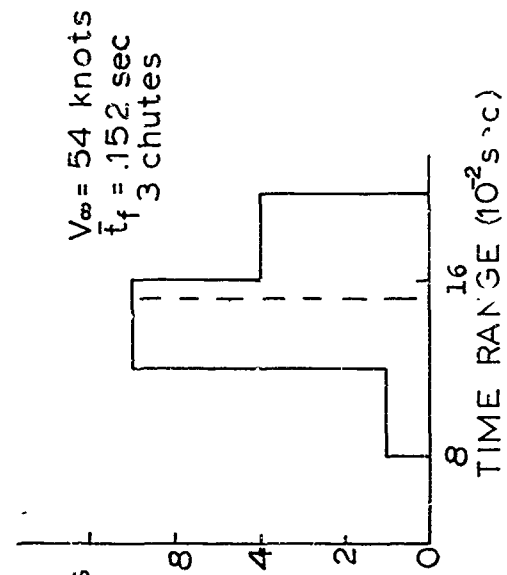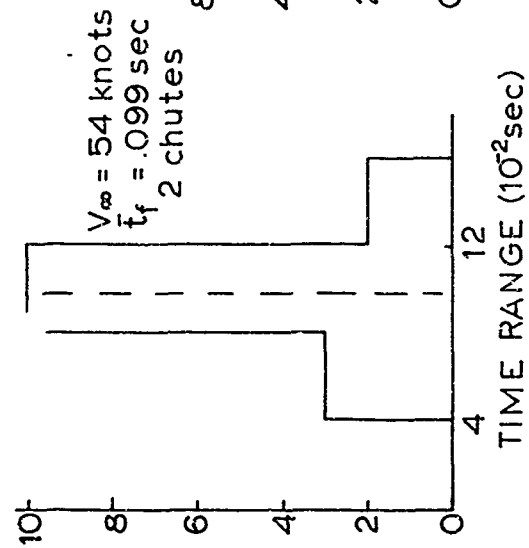
Fig 44. t_f Distributions for 1, 2, 3 and 4 Solid Flat Parachutes in Freestream
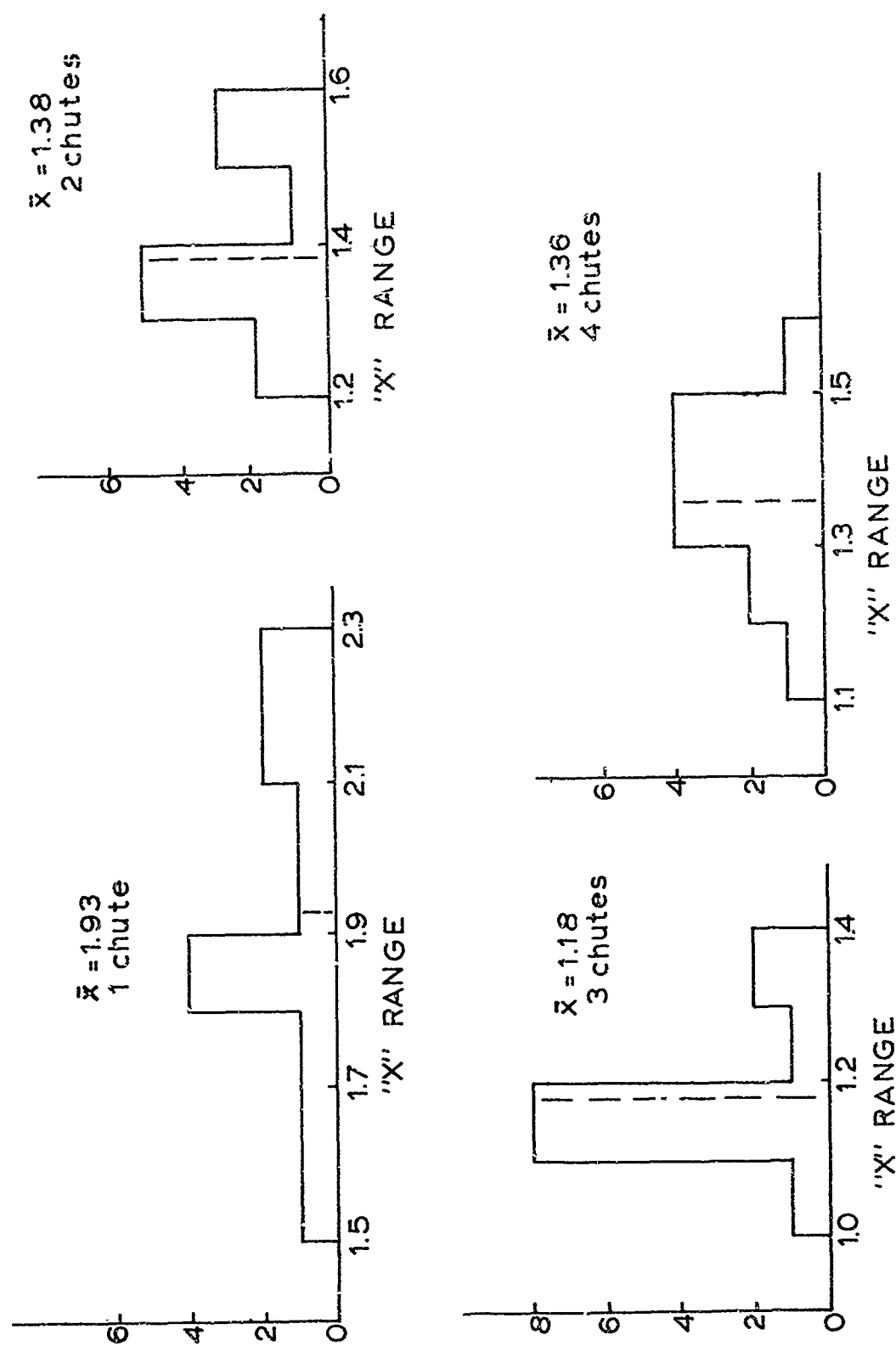
Fig 45. X Distributions for 1, 2, 3 and 4 Solid Flat Parachutes in the Aircraft Wake. V_∞ = 54 knots.
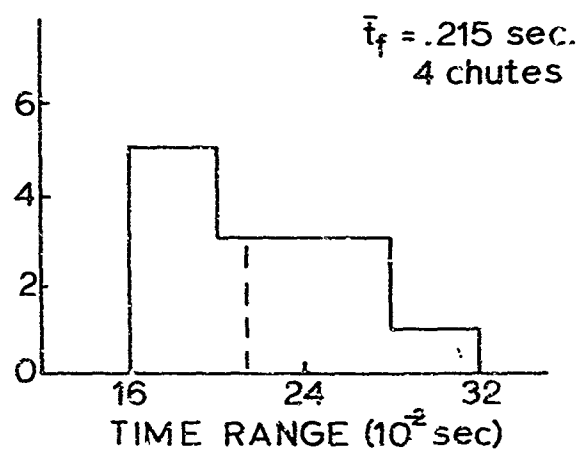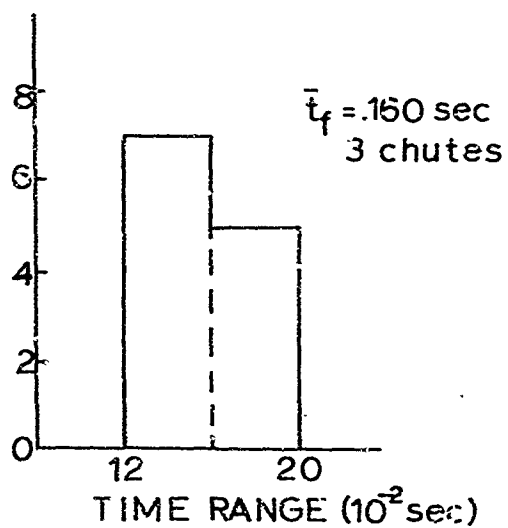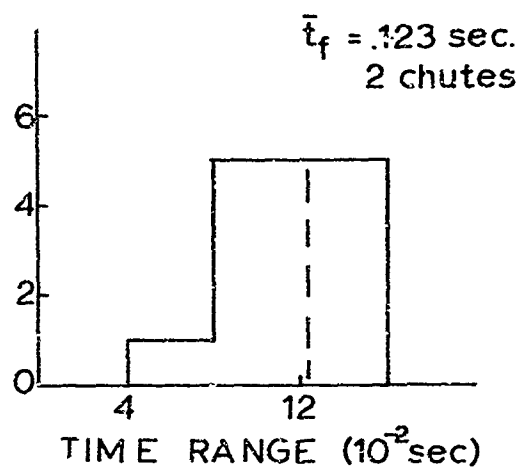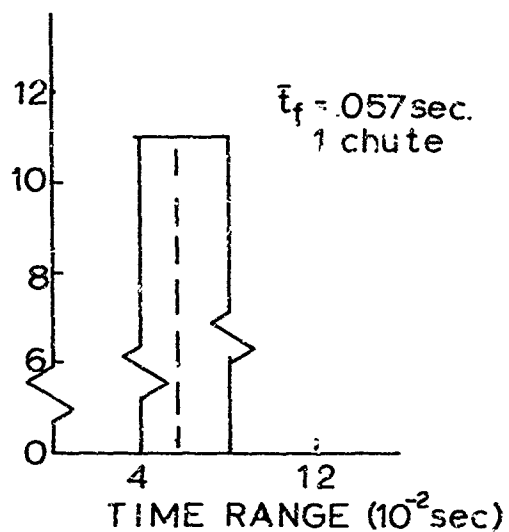
Fig 46. t_f Distributions for 1, 2, 3 and 4 Solid Flat Parachutes in the Aircraft Wake. $V_\infty = 54$ knots.

71
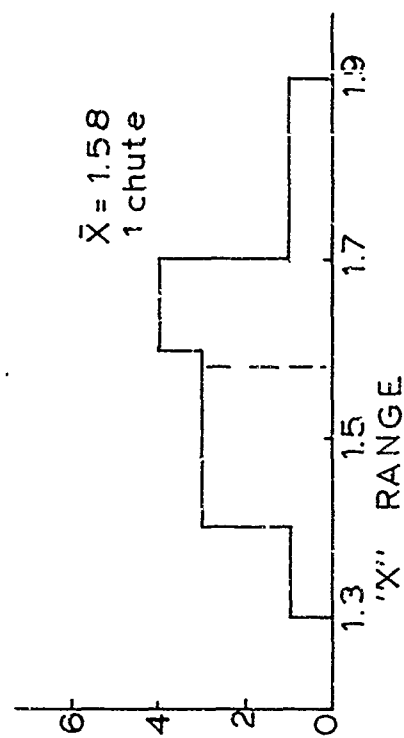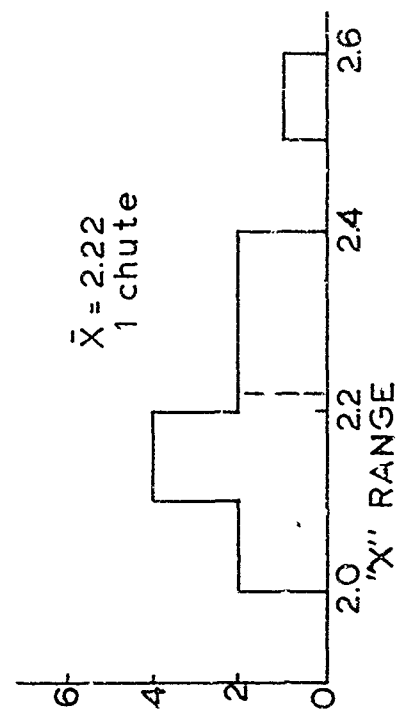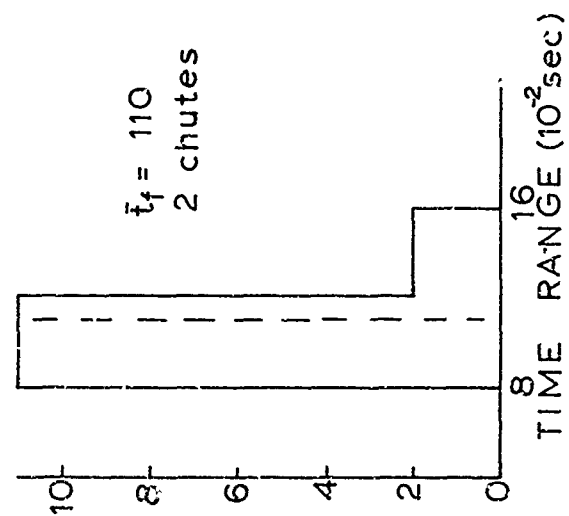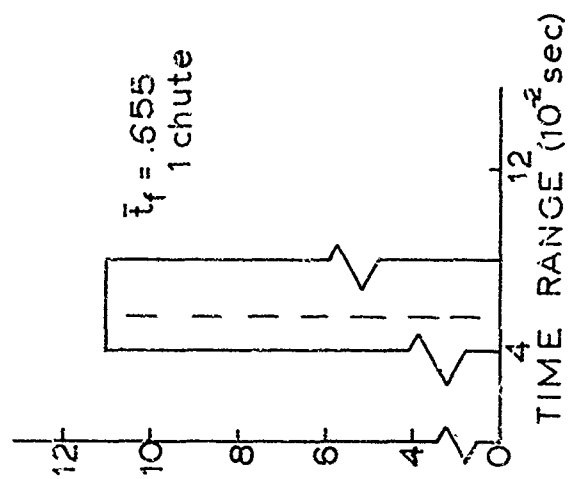
Fig 47. X and t_f Distributions for 1 and 2 Solid Flat Parachutes with Ground Effect. $V_\infty = 54$ knots.
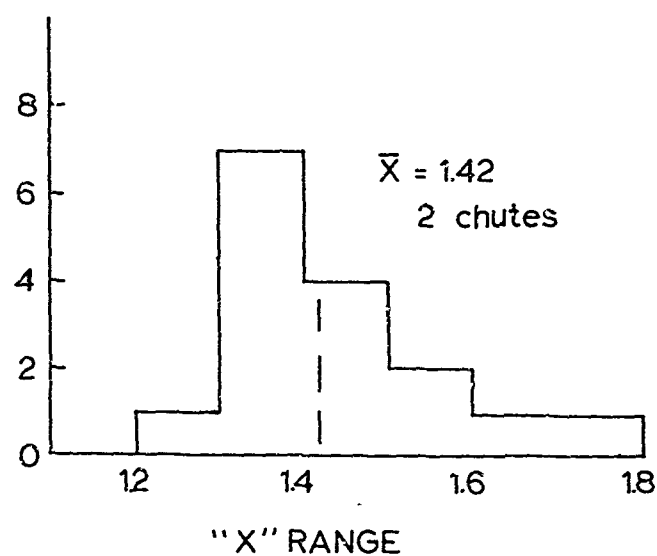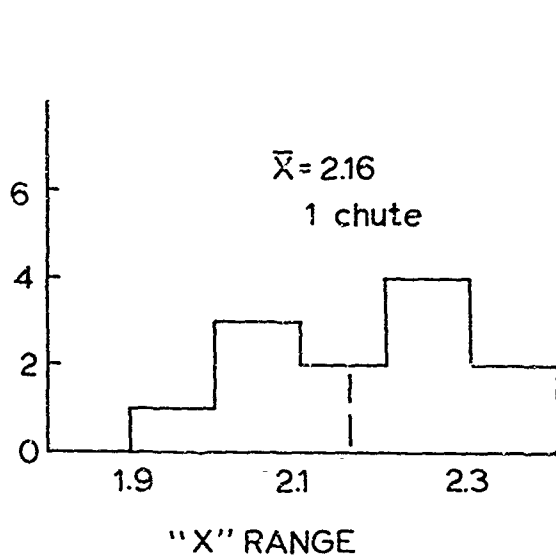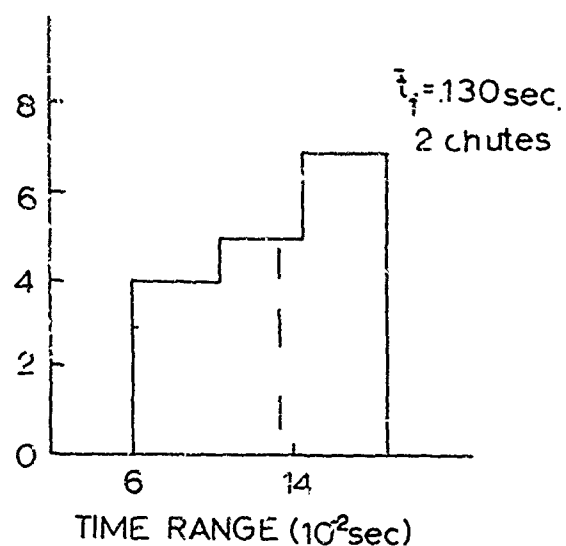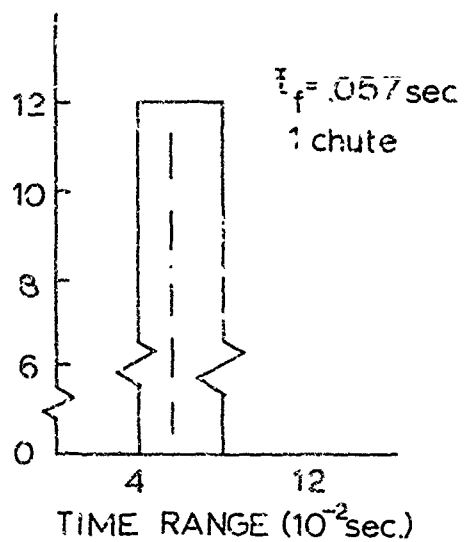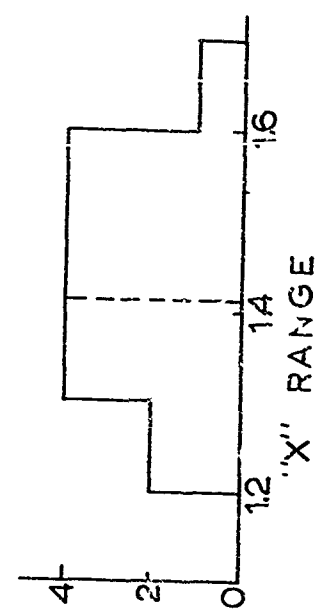
Fig 48.   X and t_f Distributions for 1 and 2 Solid Flat
Parachutes in the Aircraft Wake with Ground Effect
$V_\infty = 54$ knots.

73
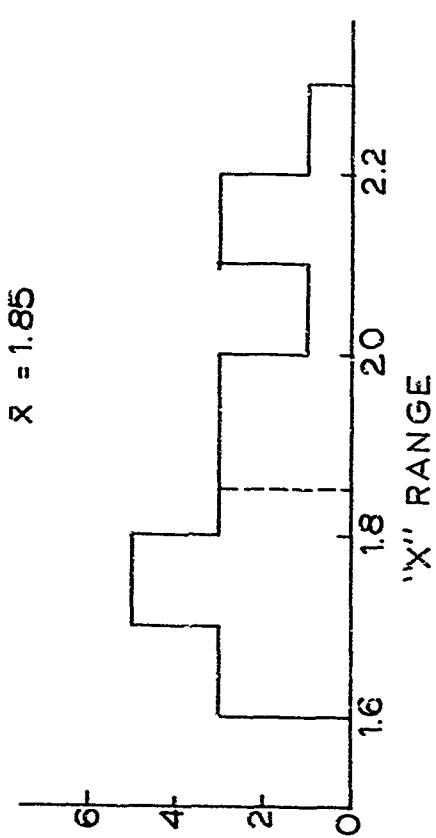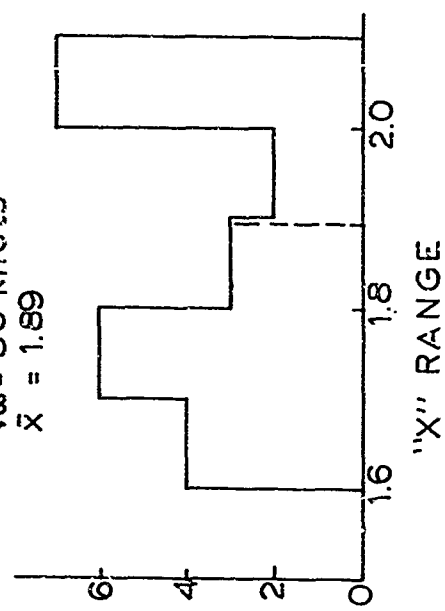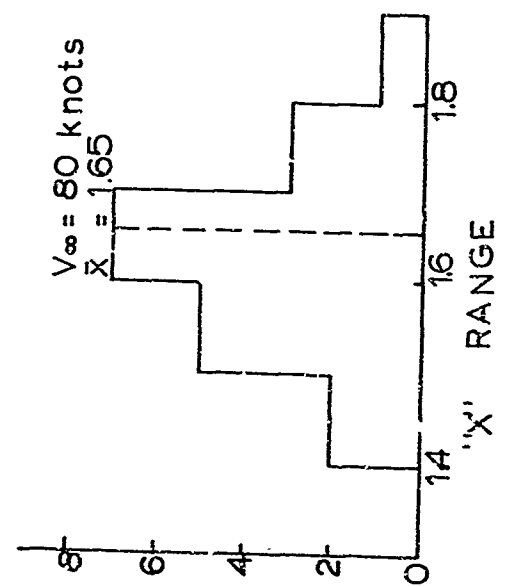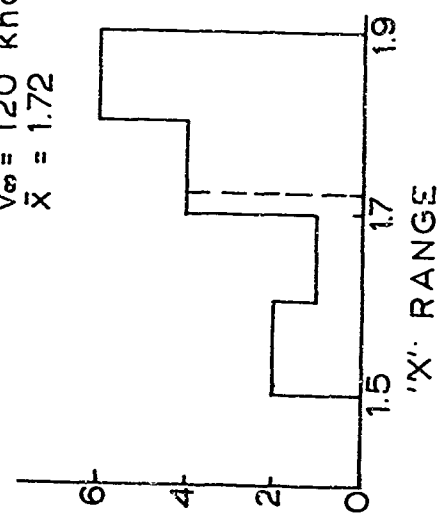
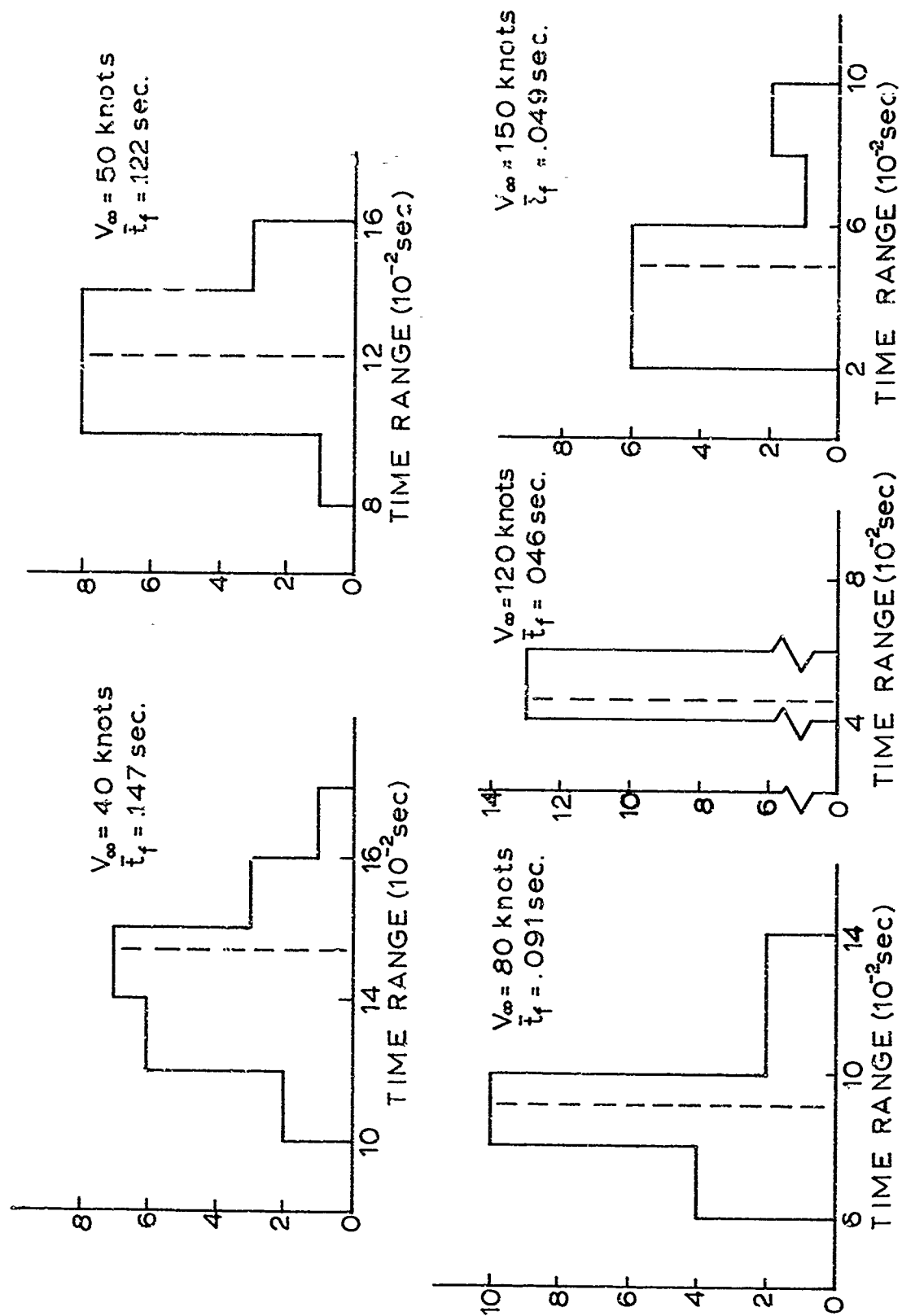Fig 49. X Distributions for 1 Ringslot Parachute in Freestream at Velocities from 40 to 150 knots.

74

Fig 50. t_f Distributions for a Single Ringslot Parachute in Freestream at Velocities from 40 to 150 knots.
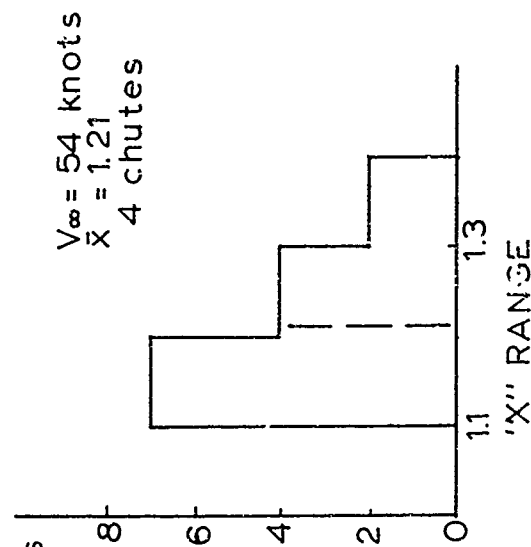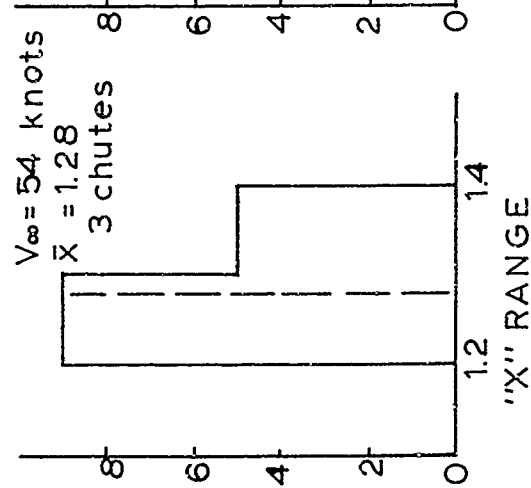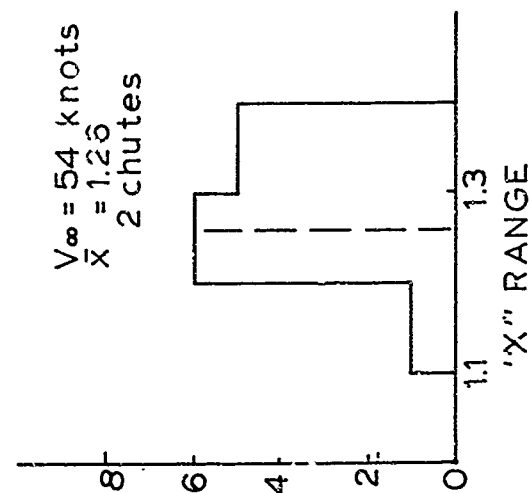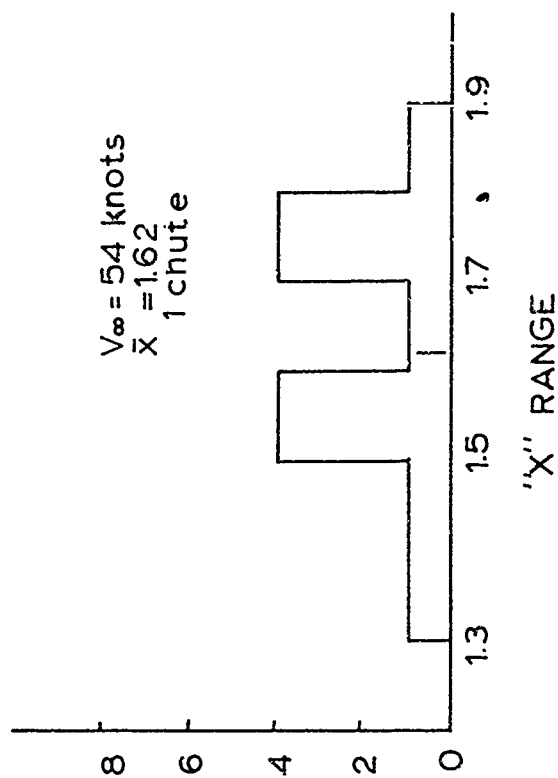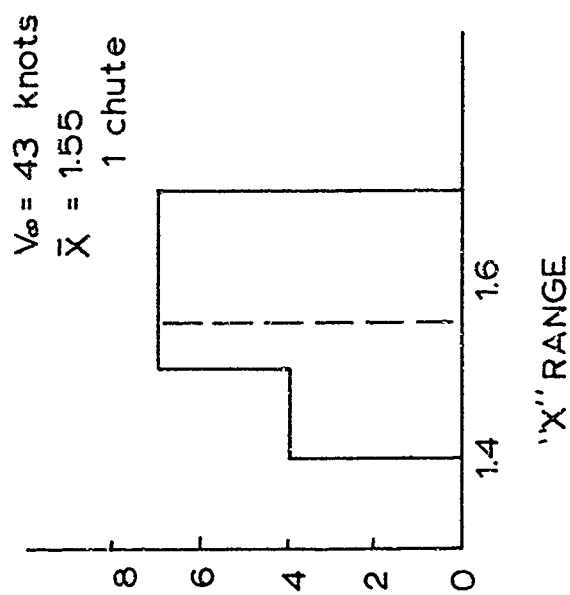
Fig 51. X Distributions for 1, 2, 3 and 4 Ringslot Parachutes in Freestream.

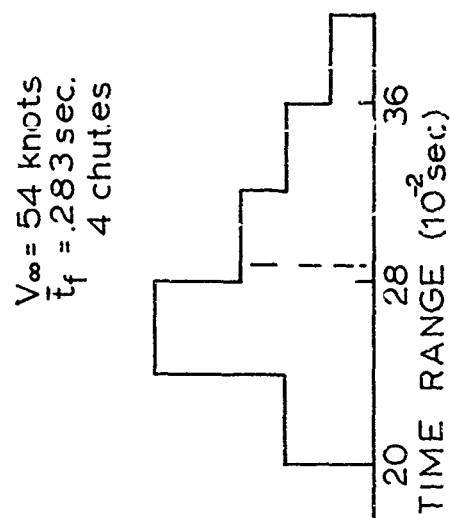Fig 52. t_f Distributions for 1, 2, 3 and 4 Ringslot Parachutes in Freestream.

77

Fig 53. X Distributions for 1, 2, 3 and 4 Ringslot Parachutes
in the Aircraft Wake. $V_\infty = 54$ knots.
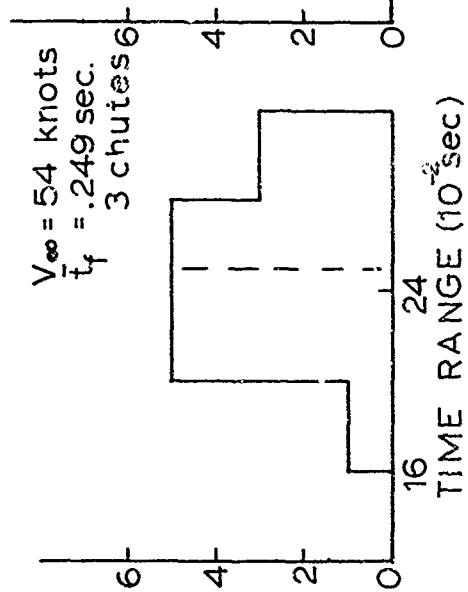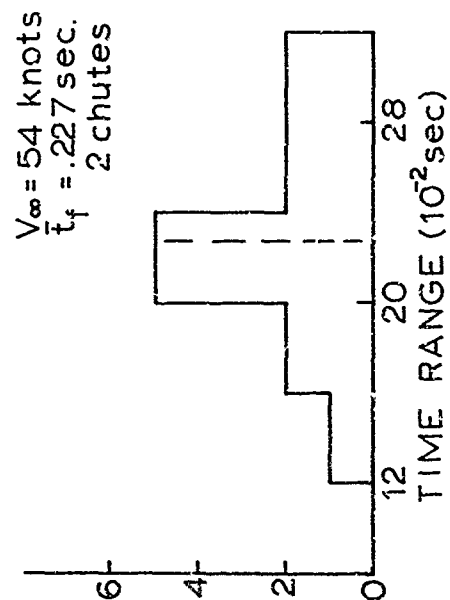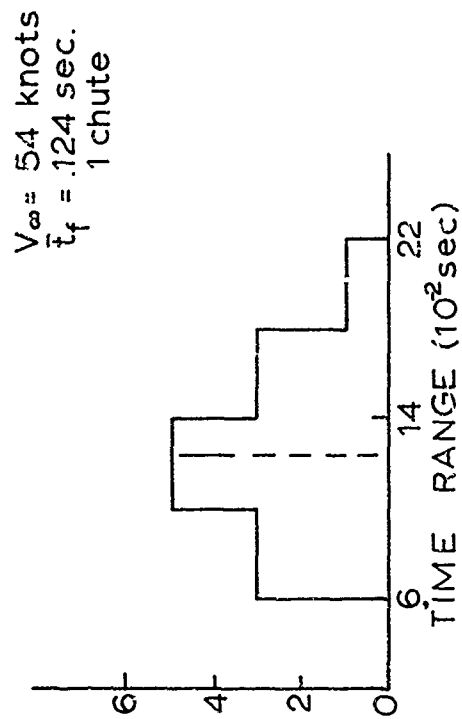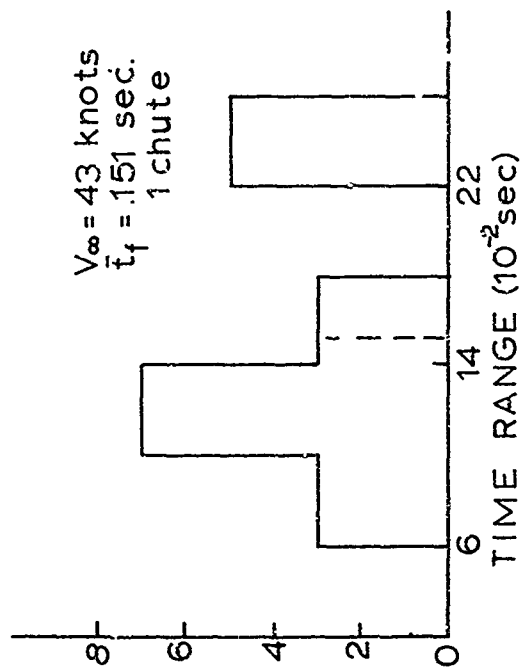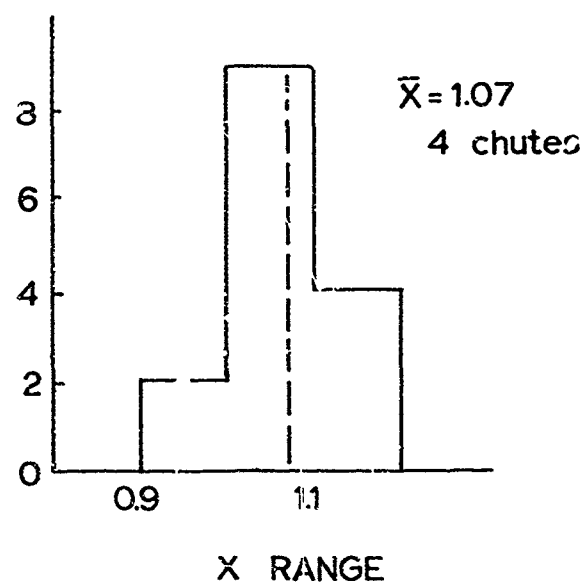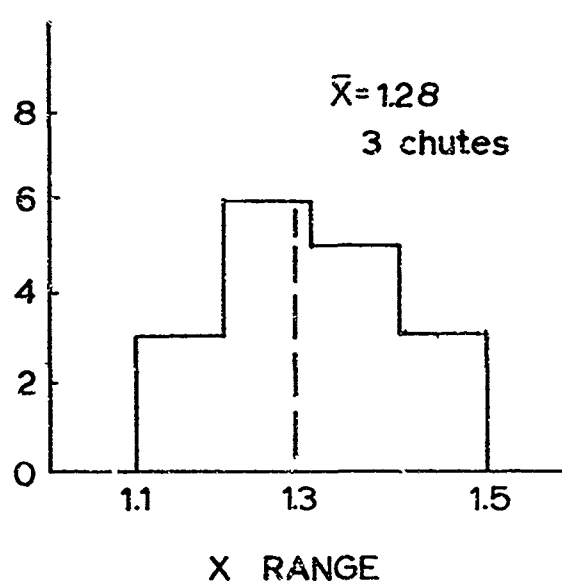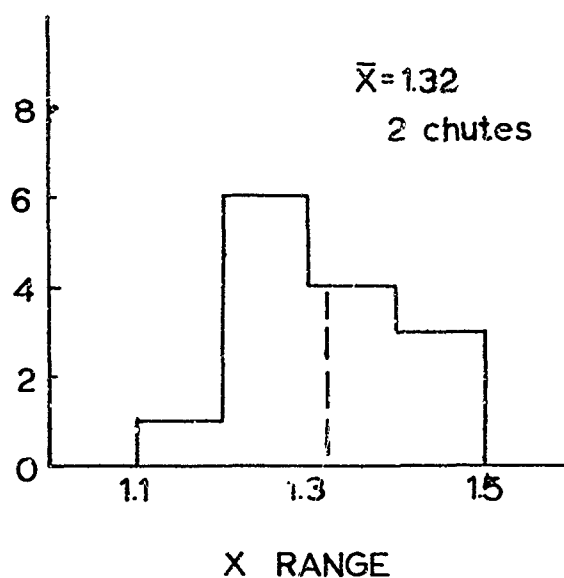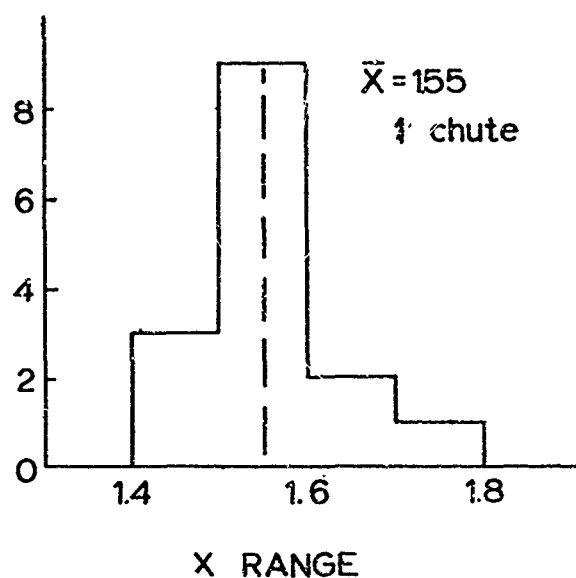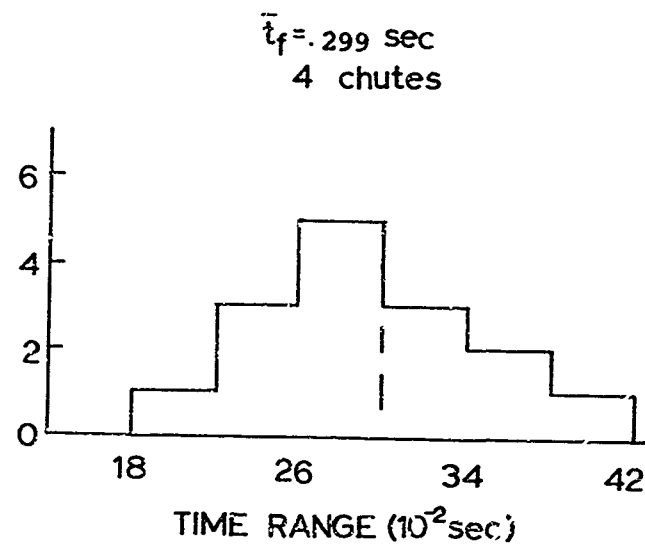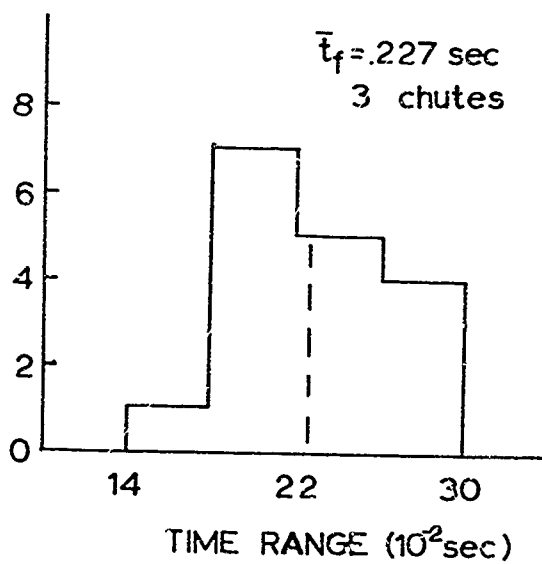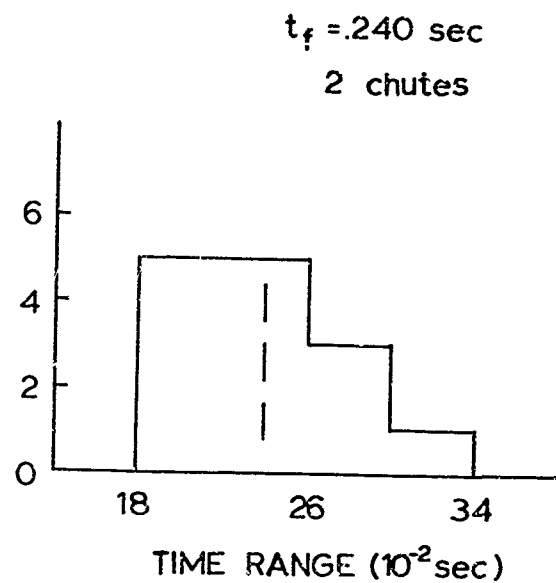
Fig 54. t_f Distributions for 1, 2, 3 and 4 Ringslot Parachutes in the Aircraft Wake. $V_\infty = 54$ knots.
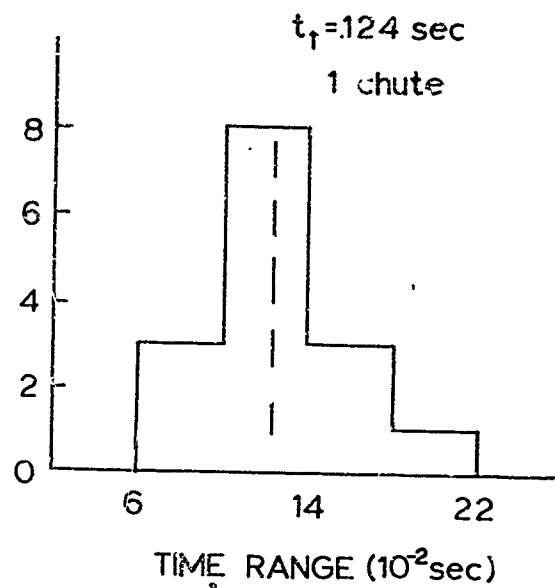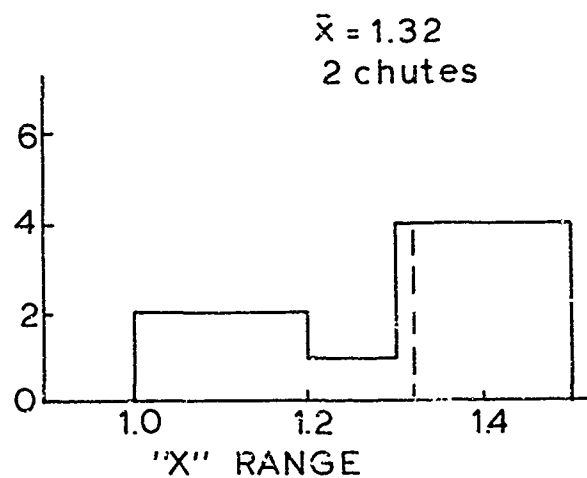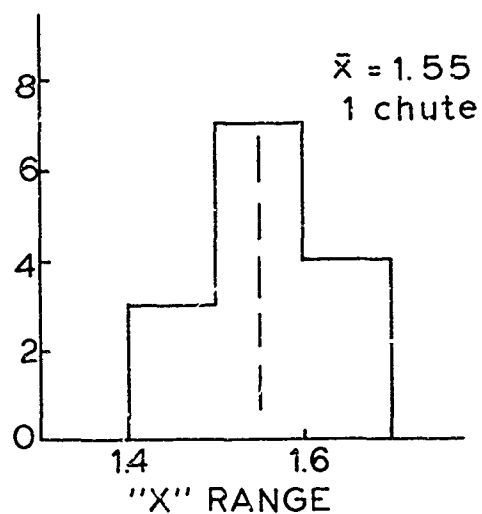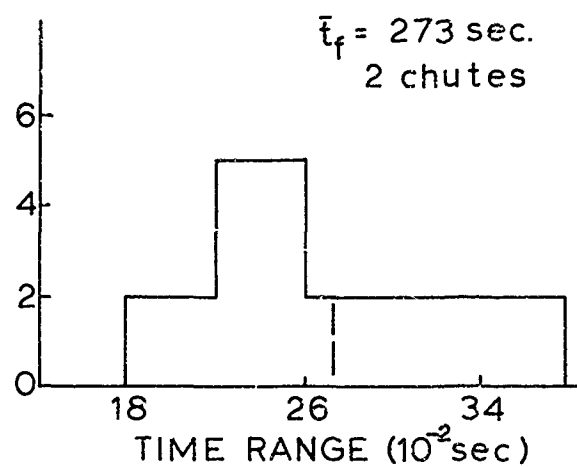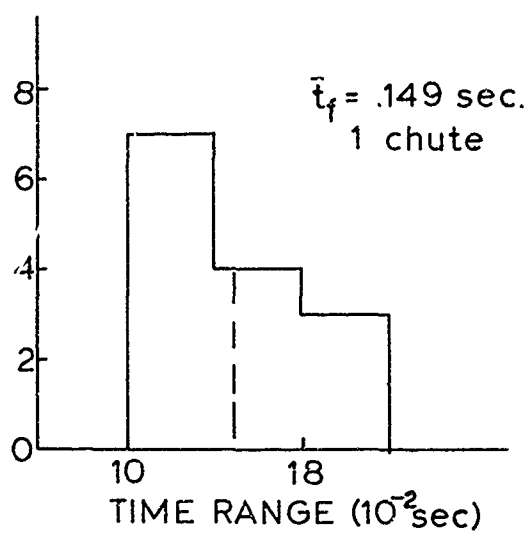
Fig 55. X and t_f Distributions for 1 and 2 Ringslot Parachutes with Ground Effect. $V_\infty = 54$ knots.
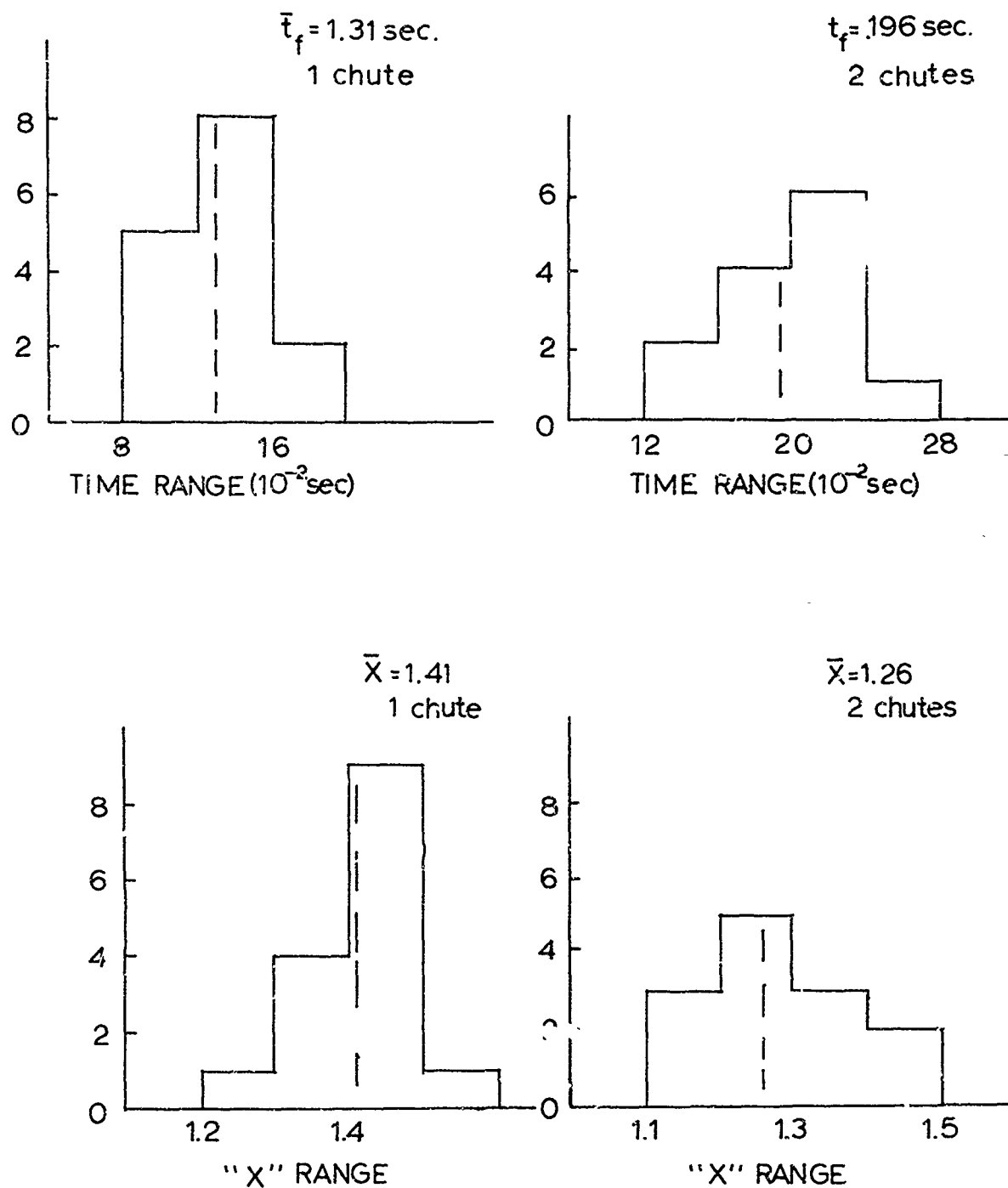
Fig 56. X and t_f Distributions for 1 and 2 Ringslot Parachutes in the Aircraft Wake with Ground Effect. $V_\infty = 54$ knots.

81

DOCUMENT CONTROL DATA - R&D

(Security classification of title, body of abstract and indexing annotation must be entered when the overall report is classified)

1. ORIGINATING ACTIVITY (Corporate author)	2a. REPORT SECURITY CLASSIFICATION
University of Minnesota Minneapolis, Minn. 55455	Unclassified
	2b. GROUP n/a

3. REPORT TITLE

Drag and Dynamics of Single and Clustered Parachutes in Freestream, and With Wake and Ground Effects.

4. DESCRIPTIVE NOTES (Type of report and inclusive dates)

Final Report. April 65 - April 66.

5. AUTHOR(S)

Heinrich, H. G.
Noreen, R. A.

6. REPORT DATE	7a. TOTAL NO. OF PAGES	7b. NO. OF REFS
November 1966	81 p.	2

8a. CONTRACT OR GRANT NO. AF33(615)-2554	9a. ORIGINATOR'S REPORT NUMBER(S)
b. PROJECT NO. AF-6065	AFFDL-TR-66-104
c. Task No. 606503	9b. OTHER REPORT NO(S) (Any other numbers that may be assigned this report)
d.	

10. AVAILABILITY/LIMITATION NOTICE Qualified users may obtain copies of this report from the Defense Documentation Center. Release to CFSTI is not authorized. This document is subject to special export controls and each transmittal to foreign governments or foreign nationals may be made only with prior approval of the Air Force Flight Dynamics Laboratory.

11. SUPPLEMENTARY NOTES	12. SPONSORING MILITARY ACTIVITY
	AFFDL (FDFR) Wright-Patterson AFB, Ohio

13. ABSTRACT

Results of wind tunnel studies concerned with transient and steady state performance of single and clustered parachutes in cargo extraction systems are presented.

In Part I, circular flat and ringslot canopies single suspended and in clusters of 2, 3, and 4, were deployed in freestream, in the wake of an aircraft, and near a simulated ground.

As a further means of analysis, wake pressure surveys were performed on the DHC-4 Caribou and the C-130 Hercules aircraft and are presented in Part II.

(232510)

DD FORM 1473 1 JAN 64

Unclassified
Security Classification

| 14 | LINK A | | LINK B | | LINK C | |
KEY WORDS	ROLE	WT	ROLE	WT	ROLE	WT
Parachutes						
Cargo extraction						
Ring slot						
Solid flat circular						
Clustered parachutes						
Aircraft wake						
Ground effects						
C-130 aircraft						
DHC-4 Caribou aircraft						

INSTRUCTIONS

1. ORIGINATING ACTIVITY. Enter the name and address of the contractor, subcontractor, grantee, Department of Defense activity or other organization (corporate author) issuing the report.

2a. REPORT SECURITY CLASSIFICATION: Enter the overall security classification of the report. Indicate whether "Restricted Data" is included. Marking is to be in accordance with appropriate security regulations.

2b. GROUP: Automatic downgrading is specified in DoD Directive 5200.10 and Armed Forces Industrial Manual. Enter the group number. Also, when applicable, show that optional markings have been used for Group 3 and Group 4 as authorized.

3. REPORT TITLE: Enter the complete report title in all capital letters. Titles in all cases should be unclassified. If a meaningful title cannot be selected without classification, show title classification in all capitals in parenthesis immediately following the title.

4. DESCRIPTIVE NOTES: If appropriate, enter the type of report, e.g., interim, progress, summary, annual, or final. Give the inclusive dates when a specific reporting period is covered.

5. AUTHOR(S): Enter the name(s) of author(s) as shown on or in the report. Enter last name, first name, middle initial. If military, show rank and branch of service. The name of the principal author is an absolute minimum requirement.

6. REPORT DATE: Enter the date of the report as day, month, year; or month, year. If more than one date appears on the report, use date of publication.

7a. TOTAL NUMBER OF PAGES: The total page count should follow normal pagination procedures i.e., enter the number of pages containing information.

7b. NUMBER OF REFERENCES: Enter the total number of references cited in the report.

8a. CONTRACT OR GRANT NUMBER. If appropriate, enter the applicable number of the contract or grant under which the report was written.

8b, &, & 8d. PROJECT NUMBER: Enter the appropriate military department identification, such as project number, subproject number, system numbers, task number, etc.

9a. ORIGINATOR'S REPORT NUMBER(S): Enter the official report number by which the document will be identified and controlled by the originating activity. This number must be unique to this report.

9b. OTHER REPORT NUMBER(S): If the report has been assigned any other report numbers (either by the originator or by the sponsor), also enter this number(s).

10. AVAILABILITY/LIMITATION NOTICES: Enter any limitations on further dissemination of the report, other than those

imposed by security classification, using standard statements such as:

(1) "Qualified requesters may obtain copies of his report from DDC."

(2) "Foreign announcement and dissemination of this report by DDC is not authorized."

(3) "U. S. Government agencies may obtain copies of this report directly from DDC. Other qualified DDC users shall request through

_____."

(4) "U. S. military agencies may obtain copies of this report directly from DDC. Other qualified users shall request through

_____."

(5) "All distribution of this report is controlled. Qualified DDC users shall request through

_____."

If the report has been furnished to the Office of Technical Services, Department of Commerce, for sale to the public, indicate this fact and enter the price, if known.

11. SUPPLEMENTARY NOTES: Use for additional explanatory notes.

12. SPONSORING MILITARY ACTIVITY: Enter the name of the departmental project office or laboratory sponsoring (paying for) the research and development. Include address.

13. ABSTRACT: Enter an abstract giving a brief and factual summary of the document indicative of the report, even though it may also appear elsewhere in the body of the technical report. If additional space is required, a continuation sheet shall be attached.

It is highly desirable that the abstract of classified reports be unclassified. Each paragraph of the abstract shall end with an indication of the military security classification of the information in the paragraph, represented as (TS), (S), (C), or (U)

There is no limitation on the length of the abstract. However, the suggested length is from 150 to 225 words.

14. KEY WORDS: Key words are technically meaningful terms or short phrases that characterize a report and may be used as index entries for cataloging the report. Key words must be selected so that no security classification is required. Identifiers, such as equipment model designation, trade name, military project code name, geographic location, may be used as key words but will be followed by an indication of technical context. The assignment of links, rules, and weights is optional.

Unclassified
Security Classification